

DOPPLER RADAR TECHNIQUES FOR DISTINCT RESPIRATORY PATTERN
RECOGNITION AND SUBJECT IDENTIFICATION

A DISSERTATION SUBMITTED TO THE GRADUATE DIVISION OF THE UNIVERSITY OF
HAWAII AT MĀNOA IN PARTIAL FULFILLMENT OF THE REQUIREMENTS FOR THE
DEGREE OF

DOCTOR OF PHILOSOPHY

IN

ELECTRICAL ENGINEERING

JUNE 2017

By

Ashikur Rahman

Dissertation Committee:

Victor M. Lubecke, Chairperson

Olga Borić-Lubecke

Jan Prins

Aaron Ohta

David Garmire

Keywords: radar, RF tags, low intermediate frequency, subject identification, respiration

Copyright

Ashikur Rahman

Dedicated to

My father Akbar Hossain (late) and my mother Ayesha Akter

ACKNOWLEDGEMENTS

I am grateful to many individuals who supported me as a mentor, colleague, and advisor. This acknowledgment may not include everyone, but I must mention some very influential people. Dr. Victor Lubecke, my adviser and committee chair is supreme in many distinguishable qualities. The mentorship I received from him surpassed all others. The inherent composure yet very powerful speech delivery capability in his nature always kept me motivated and helped me in carrying on my work. His forbearance on dealing with my initial superficial research or silly mistakes is splendid. I consider myself a very lucky person to have such an experienced and knowledgeable adviser. He could grasp the idea of my research very quickly and guide me readily towards the next steps. I have heard many unsuccessful relations between a supervisor and a graduate student. Luckily, I never felt anything that could create the slightest discomfort in between us. He is such a sensible person who would ensure that his students receive the best support to carry on our research. He used to call his past students, colleagues for any information, if needed, without any delay, considering my need as a priority. I will ever be grateful to him for ensuring very pleasant graduate life experience.

I wish to thank Dr. Olga Borić-Lubecke for her excellent support as a mentor and committee member. She is very detailed oriented, and her assessment on any research topic is unprecedented. She has been a great support for me. She not only mentored me with useful suggestions in my research but also handled other needs that graduate students usually face. She has always been a source of financial support to carry on my research and saved me from any financial hardship.

It was a great privilege to receive support from the alumni group of the lab. Aditya Singh must be given a lot of credit for his guidance in different stages of my research. He pioneers the uses of frequency altering tags and their uses in medical radar. He was a great resource to me for further development and applications of low-IF tags that consist a substantial part of the dissertation.

I also want to mention Mehran Baboli, Shuhei Yamada, Noah Hafner and Isar Mostafanezhad, Robert Nakata who shared useful insights when I faced obstacles in my research.

Ehsan Yavari has been my great colleague and guide. He showed the path towards publishing my first paper and greatly contributed to the writing. Since then he remained a very reliable colleague and friend in my research activities. Having him as a colleague was great. Otherwise, I would have wasted lot of time reinventing the wheels. I am very grateful to my supportive colleague Xiaomeng Gao. He is very energetic and dedicated person. Xiaomeng helped me greatly, in the beginning, to learn to use the lab equipment. He always considered my needs as a great priority and helped me set up many experiments and shared ideas throughout the Ph.D. endeavor. Master students Jia Xu and Alexander Lee have been very good company. Their support in conducting experiments was remarkable.

I must give a lot of credit to my dearest friend Nilufar Islam. Even though she lived in long distance, she kept me motivated every day by saying encouraging words. Her care made me believe in myself. Additionally, she spared much practical suggestion relating to general hurdles of graduate life. I used to receive surprising presents coming from another country which made me feel special.

Finally, my parents Akbar Hossain and Ayesha Akter played the main role by seeding the idea of coming to graduate school. Their dream was always to see me as a scholar. Their dreams inspired me greatly. My parents sacrificed a lot so that I can pursue Ph.D. In the absence of me, my sister Mahmuda supported my family with all her heart. Without her contribution, it would have been very difficult to continue my studies abroad.

ABSTRACT

Stationary continuous wave Doppler radar has been used for displacement measurement and vital signs detection in many state-of-the-art studies. However, further improvement, i.e., accurate radar characterization of respiration, may allow sleep diagnostics and unique subject identification. A low distortion DC coupled system with high signal to noise ratio is required for such characterization and classification, which is especially critical with small signals, as with through wall measurements which suffer from poor signal to noise ratio (SNR). This thesis proposes techniques to improve the signal to noise ratio by DC offset management and using the method of zooming in on fractions of the respiratory cycle waveform. A month-long study of six human subjects was performed and the developed Doppler radar system with classification algorithms has shown promising results in unique identification (vital signs based fingerprint) with more than 90% accuracy. Measurement time sample can be as low as 30 seconds. Neural networks, minimum distance classifiers, and majority vote algorithms were fused on multi-feature spaces to make classification decisions. Training and testing were performed on the extracted features such as variation in their breathing energy, frequency, and patterns captured by the radar. The system has shown the advantages of non-contact unique-identification where camera-based systems are not preferred or are incapable. This study also has an impact on radar-based breathing pattern classification for health diagnostics.

This research also investigates the poor SNR problem associated with mobile platform as measurements, which become challenging due to motion artifacts induced by the platform. To implement a feasible field applicable solution, low intermediate frequency (IF) techniques for non-invasive detection of vital signs from a mobile short-range Doppler radar platform were proposed and validated through mechanical and human experiments. A low IF radar architecture using RF tags is employed to extract desired vital signs motion information even in the presence of large platform motion. Upon researching SNR improvement and developing algorithms, this research took one step further for unique identification of human subjects behind the walls. Many potential applications for such technology, such as security, health monitoring, IoT, virtual reality, and health diagnostics, will benefit from such ubiquitous monitoring, leading to have benefits for human society and sustainable existence of humans and nature.

TABLE OF CONTENTS

ACKNOWLEDGEMENT	iv
ABSTRACT	vi
LIST OF TABLES	x
LIST OF FIGURES	xi
CHAPTER 1. INTRODUCTION.....	1
1.1 SCOPE OF THE DISSERTATION.....	4
CHAPTER 2. RADAR.....	6
2.1 RADAR	6
2.2 RADAR RANGE EQUATION.....	6
2.3 RADAR HISTORY.....	8
2.3.1 Early experiments.....	8
2.3.2 First military radars.....	8
2.3.3 Advances during World War II.....	8
2.3.4 Radar in the digital age	9
2.3.5 Doppler radar measurement for physiological motion.....	9
2.4 TYPES OF RADAR.....	9
2.5 DOPPLER RADAR.....	10
2.6 PULSE DOPPLER RADAR	11
2.7 PHASE MODULATION	12
2.8 RADAR APPLICATION	13
2.9 SINGLE CHANNEL AND QUADRATURE RADAR.....	15
2.10 SHORT DISTANCE RADAR: PHYSIOLOGICAL APPLICATIONS.....	15
CHAPTER 3. DEMODULATION	18
3.1 SINGLE CHANNEL RECEIVER LIMITATIONS	18
3.2 QUADRATURE RADAR USING SINGLE CHANNEL RADARS	20
3.3 CONTINUOUS WAVE (CW) QUADRATURE DOPPLER RADAR:.....	24
3.4 LINEAR DEMODULATION	25
3.5 ARCTANGENT DEMODULATION:	27
3.6 CHANNEL IMBALANCE CORRECTION.....	29
CHAPTER 4. RADAR SIGNAL CLASSIFICATION.....	33
4.1 FUTURE OF RF ACTIVITY CLASSIFICATION	34
4.2 THEORY OF RF ACTIVITY CLASSIFICATION	36
4.2.1 Sensing techniques	36

4.2.2 Useful information extraction.....	38
4.2.3 Turning data into knowledge.....	40
4.3 DOPPLER RADAR-BASED UNIQUE IDENTIFICATION SYSTEM.....	41
4.3.1 System setup.....	43
4.3.2 Feature extraction.....	44
4.3.3 Method and results.....	45
4.4 CONCLUSION.....	47
CHAPTER 5. MOBILE PLATFORM RADAR.....	48
5.1 PLATFORM MOTION COMPENSATION	49
5.2 MOTION COMPENSATION EXPERIMENT	50
5.3 SEE-THROUGH-THE-WALL (STTW) LIFE SIGN DETECTION FROM A MOBILE PLATFORM	51
5.3.1 Theory of mobile STTW radar.....	53
5.3.2 Experiment.....	56
5.4 CONCLUSION.....	60
CHAPTER 6. LOW-IF TAG BASED COMPENSATION	61
6.1 LOW IF BACKGROUND	61
6.2 THEORY OF OPERATION OF LOW-IF MOTION COMPENSATION TAG.....	64
6.3 EXPERIMENT AND RESULTS	71
CHAPTER 7. SUBJECT IDENTIFICATION	77
7.1 SYSTEM REQUIREMENT.....	77
7.2 SYSTEM IMPROVEMENT	78
7.3 ENHANCED SYSTEM AND NEW ALGORITHM.....	82
7.4 FEATURE SPACE 1:	83
7.4.1 Breathing Rate.....	83
7.4.2 Average exhale-start cycle period T_{ex} :	83
7.4.3 Standard deviation of exhaling-start period over N cycles.....	84
7.4.4 Average inhale-start cycle period T_{in} :.....	85
7.4.5 Standard deviation of T_{in} over N cycles	85
7.4.6 Speed of exhaling	85
7.4.7 Speed of inhaling.....	86
7.5 FEATURE SPACE 2:	86
7.5.1 Ratio of [inhale – exhale] area to [exhale-inhale area], Inhale-exhale-trapezium / Exhale-inhale-trapezium	86
7.6 FEATURE SPACE 3:	88
7.6.1 Signal complexity prior and after lung volume full.....	88
7.7 IDENTIFY ONE PERSON OUT OF A GROUP OF PEOPLE.....	90
7.8 IDENTIFY A GROUP OF PEOPLE FROM MANY	92

7.9 UNIQUELY IDENTIFY EVERYONE.....	93
7.10 CONCLUSION:.....	96
CHAPTER 8. RF UNIQUE IDENTIFICATION CHALLENGES AND FUTURE WORK.....	97
8.1 INTRODUCTION	97
8.2 ACCURACY VS. DETECTION TIME	97
8.3 LOW SUCCESS RATE SUBJECT	100
<i>8.3.1 Frequency analysis of minor components.</i>	<i>100</i>
<i>8.3.2 Algorithm for minor component feature for unique identification.....</i>	<i>102</i>
<i>8.3.3 Biometric feature summary.....</i>	<i>103</i>
<i>8.3.4 Feature fusion topology.....</i>	<i>105</i>
8.4 CONCLUSION.....	106
REFERENCES	108

LIST OF TABLES

Table 2-1 Information gathered using Different Topologies of Radar Transceivers [2]	14
Table 4-1. Respiration segment features.....	46
Table 4-2 Unique identification testing results in a confusion matrix [4]	46
Table 7-1 Features for unique identification.....	80
Table 7-2 Unique identification without gain improvement for close pairs subjects	80
Table 7-3 Gain improvement with proposed DC-offset cancellation	81
Table 7-4 Unique identification with gain improvement for close pairs subjects.....	82
Table 7-5 Ratio of [inhale – exhale] area to [exhale-inhale area] – Feature space 2	92
Table 7-6 Fraction of times inhale-exhale transition speed is greater than unity – Feature space 3	93
Table 7-7 Training data collection from subjects – October 10 – October 20, 2016.....	95
Table 7-8 Training data collection from subjects – October 21 – November 20, 2016.....	95
Table 8-1 Accuracy and breakdown testing with varied testing time on subject #2.....	98
Table 8-2 Accuracy and breakdown testing with varied testing time on subject #3.....	99
Table 8-3 Longer sample-time experiment for low success-rate subject.....	100
Table 8-4 Biometric features [112].....	104
Table 8-5 Biometric features continued [112].....	105

LIST OF FIGURES

Figure 1.1 The scope of the dissertation (a) displacement measurement (b) unique identification	4
Figure 2.1 An illustration of the radar system.	7
Figure 2.2 A simplified classification approach for radars. PRF stands for pulse repetition frequency. CW stands for continuous wave.	10
Figure 2.3 Continuous wave (CW) radar classification based on operating distance.	10
Figure 2.4 Pulse Doppler radar [15]	12
Figure 2.5 Continuous wave (CW) radar classification	13
Figure 2.6 A single channel CW radar transceiver is shown. The RF signal is split into a carrier for the transmitter and local oscillator. Transmitter couples RF_{out} and receiver demodulates RF_{in} [2]	15
Figure 3.1 A simplified classification of CW short distance radar based on receiver architecture.....	19
Figure 3.2 The occurrence of null and optimum based on the nominal distance between the radar and target is shown (Single-channel radar).	20
Figure 3.3 Quadrature radar assembly is illustrated. A physical offset of approximately 3.5 mm has been kept between the two MDU1020 single channel x-band radars [69].	21
Figure 3.4 Experimental setup of the quadrature radar, assembled using two single channel radars (a), a motorized mover with a mounted reflector (torso representation) was used to simulate periodic motion. (b), human experiment.	22
Figure 3.5 (a) The top two plots are the output of the two radars and the bottom plot is the result of linear demodulation of the two radars, (b) and (c) shows the same when the nominal distance is gradually changed. It is evident that one radar suffers distortion, but the other radar helps to demodulate the correct signal. (d) Shows a human experiment result, the bottom curve compares demodulation result with a respiration belt [69].	24
Figure 3.6 Doppler radar vital sign measurement assembly is shown. The quadrature receiver includes RF mixer and dividers.	25
Figure 3.7 Linear demodulation, graphical illustration. a) shows arc created plotting I data vs Q data, the projections are taken on both axis, b) rotates the arc for projection on the larger side, c) shows the projection or linearization of the arc, and d) shows if the case were opposite, i.e., larger projection is on I axis.	26
Figure 3.8 Sources of the DC offset in Doppler radar system.	28
Figure 3.9 A reflector was moved in periodic sinusoidal motion in front of a quadrature radar, with the balanced channel the IQ plot would have been an arc of a circle. a) shows time series of I and Q channel, displacement is more than a quarter circle in IQ plane, b) IQ plot to show channel imbalance, it is evident from the elliptic shape.	30
Figure 3.10 a) shows imbalance correction using the method described in this section (ellipse fit), and b) shows circle fitting using GS method.	31
Figure 3.11 Demodulated output after imbalance correction, which resembles the sinusoidal movement.	32
Figure 4.1 Samsung's smart home service architecture [78].	35
Figure 4.2 The author's vision for indoor RF activity sensing and classification [79]	36

Figure 4.3 Time domain data and corresponding IQ plot, for Doppler radar measurement of sinusoidal motion in (a), and (b) shows the same for a series random linear movement [79].	37
Figure 4.4 Doppler radar vital sign measurement assembly is shown. The quadrature receiver includes RF mixer and dividers.	42
Figure 4.5 Epoch features for neural network training are illustrated. a) Time series of respiration record b) Power spectral density c) Peak line fit and error d) Packing density [4] [79].	45
Figure 5.1 Mobile quadrature Doppler radar system. The transceiver is mounted on a linear stage which can move the radar.	50
Figure 5.2 Linear stage mounted radar system moving with 2 Hz sinusoidal having 4 mm amplitude. a) Linear demodulated the signal from radar system b) radar displacement (mm) from the nominal reference position with infrared tracking system c) comparison of extracted respiration rate using IIR filter (blue) and respiratory belt transducer (red) [5].	52
Figure 5.3 Radar system is moving with 1.2 Hz sinusoidal having 4 mm amplitude [5].	53
Figure 5.4 Mounted radar system running with 0.2 Hz sinusoidal having 4 mm amplitude. a) Linear demodulated the signal from radar system b) radar displacement (mm) from nominal reference position c) plot showing respiration rate from ANC (black) filter, IIR notch filter with 0.2 Hz center (red) and chest belt (blue) reference. In extreme aliasing case (0.2 Hz radar motion) ANC showed much better performance in respiration measurement [5].	53
Figure 5.5 See through wall vital sign detection for a stationary human target and stationary radar using continuous wave radar [1]. Ultra-wide band (UWB) pulse radars also used for STTW applications [97].	55
Figure 5.6 See-through wall visualization with Doppler radar transceiver. The radar is on a mobile platform. A mechanical target (chest phantom) can be moved on a linear stage [97].	56
Figure 5.7 Flow chart is showing motion compensation procedure. Radar output is continuously checked against a threshold. Motion compensation is only performed on the data that is within the limit. Various motion compensation techniques are applied such as spectral filtering, adaptive noise cancellation, or sometimes fixed filtering [97].	57
Figure 5.8 Through wall experiment in the laboratory [97].	57
Figure 5.9 Implementation of the adaptive algorithm as shown in Fig. 5.8. Any turbulent motion causes the radar signal to be severely saturated and throws in the nonlinear region for that is not suitable for vital sign detection. The filtering only takes place when the motion is within the limit of the threshold, (a) shows the output of the radar for a two-minute span of time, (b) shows the same for ultrasound sensor.	58
Figure 5.10 Frequency response of radar output in (a), and ultrasonic sensor's output in (b). Both outputs show that a common 1 Hz is present which is platform's motion [98].	59
Figure 5.11 Radar output is shown in (a) which comprises voltage output due to the motion of platform and target. (b) shows the output of ultrasonic sensor capturing voltage due to platform motion, and (c) is the output of filtering of platform motion from the radar output resulting in the voltage proportional to the motion of the target which fairly compares well with the reference of the target [97].	59
Figure 6.1 Application of RFID tagging in Doppler radar motion sensing. A stationary radar and subject, (a), a subject tagged to cancel (ignore) unwanted hand movement, (b), and the proposed system where the radar	

itself is in movement, (c), are shown. In (c), the stationary tag is used to find the radar motion and cancel it from another motion measurement [97].....	64
Figure 6.2 Mobile quadrature Doppler radar system. The transceiver is mounted on a linear stage which can move the radar. BB refers to baseband [96].	65
Figure 6.3 RF tag device includes a mixer, an on-board oscillator, and an antenna [96].	66
Figure 6.4 Theoretical frequency domain response of the demodulated RF signal [96].	69
Figure 6.5 Fabricated IF tag and ADS simulation circuit [96].	72
Figure 6.6 Platform motion detection using IF tag. The radar-carrying linear stage was programmed to move in 1.2 Hz with 8mm displacement. The IF filter output from I channel, (a), the Fourier transform of the 1531 Hz IF signal amplitude modulated by the motion of radar module, (b), and the IF demodulated signal which is proportional to the displacement, (c), are shown. It is evident that 1.2 Hz sinusoidal motion is detected [96].....	73
Figure 6.7 Similar plots are shown for Q channel. To avoid the null problem both I and Q channels are required. Therefore, both I and Q measurements are taken to perform linear demodulation [96].	73
Figure 6.8 Tag performance for motion compensation. Radar output is showing baseband data comprised of (a voltage proportional to) platform motion and respiratory effort, (a); demodulated IF signal representing the voltage proportional to platform motion. The platform motion is filtered out from baseband data to retrieve respiration signal, (b); and a comparison of motion compensated radar result and reference chest belt, (c), are shown. The results are comparable to the infrared camera tracker system (8 mm, 1.2 Hz motion of the platform) [5].	74
Figure 6.9 Respiration signal retrieved using adaptive filters. Radar output showing baseband data comprising (a voltage proportional to) platform motion and respiratory effort, (a), demodulated IF signal representing the voltage proportional to platform motion, (b), and a comparison of the motion compensated radar result and chest belt reference, (c), is shown [96].	75
Figure 6.10 Experiment setup in the laboratory. Front view and a side view shows the placement of radar, RF tag, and human subject [96].	76
Figure 7.1 Radar output of displacement of a very simplified mechanical breathing simulator. Both AC coupled, and DC coupled measurements are presented. When a rest in between inhale and exhale is simulated, DC coupling preserves the state in its displacement measurement. However, AC coupled measurement is distorted [111].	78
Figure 7.2 Replication of Levenberg-Marquardt method based circle fitting on the very short arc. The operating frequency is 2.4GHz. The nominal displacement simulated is 2 mm, which is equivalent to 3.2% of a full circle. A 30dB white Gaussian noise (AWGN) was added to baseband signals [111].	79
Figure 7.3 Proposed method for dynamic range improvement. Required DC offset cancellation margin is calculated in the beginning and subtracted/added from the down-conversion output which enhances the margin of amplification without saturating LNA with lower gain. Table III shows some gain improvement in two different target distances [111].	81
Figure 7.4 4 cycles of respiration signal from subject 1 measured using the proposed system in Fig.4. This high DR system allows zooming in the fractions of breathing cycle without distorting useful patterns. The	

intactness of these patterns produces good unique identification accuracy while using wavelet complexity analysis [111].	82
Figure 7.5 Finding the respiration rate using FFT	83
Figure 7.6 Breathing depth estimation after peak searching.	84
Figure 7.7 Dynamic segmentation of [30%-70%] displacement in each breathing cycle.	86
Figure 7.8 Dynamic segmentation of [30%-70%] displacement in each breathing cycle, and area ratio calculation, [inhale-exhale]/[exhale-inhale]	87
Figure 7.9 The summary of the algorithm (flow chart) of determining the ratio feature	87
Figure 7.10 Signal pattern which relates to the dynamics of breathing near the points where exhale- inhale transition occurs.	88
Figure 7.11 a) shows the color coded 100 samples prior and after the apex occurs. This apex is considered as the full lung volume; exhalation starts from apex; b) depicts the summary of the algorithm (flow chart) of determining the signal feature near breathing transition (exhale-inhale handover)	89
Figure 7.12 Hypothetical setup of a system where one individual is identified out of a group.	90
Figure 7.13 Signal pattern which relates to the dynamics of breathing near the points where exhale- inhale transition occurs. This subject shows a constant pattern of slow-down in transition.	91
Figure 7.14 There is no fixed pattern; rather the subject shows variable nature, slow or fast either.	91
Figure 7.15 shows hypothetical class boundaries of subjects S1 through S6. These boundaries have been found by training data and fusing some features and taking a weighted average. The ranges of the feature values overlap which means we can identify a group of people (if not an individual) from a larger set.	92
Figure 7.16 Majority vote concept from multiple feature space is illustrated. A test data evaluates to the class of S1/S3 in feature space 2. However, same test data evaluates to S1/S2 in feature space 3. Now, the majority vote goes to S1. The decision is made based on most likely probability.	93
Figure 7.17 a) shows the stages of feature extraction for identifying one person trivially from a group, a group of people from many, and uniquely identifying an individual from a group of people, b) shows steps to evaluate identification. The average value of each feature was calculated and saves in the database in the training process. Table 7-7 shows the collection of training data.	94
Figure 7.18 A minimum distance classifier was used if the testing data did not identify the person in stage 1 and 2. In this figure S1 through Sn are the sum of the feature values in feature space 1 and the each point value indicates individuals in the database system. The data point is evaluated on the same feature space, and Euclidian distance is calculated to find the minimum and make decision whoever is the closest match. S2 is closest, in this case; the identification result will be subject #2.	96
Figure 8.1 Plot of the data in Table 8.1 shows sample-time versus detection accuracy curve for subject #1. Algorithm fails to run if sample time is less than 20 s.	98
Figure 8.2 Plot of the data in Table 8.2 shows sample-time versus detection accuracy curve for subject #3.	99
Figure 8.3 This figure shows frequency domain analysis of minor components for subject #1. There is a definite pattern visible. The data peaks at 1 Hz which is well contrasted with other frequency components.	101
Figure 8.4 This figure shows frequency domain analysis of minor components for subject #4. If this data is compared to subject #1, a clear difference is visible. The data peak is at nearly 1.1 Hz. The other	

frequency components are relatively much more dominant than the subject #1. Also, there a second peak noticed almost same distance for all the four samples.	102
Figure 8.5 In (a) the algorithm of using minor component of demodulated high passed IQ data is presented for unique identification, (b) shows the plot of major versus minor components of high passed demodulated radar data for one of the subjects in the experiment.....	103
Figure 8.6 Algorithm shows the prospective feature fusion method that can be used to enhance the performance of radar-based unique identification.....	106

CHAPTER 1. INTRODUCTION

Short range microwave Doppler radar has been employed for non-invasive monitoring of human cardiopulmonary activity [1]. A Doppler radar motion sensing transceiver transmits a continuous microwave signal and demodulates the signal reflected from a target.

According to Doppler theory, if the target has a time-varying displacement having zero net velocity, the reflected signal is phase-modulated in proportion to the position of the object rather than the velocity [2]. Thus, the phase of a reflected signal will be directly associated with positional changes of the chest surface due to the lungs and heart movements [2].

Chapter 2, 3 describes the background of radars and demodulation process.

Adult human breathing patterns at rest are different not only with respect to tidal volume and, inspiratory and expiratory duration, but also in airflow profile [3]. Besides this diversity, in every recording of ventilation at rest in a steady-state condition, breath to breath fluctuations are observed in ventilatory variables [3]. This variability is non-random and may be explained either by a central neural mechanism or by instability in the chemical feedback loops. Beyond this variability, everyone appears to select one pattern among the infinite number of possible combination of ventilatory variables and airflow profile [3]. Any collection of information generated by monitoring that person's health may uniquely identify a person or a group of people, which is crucial in the unique identification of, or creation of a unique medical identity for people. Unique-identification based on vital signs may add another dimension to traditional fingerprint systems. Camera based unique identification can be inappropriate due to privacy concerns. This thesis proposes a Doppler radar based system,

capable of recording and classifying vital signs such as respiration and heart signal for biometric identification.

Abnormal respiration results in distinctive patterns which are indicative of specific health disorders. Breathing could be normal, Cheyne-stokes, central neurigenci-hyperventilation, ataxic-breathing, and cluster-breathing to cite some examples. Simple inspection of the respiratory cycle, rate, rhythm, inspiratory volume, and effort of breathing, are useful parameters in finding any abnormality [4]. Finding differences in normal breathing from person to person needs further careful analysis and observation which is the prime motivation of this thesis. However, these abnormalities are relatively easier to detect since each one shows a definitive pattern. Useful features can be extracted and an artificial intelligence network can be trained for classifying the signals. This classification can represent a unique identification of the person or a group of persons [4]. Chapter 4 presents the basics of data classification. A study on unique identification is performed to evaluate the radar based system's potential. The process and results are presented in chapter 4.

Signal to noise ratio (SNR) can be greatly reduced if the vital sign is measured from a mobile radar system. Correct measurement of vital signs is challenging due to possible aliasing, phase distortion and occurrence of non-linear distortion. These problems occur due to variable traveling distance from moving radar antennas and target [5]. If tracked radar motion is simple and precisely detected, IIR filtering techniques can remove the motion artifact. However, in cases of extreme aliasing advanced noise cancellation techniques are required. Some work has been published addressing motion artifacts due to hand shake for Doppler radar sensors. One way of tackling this problem is using a sensor node [6]. Empirical mode decomposition techniques were discussed for removing fidgeting interference in Doppler radar life signs monitoring devices [7]. This thesis further analyses the noise compensation not only for transmit antenna, but also the whole radar module for continuous motion of larger amplitude to use the system in vehicle mounted devices. The sensor node technique is not always feasible because it requires an additional device nearby a subject. In the EMD method intrinsic mode functions (IMFs) should be selected by the user, which is not always possible, and it is more computationally complex [7]. Chapter 5 begins discussion on theory and experiments of motion artifact cancellation. This chapter extends on the techniques of through wall measurements.

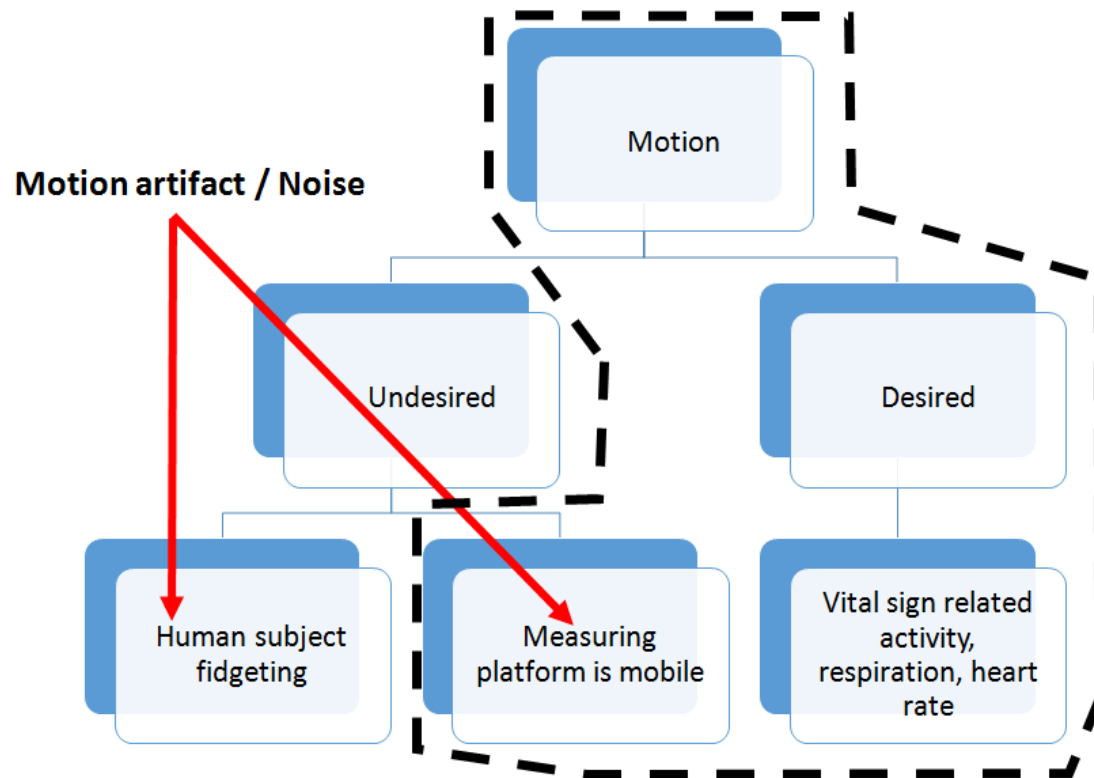
To enhance radar-based system's capability, the see-through-wall measurement technique is very crucial. A through wall radar has many civil and military applications, for

instance, in rescue missions, behind-the-wall target detection, surveillance, and reconnaissance. Some challenges in see-through-wall measurements have been addressed in subsequent chapters.

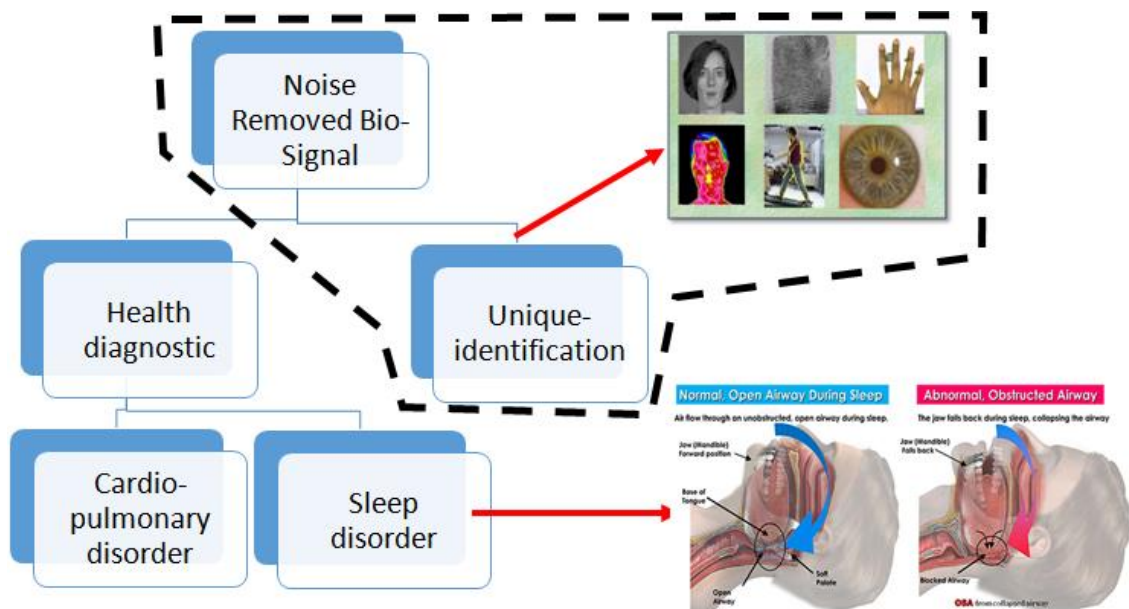
Some experiments presented in Chapter 5 to overcome motion artifact problem, however, only validating limited indoor cases using expensive precise infrared cameras. Motion artifact problems require more techniques for field application cases. This dissertation further presents a great deal of experiments and results on the analysis of noise compensation methods suitable for the motion of the whole radar system, which can be applied to large amplitude motion as would be expected in vehicle mounted applications. RF tag is introduced for motion artifact compensation. The original idea of using RF tag for platform motion cancellation is inspired by prior work [8] [9] where motion artifact cancellation for a moving target (stationary radar) was investigated via the use of a harmonic radar tag which provided a reference signal for the motion content to be canceled. Chapter 6 presents the details of using Low-IF tags for motion artifact cancellation.

Preliminary work in Doppler radar-based unique identification has been discussed in Chapter 4. However, published results in [4] did not incorporate any physical obstacle in the field of view; hence a fair SNR enabled unique feature detection. The training data and testing data both were collected from sedentary subjects. Breathing rate was a major feature for unique identification in [4]. However, subjects whose breathing rates are close will create ambiguity and false identification. Breathing depth also changes depending on subject's mood and physical condition. So, further research was required to identify distinct patterns of breathing. Additionally, a wall in between target and radar transceivers significantly lowers the SNR which hampers the possibility of detecting very subtle and unique signatures in human vital signs. In summary, a very good SNR system is required to achieve micro signatures in breathing patterns. This thesis finally puts efforts in achieving good SNR in DC coupled CW Doppler radar system and its impact on a robust system and signal processing algorithm to avoid any false detection in unique identification using Doppler radar. Algorithms were researched and reported on Doppler radar-based unique identification for a larger set of subjects. Chapter 7 presents these newly developed algorithms. The dissertation is concluded in chapter 8, which discuss some challenges and future direction. The overall scope of the dissertation is depicted in Figure 1.1. The challenge of isolating chest wall motion from other sources of motion is addressed. After achieving acceptable noise

1.1 Scope of the dissertation



(a)



(b)

Figure 1.1 The scope of the dissertation (a) displacement measurement (b) unique identification

reduced bio-signals (cardio-pulmonary), research efforts were made to recognize patterns in human subjects for unique identification.

CHAPTER 2. RADAR

2.1 Radar

The term Radar is derived from the original name given to this technique that was **R**adio **D**etection **A**nd **R**anging [2]. Pulses of electromagnetic waves (EM) are generated by the transmitter and sent to a radiating antenna which usually focuses the EM wave energy into a beam towards the target [10]. The received signal is received by the same antenna (duplex) or a different antenna and is sent to the receiver which proceeds signal processing system (Figure 2.1). After the signal processing, the results are displayed. The radar is designed to search and detect the target of interest and to determine certain target parameters [10].

2.2 Radar range equation

Determination of radar range is very crucial in designing or evaluating a radar's performance. A very simplified range equation is given below [10]-

$$R_{max} = \left[\frac{P_t A_e G \sigma}{(4\pi)^2 S_{min}} \right]^{1/4} \quad (2.1)$$

The parameters are described below.

P_t = transmitted power, W

A_e = Antenna effective aperture, m²

G = Antenna gain,

σ = Radar cross section of the target, m^2

S_{min} = Minimum detectable signal, W

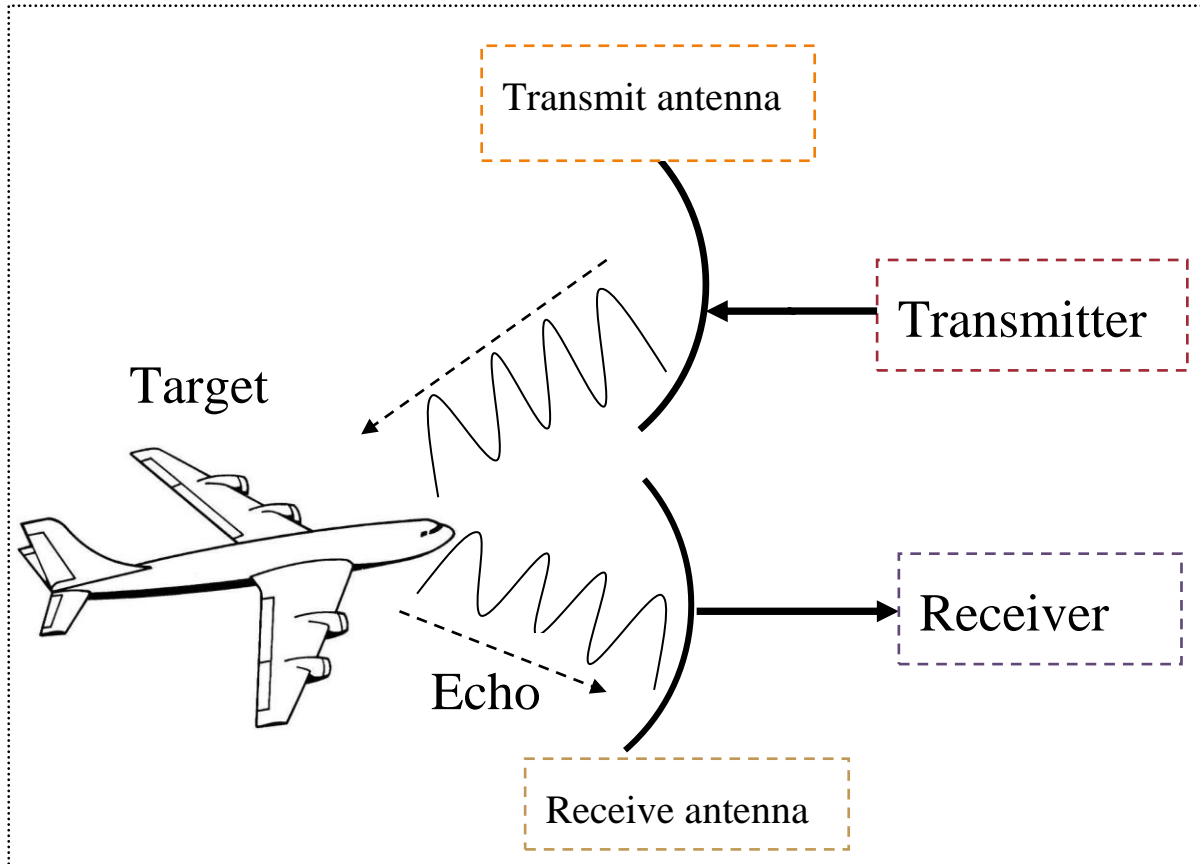


Figure 2.1 An illustration of the radar system.

The parameters of this maximum range equation can be designed; however, the designer cannot control the target's radar cross section. To achieve long range the transmission power should be higher. For short range operation, the transmission power can be kept considerably low; the energy radiation not necessarily has to be a very narrow beam, a small aperture antenna can receive the echo energy. All these design parameters present the trade-offs between having a large range versus small power small sized radar system [10].

The actual range is a function of many factors and may vary due to the following facts-

- 1) The minimum detectable signal is not a fixed number/quantity. Usually, it is determined by receiver noise
- 2) Fluctuations and uncertainties in target radar's cross section
- 3) Free space loss, other losses experienced in hardware
- 4) Propagation effects (composition of walls and clutters in indoor scenario)

2.3 Radar history

2.3.1 Early experiments

The basic idea of radar had its origins in the classical experiments on electromagnetic radiation conducted by German physicist Heinrich Hertz during the late 1880s. Later solemn developmental work on radar began in the 1930s. Hertz work relates to scientist Maxwell's work. Maxwell had formulated the general equations of the electromagnetic field, determining that both light and radio waves are examples of electromagnetic waves. These waves are governed by the same fundamental laws but having widely different frequencies which led to the conclusion that radio waves can be reflected from metallic objects and refracted by a dielectric medium, just as light waves can. Hertz demonstrated these properties in 1888, using radio waves at a wavelength of 66 cm associating a frequency of about 455 MHz) [11].

2.3.2 First military radars

The first radars developed by the U.S. Army were the SCR-268. The frequency of operation of the SCR-268 was 205 megahertz. To detect aircraft Britain commenced radar research (1935). In September 1938 the first British radar system, the Chain Home, had gone into 24-hour operation. Soviets had developed several different types of radars and had in production aircraft detection radar that operated at 75 MHz during World War II [11].

2.3.3 Advances during World War II

The successful development of innovative and important microwave radars at the MIT Radiation Laboratory has been accredited to the urgency for meeting new military capabilities. Many different radar systems were developed because of the laboratory's program during the five years of its existence (1940–45). One of the most noteworthy microwave radars developed by the MIT Radiation Laboratory was the SCR-584. SCR-584 was widely used for gunfire control system. The conical scan tracking of SCR-584 had a single offset (squinted) radar beam that is continuously rotated about the radar antenna's central axis [11].

2.3.4 Radar in the digital age

With the advancement of digital technology airborne pulse Doppler radars were developed during 1970, greatly enhancing its ability to detect aircraft amid the heavy ground clutter. The U.S. Air Force's airborne-warning-and-control-system (AWACS) radar and military airborne intercept radar relies on the pulse Doppler principle. Additionally, radar was also used in spacecraft for remote sensing of the environment during the 1970s. Advances in digital technology in the first decade of the 21st century helped further improvement in signal and data processing, with the goal of developing (almost) all-digital phased-array radars. High-power transmitters became accessible for radar application in the millimetre-wave portion of the spectrum (typically 94 GHz), with higher power [11].

2.3.5 Doppler radar measurement for physiological motion

In 1975 James Lin measured respiration signal of rabbit and human from a 30 cm distance using X-band sweep oscillator equipped with a rectangular horn antenna. He and his team continued research on using the microwave for detecting apnea noninvasively and was published in 1977. Researchers also wanted to find both the respiration and heart rate. With the advancement of analog and digital signal processing, Chan and Lin could obtain heart and respiration signals separately in 1987. In 2002 Lubecke invented methods to make add-on module that uses signals from existing wireless devices to measure heart and respiration rates. Quadrature Doppler radars were developed and different modulation techniques were proposed for accurate respiration and heart signal measurement. Techniques were also developed in last decades to compensate for distortion such as AC coupling distortion, I/Q channel imbalances, random body motion cancellation. Hybrid FMCW-interferometer radar was proposed for precise 2-D positioning and life activities surveillance. The proposed hybrid radar works in the 5.8 GHz ISM band with a 160 MHz bandwidth [11].

2.4 Types of radar

Since the invention, radars have been designed and used for many applications. Even though the basic principle remained same, many kinds of radars have evolved over the years. Radars can be categorized in domains and subdomains depending on the architecture and the waveforms used for various applications.

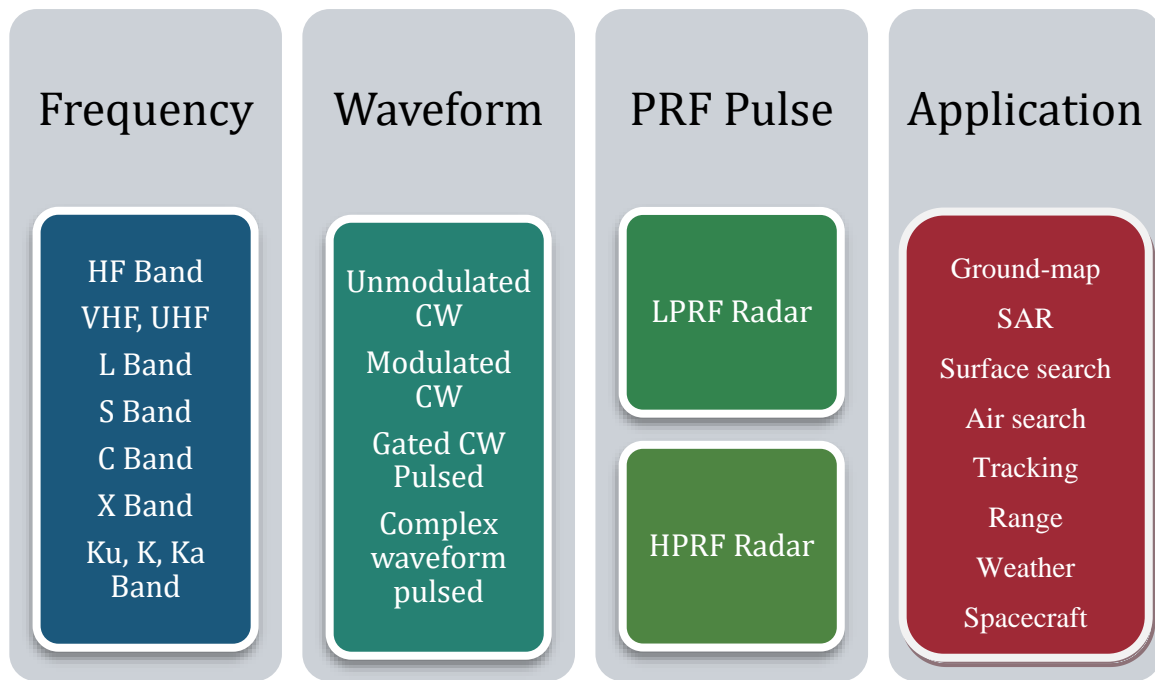


Figure 2.2 A simplified classification approach for radars. PRF stands for pulse repetition frequency. CW stands for continuous wave.

To illustrate an example that some radars from one of the domains in Figure 2.2 may be classified in sub-domains as is shown in Figure 2.3.

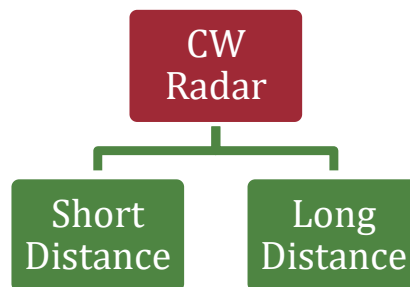


Figure 2.3 Continuous wave (CW) radar classification based on operating distance.

2.5 Doppler radar

In radar theory, Doppler effect is very well-known concept [12] [13]. To detect or characterize a moving object Doppler theory plays an important role and receivers are designed accordingly. According to Doppler theory while tracking a moving object, received RF signal's frequency shift is caused by motion that changes the number of wavelengths between the reflector and the radar. This process can corrupt or enhance radar performance

depending upon how that affects the detection process. Many applications such as sea-based radar systems, semi-active radar homing, active radar homing, military aircraft, weather radar, and radar astronomy rely on the enhancement effect of Doppler [14].

Doppler radar produces information about target velocity during the detection process. The information also allows small objects to be detected in an environment where there is a big contrast of velocities, for instance, the object of interest is moving relatively faster surrounded by slow moving objects [14]. Doppler shift subject the radar configurations, either if active or passive. The active radar transmits a signal, and the receiver receives the reflected signal. Passive radar receives signals from the object itself.

The Doppler frequency depends on the speed of light. The received frequency from a moving target is given by [15]–

$$f_r = f_t \left(\frac{1+\frac{v}{c}}{1-\frac{v}{c}} \right) \quad (2.2)$$

$$f_d = f_r - f_t = 2v \left(\frac{f_t}{c-v} \right) \quad (2.3)$$

$$f_d = f_r - f_t \approx 2v \left(\frac{f_t}{c} \right) \quad (2.4)$$

Where f_r, f_t, f_d, v, c denote the transmitter frequency, received frequency, Doppler or beat frequency, speed of the moving target and speed of the light in the medium (usually air for radars). Now the speed of the EM wave/light is usually much higher than the speed of the targets in our world applications. In such case, Doppler frequency can be expressed in more simplified form as shown in 2.4.

2.6 Pulse Doppler radar

It is important to understand the principle of pulse Doppler radar because it leads us to the understanding of phase modulation. Radial velocity is required for pulse-Doppler radar operation. Pulse radar sends out pulse RF with some interval. As the target moves between each transmit pulse the return signal will undergo a phase change from pulse to pulse, thus creating Doppler modulation. The amplitude of the successively returning pulse from the target is almost equal –

$$V = V_0 \sin \left(\frac{4\pi(d_0 + v\Delta t)}{\lambda} \right) = V_0 \sin(\phi_0 + \Delta\phi) \quad (2.5)$$

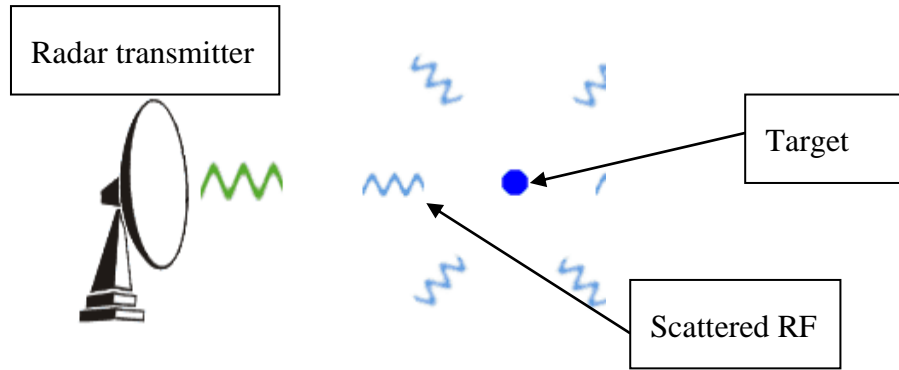


Figure 2.4 Pulse Doppler radar [15]

where

d_0 = distance between the radar and the target

λ = Wavelength of the transmitted signal

Δt = time interval between two pulses

$$\Delta\phi = \frac{4\pi(v\Delta t)}{\lambda} \quad (2.6)$$

Now if the phase shift can be measured in 2.6, the velocity can be found having other parameters known. Interestingly, only the radial component of the velocity is applicable. In case the target is moving at right angle to the radar beam, it has no relative velocity. Maximum Doppler frequency shift is found in the vehicles and weather move parallel to the radar beam.

2.7 Phase modulation

Consider a case where a target has a low-frequency oscillating motion on a fixed nominal distance from radar. The target is neither going away nor coming towards the radar. So, the net velocity of the target is 0. In short distance application, a target having a net 0 velocity the Doppler frequency shift measurement is hard to produce good results, it will be almost 0 which can be realized analyzing equation 2.4. We may use phase modulation information instead of Doppler frequency shift to track the low-frequency motion of the slow moving torso of the target. For this special case, we can modify the Equation 2.5. If a continuous wave radar is used instead of pulse radar,

$$v\Delta t = x(t) \quad (2.7)$$

$$V = V_0 \left(\frac{4\pi(d_0 + x(t))}{\lambda} \right) = V_0 \sin(\phi_0 + \Delta\phi) \quad (2.8)$$

$$\Delta\phi = \frac{4\pi x(t)}{\lambda} \quad (2.9)$$

where

$x(t)$ = time varying position of the reflector / target.

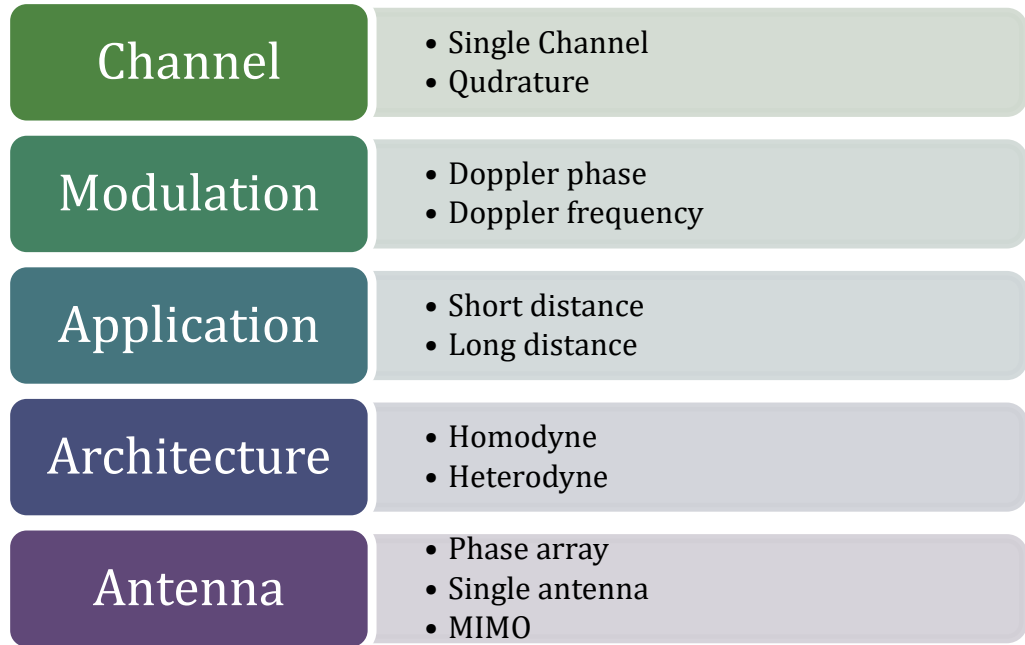


Figure 2.5 Continuous wave (CW) radar classification

Continuous wave Doppler radars are the kind that transmits RF signal towards the target ceaselessly. This kind of radar has some advantages over pulse radar. Continuous wave radar can completely produce the motion of a target within the environment of a stationary clutter. This type of radars has many applications in the field of biomedical science. Continuous wave radars can be classified in many ways as shown in Figure 2.5.

2.8 Radar application

Radar provides a range (and therefore position) of the object from the radar scanner. It is thus used in many different fields where the need for such positioning is critical. The first use of radar was for military drives as it facilitates in locating air, ground and sea targets [2]. Later civilian fields used radars extensively into applications for aircraft, ships, and roads. With improvements of different types of radar technologies, it is possible to also obtain information such as velocity, angle, size and shape, and radial velocity. These capabilities

(shown in Table 2.1) of radar technologies attracted many applications beyond aviation and war assisting system.

Table 2-1 Information gathered using Different Topologies of Radar Transceivers [2]

Information	Method of Determination	Required Topology
Range	Time Delay	Any but not CW, need enough range resolution
Velocity	Doppler Shift	Any, pulse radar with enough velocity resolution
Angle	Direction of Reflection	Any, array antenna
Size and Shape	Received Power	Any but CW, high resolution
Radial velocity	Doppler Shift and Time Delay	CW

In aviation, aircraft are armed with radar devices that notify of aircraft or other obstacles in or approaching their path, display weather information, and give precise altitude readings. One of the early stage radar was used in civil aircraft that can land in fog at airports equipped with radar. The landing was very precise, and radar-assisted ground-controlled approach systems were utilized.

Marine radars can help to measure the bearing and distance of ships to prevent collision with other ships, to navigate, and to fix their position at sea when within the range of shore or other fixed references such as islands, buoys, and lightships [2]. Vessel-traffic service radar systems are used to monitor and regulate ship movements in busy waters in the harbor.

Radar is used by meteorologists to monitor precipitation and the wind. Radar has become the key tool for short-term weather forecasting and watching for severe weather such as thunderstorms, tornadoes, winter storms, precipitation types, etc. Geologists use specialized ground-penetrating radars to record the composition of Earth's crust. Police forces use radar guns to screen vehicle speeds on the roads. Smaller radar systems are used to sense human movement. Examples are breathing pattern detection for sleep monitoring and hand and finger gesture detection for computer interaction.

2.9 Single channel and quadrature radar

One way to categorize CW radar is a single channel and quadrature radar. The simple architecture has been used by many researchers over the years to monitor physiological signals of human subjects in short-range scenarios. While single-channel radars have some practical limitation quadrature radar overcomes the limitations (shown in Figure 2.7). The working principle and demodulation techniques will be discussed in detail in next chapter.

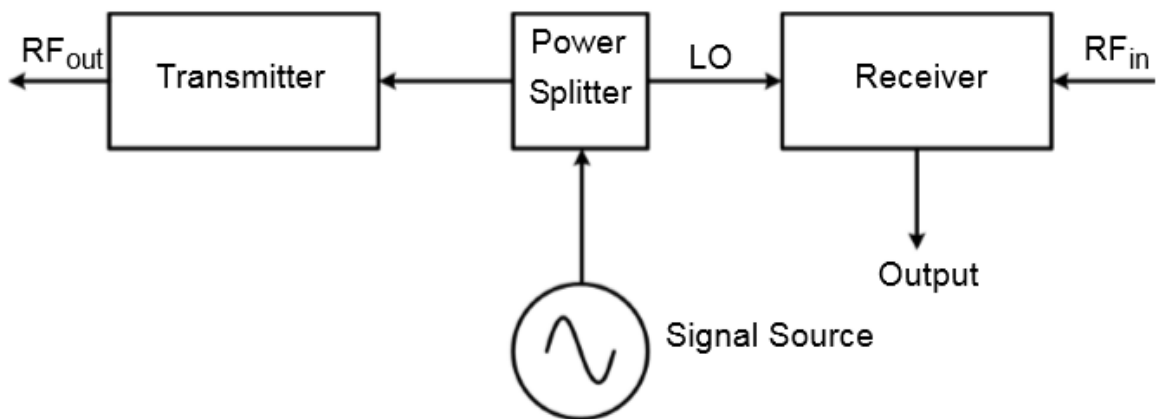


Figure 2.6 A single channel CW radar transceiver is shown. The RF signal is split into a carrier for the transmitter and local oscillator. Transmitter couples RF_{out} and receiver demodulates RF_{in} [2]

Another kind of radar is popular among researchers. The ultra-wideband radar has also been deployed for vital sign measurements. The ultra-wideband radar has some advantages and disadvantages compared to CW radar [16]. UWB radars are used as pulsed radar and require very complicated hardware for receiving and may suffer range ambiguity. However, the good side is it is very low power radar [17].

2.10 Short Distance Radar: Physiological applications

Recent developments in non-invasive radar measurement of small-scale motion offer great potential for indoor activity classification in applications such as health diagnostics, health monitoring, surveillance, product tracking product, occupancy sensing, and animal research [18] [19] [20]. Combined with wireless body area networks and indoor localization technology, measurement, and recognition of biological motion patterns will shape the future of home and workplace security, safety and comfort [21] [22] [23].

Many researchers chose many different topologies for physiological monitoring of human subjects. Two frequency radars, single channel radars, MIMO system radars, radars with varying waveforms and technologies have been reported in the literature [24]. Different types of radar provide different features, and almost all of those has trade-offs. Some concerns on displacement detection, some on rate, some are focused on respiratory patterns whereas some are designed to detect heart signals [25].

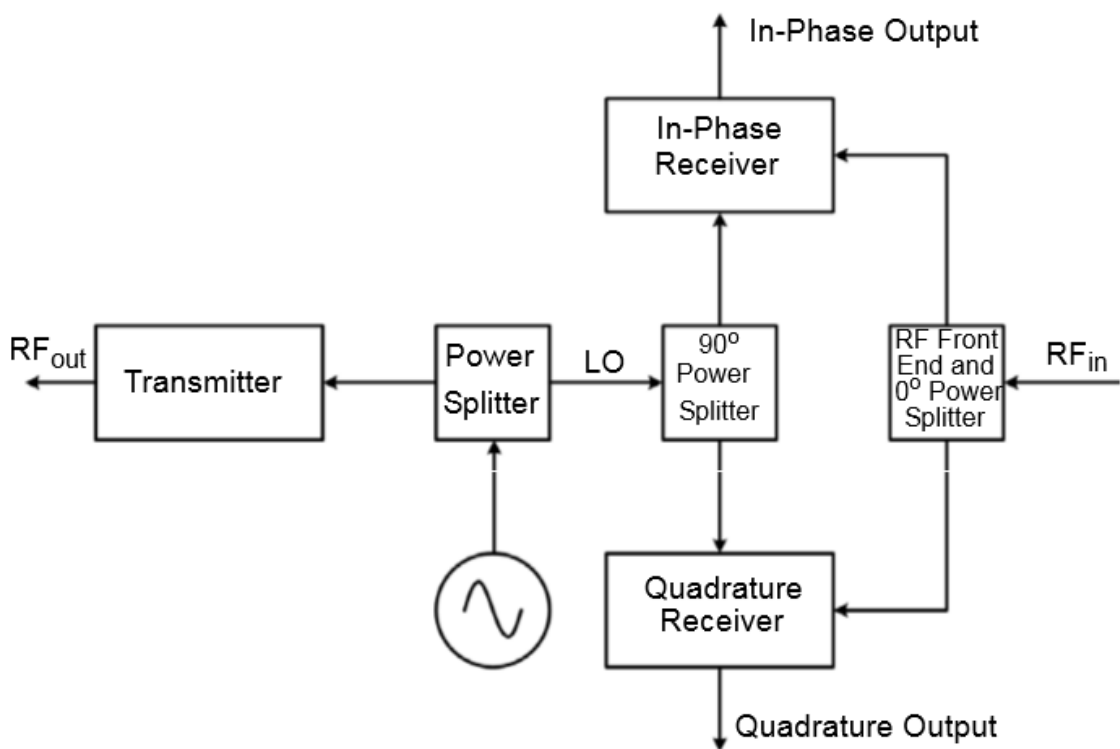


Figure 2.7: Block diagram of a CW quadrature radar system. Unlike single-channel radar, the LO is split with 90-degree phase shift. The received RF_{in} is then mixed with phase shifted LO's to generate two outputs, namely, in-phase (I) and quadrature phase (Q) which are orthonormal to each other [2].

Quadrature-radar is very popular for vital sign monitoring and accurate displacement measurement which came to maturity after solving many problems relating signal to noise ratio [26] [27] [28]. Digital signal processing also enhanced the usefulness of such radars [29] [30] [31] [32] [33].

In the last decade, new front-end architectures, baseband signal processing methods, and system-level integration technologies have been proposed by many researchers in

biomedical radar to improve detection accuracy and robustness [13] [34] [35] [36]. The advantages of non-contact detection have drawn interest for various applications, such as energy management in smart homes, occupancy monitoring [37], baby monitoring [38], cardiopulmonary activity assessment, and tumor tracking [39] [40] [41]. Radar can be used to monitor older adults, and that can work as an aid to medical emergency notification [42]. Advances in biomedical radar technology have also opened the door to many indoor activity monitoring applications, only limited by the imagination [43] [44] [45] [46]. Beyond the measurement of heart and respiratory rate, this technology enables us to measure the effective radar cross section (ERCS) yielding information about body orientation, torso displacement, and physical characteristics of human subjects [47]. Heart rate variability and tidal volumes are very important parameters that can be measured with radars [48] [49]. Sleep is widely understood to play a key part in physical and mental health [50] [51]. The quality and quantity of sleep that an individual experience can have a substantial impact on learning and memory, metabolism and weight, safety, mood, cardiovascular health, disease and immune system function. Research indicates that in America alone 40 million people suffer from insomnia and chronic sleep disorders [52] [41]. Doppler radar technology shows a promising non-invasive way of monitoring sleep behavior with automated pattern recognition. This technology can potentially provide a huge cut in the cost of sleep studies [53] [54]. Some work has been reported in the literature on EEG analysis of sleep behavior detection [39] [50]. A similar approach can be adopted for the radar based monitoring system. In addition to recognition, artificial neural network based automatic classifiers will be very useful in the diagnosis of diseases and physiological conditions [55] [36] [56] [57]. Radar technology may also provide a non-contact, low cost, fast, unique identification solution without the privacy concerns associated with camera-based monitoring systems [4].

Doppler radar offers a convenient method for monitoring activity of animals as well as the recognition of various behavioral events [35] [46] [40]. Using multi-radar systems provides the ability to classify motion such as walking, running, or fidgeting, which is important in animal activity monitoring of energetic cost [58] [59]. It's a demographic fact that elderly population (older than 60 years) has been gradually increasing worldwide. This change calls for greater attention to cost-effective healthcare worldwide [60]. Since falling represents a major risk for older adults who live independently, innovative techniques are required for long-term monitoring of human subjects [61] [61]. System improvement with various waveform method [62], digital processing [63], and random body motion canceling radars also opens the door for more applications [64] [65] [66].

CHAPTER 3.

DEMODULATION

This chapter presents a summary of two types of vital-sign radars and the demodulation techniques that are employed. As mentioned in earlier chapter radars can be classified from many viewpoints. Some well-known types of CW short distance radars are listed in Figure 3.1. There is always a trade-off between architectural simplicity and the desired performance. While single channel radars are very simple, these radars suffer positional sensitivity and output distortion. This thesis evaluated the need for the efficient type of Doppler radar for unique identification application.

3.1 Single channel receiver limitations

A non-invasive CW radar-based system can monitor respiration parameters of the human subject by sending RF signal to the human chest and by processing reflected signal from human torso. A Doppler radar motion-sensing transceiver transmits a continuous microwave signal and demodulates the reflected signal from a target. According to Doppler theory, if the target has a time-varying displacement having zero net velocity, the reflected signal is phase-modulated in proportion to the position of the object rather than the velocity [9]. Thus, the phase of a reflected signal will be directly associated with positional changes of the chest surface due to the lungs and heart movements [67]. CW radars can be classified in a different perspective. Some well-known types are listed in Figure 3.1. Some features are also noted for each type.

Single Channel	Qudrature	MIMO
<ul style="list-style-type: none"> • Single channel • Non-linear distortion, position sensitivity • Simple demodulation • Low cost 	<ul style="list-style-type: none"> • Two channels • Sterio vision, position sensitivity is overcome with proper demodulation • Non-linear demodulation is more complex than single-channel system 	<ul style="list-style-type: none"> • Multiple Channel • Broader application range • Complicated reciever architecture • Higher cost

Figure 3.1 A simplified classification of CW short distance radar based on receiver architecture

A typical coherent continuous wave vital sign Doppler radar system sends an RF signal towards human torso; the echo is phase modulated due to the positional variation of moving body parts. The echo is mixed and down converted to retrieve the target's displacement. The output of a single channel receiver is given by [68]

$$B(t) \approx A_B \cos \left(\theta + \frac{4\pi r(t)}{\lambda} + \frac{4\pi h(t)}{\lambda} + \Delta\phi \left(t - \frac{2d_0}{c} \right) \right) \quad (3.1)$$

where the θ is constant phase-shift and $\Delta\phi$ is residual phase noise. $A_B, \lambda, r(t), h(t)$ and d_0 are baseband amplitude, wavelength, chest movement, heart movement and nominal distance between the radar and target.

The constant phase shift in (3.1) is related to nominal distance and can be expressed as

$$\theta = \frac{4\pi d_0}{\lambda} + \theta_0 \rightarrow d_0 = \frac{\lambda(\theta - \theta_0)}{4\pi} \quad (3.2)$$

If θ is denoted as the k multiple of $\frac{\pi}{2}$

$$d_0 = \frac{\lambda \left(\frac{k\pi}{2} - \theta_0 \right)}{4\pi} \quad (3.3)$$

The baseband output $B(t)$ will be either null or optimum for an integer value of k when small signal approximation is applicable [2].

The optimum output is given by [68],

$$B(t) \approx A \sin 2\pi f_1 t + B \sin 2\pi f_2 t + \Delta\phi(t)$$

and the null output is -

$$B(t) \approx 1 - [A \sin 2\pi f_1 t + B \sin 2\pi f_2 t + \Delta\phi(t)]^2$$

From (3.1) and (3.3) we see that null and optimum baseband output occurs for the nominal distances as

$$d_{NULL} = \frac{\lambda(m\pi - \theta_0)}{4\pi}; d_{OPT} = \frac{\lambda(m\pi + \frac{\pi}{2} - \theta_0)}{4\pi} \quad (3.4)$$

m is an integer. (3) reveals that the adjacent null and optimum separation is

$$|d_{NULL} - d_{OPT}| = \frac{\lambda}{8} \quad (3.5)$$

Chest and heart movements are approximated as sinusoids of frequencies of f_1 and f_2 . Figure 3.2 depicts the null and optimum outputs.

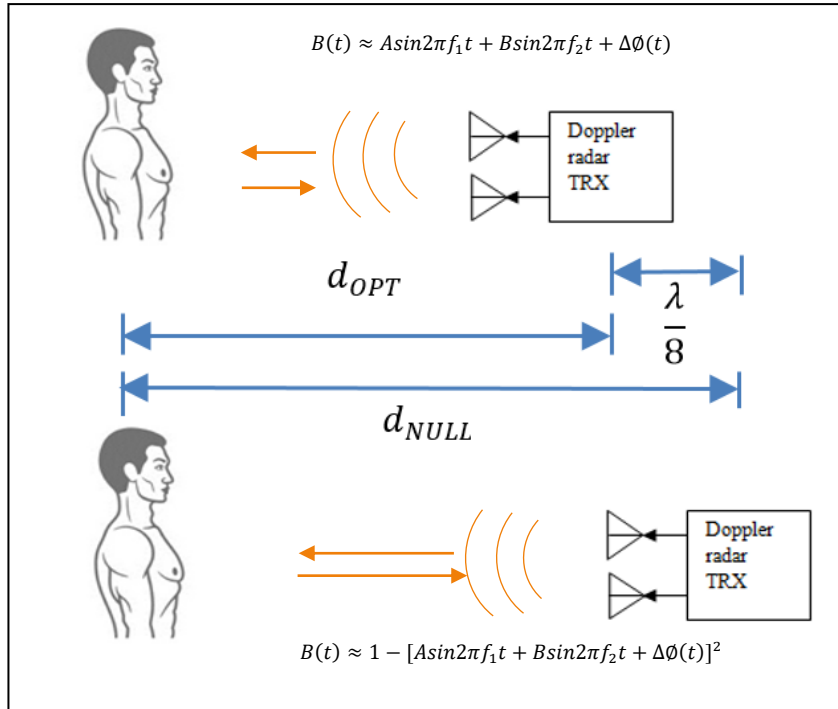


Figure 3.2 The occurrence of null and optimum based on the nominal distance between the radar and target is shown (Single-channel radar).

3.2 Quadrature radar using single channel radars

This analysis proves the fact that if two single channel radars are oriented similarly with a separation of $\frac{\lambda}{8}$ in the plane of nominal distance between the target and the radar transceivers, one of the radars will be in optimum position given that the other is in null position and vice versa. One fundamental assumption is that the difference of the residual phase noise of the radars is negligible. An experiment was performed to validate this theory.

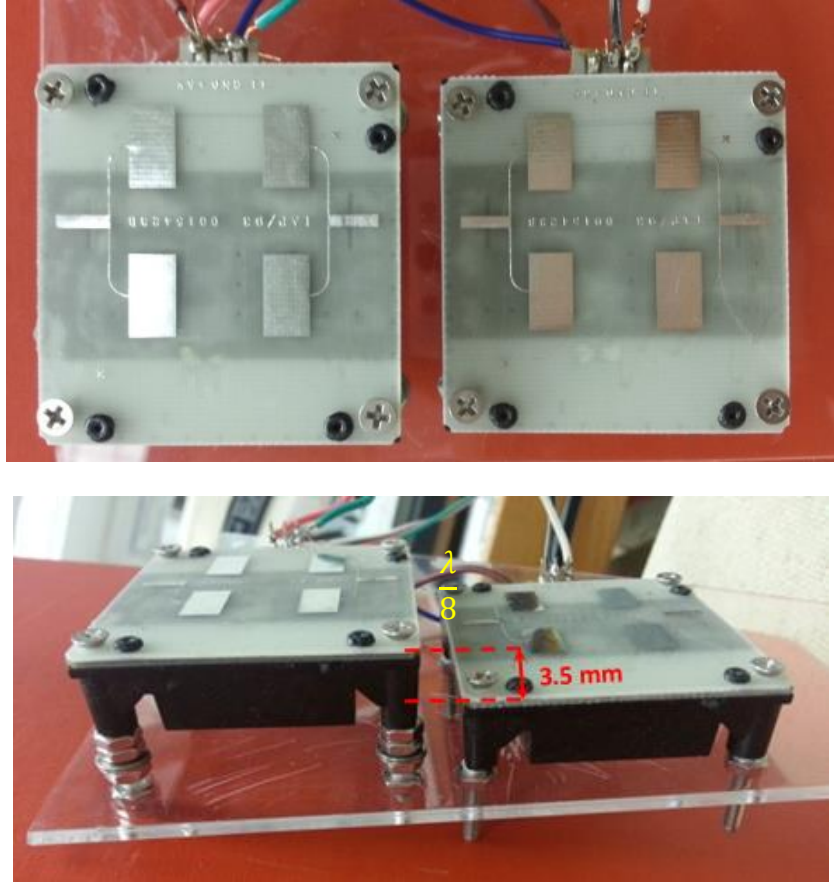


Figure 3.3 Quadrature radar assembly is illustrated. A physical offset of approximately 3.5 mm has been kept between the two MDU1020 single channel x-band radars [69].

Two MDU1020 radars were used for the experiment. MDU1020 has the operating frequency 10.525 GHz. The theoretical distance between consecutive null and optimum points is $(\frac{\lambda}{8})$ 3.5629 mm. Now creating the physical separation of this length in traveling plane of the wave should ensure one channel will be always in the optimum point. In case the nominal distance between one of the radars is in null position the other will be in optimum position. The two radars were physically separated approximately 3.5 mm. Figure 3.4 illustrates the experimental setup.

A mechanical mover was programmed to move in 1 Hz sinusoidal motion. The nominal distance between the radar pair and target was varied in the range of [0.5 m (0.5+.0035) m]. Linear demodulation has been performed using the output (a voltage proportional to displacement) of the two radars as shown in Figure 3.5.

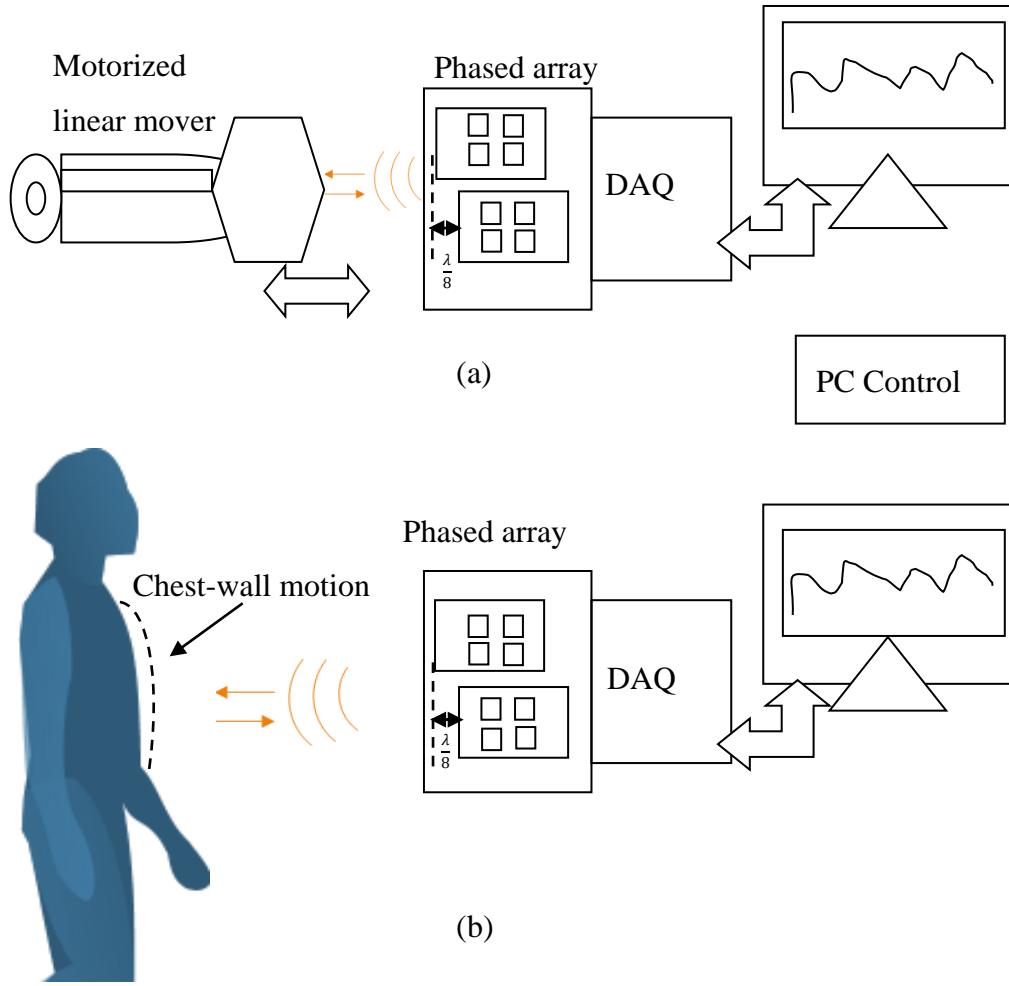
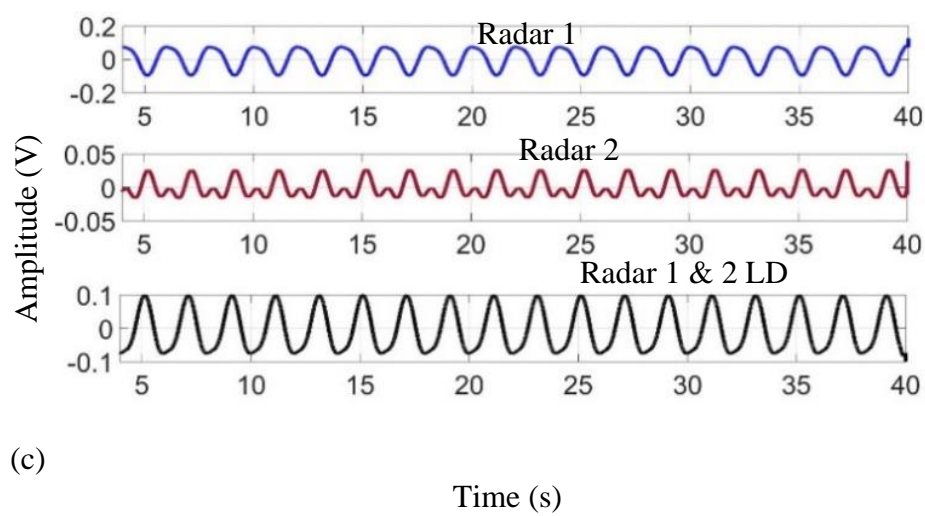
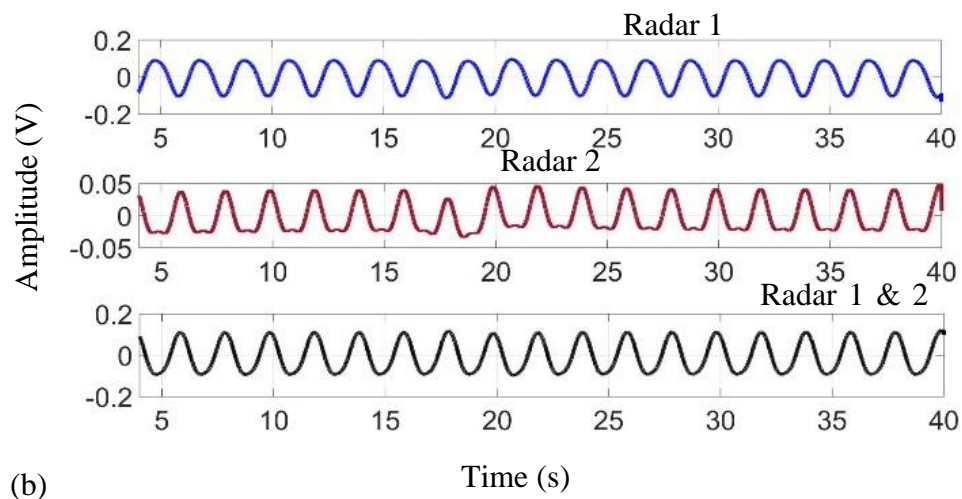
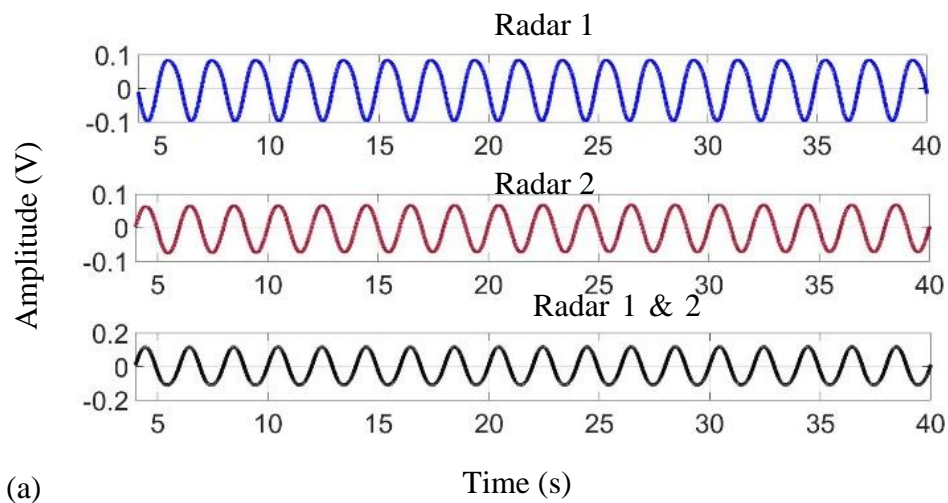


Figure 3.4 Experimental setup of the quadrature radar, assembled using two single channel radars (a), a motorized mover with a mounted reflector (torso representation) was used to simulate periodic motion. (b), human experiment.

In each subplot, the top two figures are baseband signals from the two radars. Linear demodulation (LD) [2] of the two-radar's output is also shown. Figure 3.5 (a) shows the two channels that are similar and in between null and optimum points with 180° phase shift. In Figure 3.5 (b) and Figure 3.5 (c) radar one is in optimum point while radar two is in null point and the doubled frequency is evident. Human testing was performed to compare the respiration curve with a respiration chest belt sensor's output.

Single channel radars are inexpensive. Anyone requiring IQ radar can use multiple single channel radars to create IQ radars. Experiments conducted with the mechanical target

and human subject supports the concepts of null point distortions and provides a means for avoiding it for single channel radars.



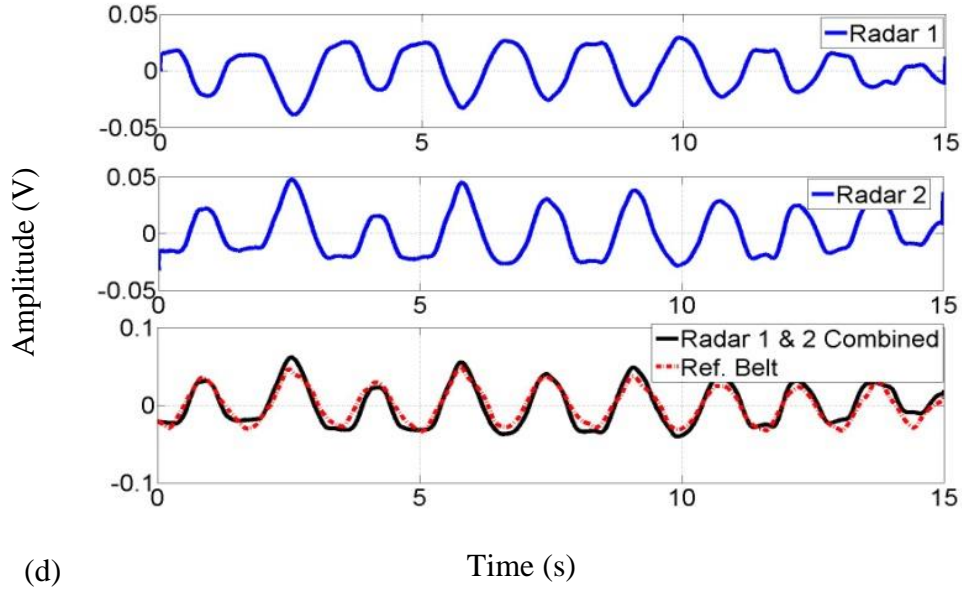


Figure 3.5 (a) The top two plots are the output of the two radars and the bottom plot is the result of linear demodulation of the two radars, (b) and (c) shows the same when the nominal distance is gradually changed. It is evident that one radar suffers distortion, but the other radar helps to demodulate the correct signal. (d) Shows a human experiment result, the bottom curve compares demodulation result with a respiration belt [69].

The experiment was performed to prove the occurrence of distortion using one-channel radar experimentally. Now, we do not have to use two separate single channel radars for such case; rather the circuit could be combined to one single circuit to make quadrature radar.

3.3 Continuous wave (CW) quadrature Doppler radar:

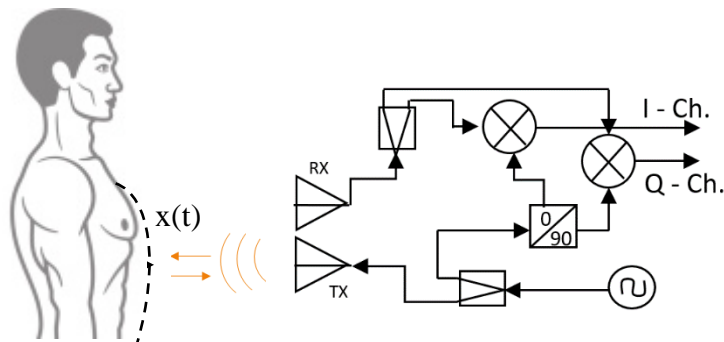
A quadrature Doppler radar provides the benefits of stereo vision. Demodulation of Single channel radars signal may become complicated and falls in the region of non-linearity at a certain distance from the radar TRX.

A typical CW quadrature Doppler radar system is shown in Figure 3.6.

The output of the quadrature receiver channels is,

$$B_I(t) = V_I + \cos\left(\phi + \frac{4\pi x(t)}{\lambda}\right) \quad (3.6)$$

$$B_Q(t) = V_Q + \sin\left(\phi + \frac{4\pi x(t)}{\lambda}\right) \quad (3.7)$$



Legends:




Mixer:  Power Splitter:  Antenna:  RF Generator: 

Figure 3.6 Doppler radar vital sign measurement assembly is shown. The quadrature receiver includes RF mixer and dividers.

where V_I , V_Q are dc offset voltages, \emptyset is phase noise, λ is wavelength and $x(t)$ is chest and heart composite displacement. After performing linear demodulation, the baseband output can be approximated as,

$$B(t) \approx A_B (4\pi x(t)/\lambda + \Delta\phi(t)). \quad (3.8)$$

3.4 Linear demodulation

The linear demodulated signal is a proportional and close approximation of torso displacement (a combination of movement due to heart pumping and breathing). Linear demodulation is straight forward, and rate estimation from this method is accurate. Accurate displacement measurement is usually avoided using this method. The steps of the linear demodulation are described below-

Step 1: DC cancellation

The mean value of both I and Q signals are calculated in post-processing.

Step 2: Covariance matrix

The covariance matrix of the I and Q signals is created from the data points. The covariance matrix generalizes the notion of variance to multiple dimensions.

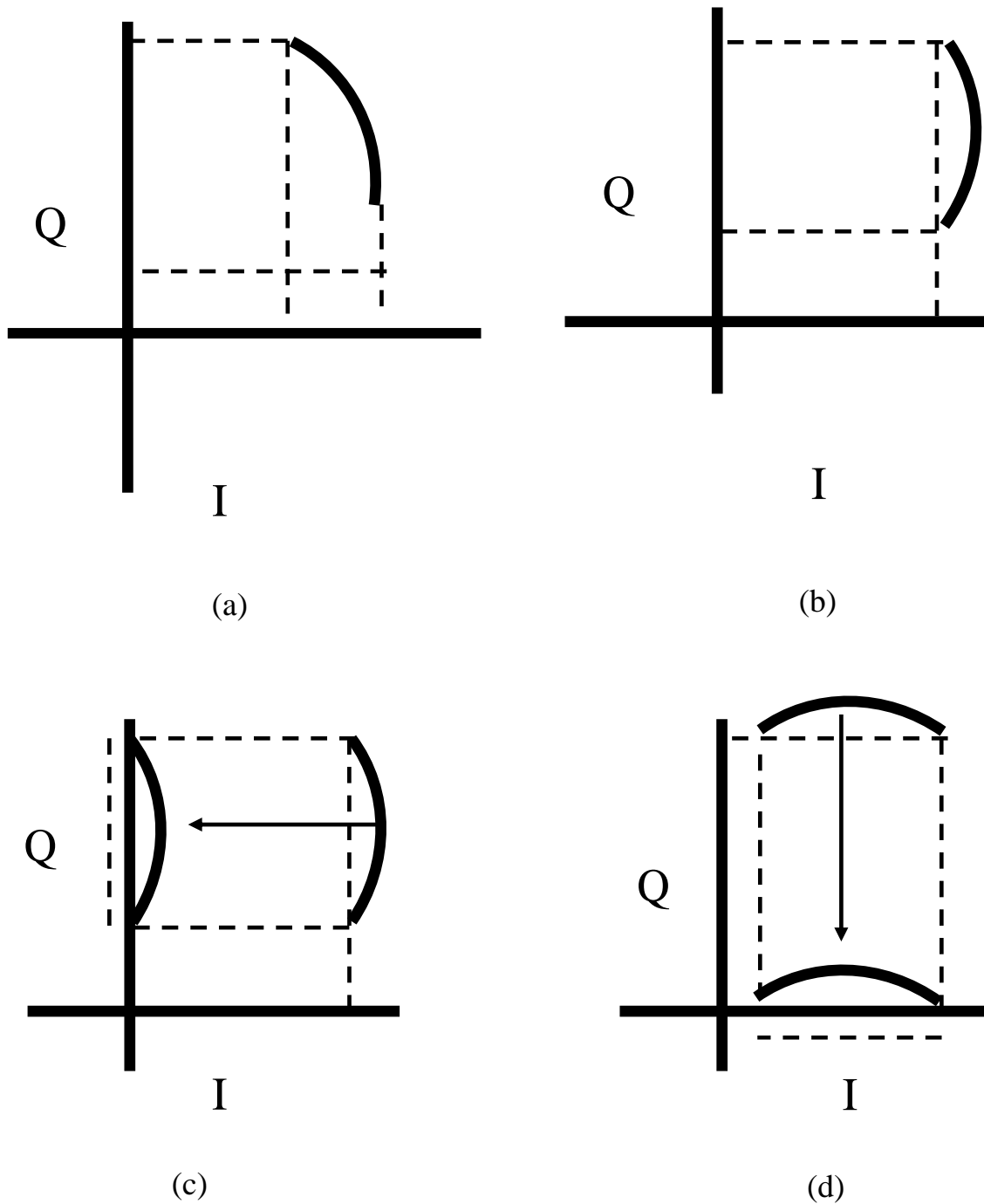


Figure 3.7 Linear demodulation, graphical illustration. a) shows arc created plotting I data vs Q data, the projections are taken on both axis, b) rotates the arc for projection on the larger side, c) shows the projection or linearization of the arc, and d) shows if the case were opposite, i.e., larger projection is on I axis.

Step 3: Eigenvectors and eigenvalues

Upon finding the covariance matrix the eigenvectors and eigenvalues are found.

Step 4: Largest variance

The Eigenvectors are multiplied with data, and the output with the largest variance is picked.

For periodic movement sensed by the radar, the demodulated baseband signals will be periodic too. However, once the demodulated signals are plotted on an IQ plane for a periodic signal, an arc will be found. The length of the arc depends on factors like wavelength. A 10 GHz radar system will create much larger arc than the signals demodulated from 2.4 GHz radar. Graphically, linear demodulation can be understood by rotating the arc of IQ data in IQ plane such that it will be in line with one of the axes resulting in maximum demodulated signal. The fundamental assumption for using linear demodulation is that the arc of IQ signals is very small such that it can be approximated with a line (hence the name linear demodulation). This supposition may not always be valid. Bigger physiological displacement or a higher RF frequency (smaller wavelength) can cause a larger arc in the IQ plane. The arc can still be approximated as a line, up to 46.8 degrees corresponding to 0.81 cm of displacement. Past that point, the linear demodulation will not give in the optimum result, and a nonlinear method must be used.

3.5 Arctangent demodulation:

The single-channel receiver Doppler radar system margins previously described can be eliminated by using a quadrature receiver system like the one shown in Figure 3.6 with both channels considered concurrently. A quadrature receiver provides two outputs that are orthogonal to each other; this ensures that when one channel is in a “null” position, the other will be in an “optimum” position [68]. Also, by combining the two channels, accurate phase demodulation can be achieved regardless of the target position or displacement amplitude. It is important to mention that the displacement amplitude is restricted to the small angle deviation condition for even the optimum case in a single channel receiver. In ideal case, the outputs of the quadrature radars are given by the following equations-

$$B_I(t) = \cos\left(\Delta\phi(t) + \frac{4\pi x(t)}{\lambda} + \theta\right) \quad (3.9)$$

$$B_Q(t) = \sin\left(\Delta\phi(t) + \frac{4\pi x(t)}{\lambda} + \theta\right) \quad (3.10)$$

As shown in (3.9) and (3.10), the I and Q outputs are the cosine and sine of a constant phase delay caused by the nominal distance to a target with a time varying phase shift that is linearly proportional to the chest displacement. By applying the arctangent operation to the I and Q output data ratio, accurate phase demodulation can always be obtained regardless of the target's position as [70],

$$\Phi(t) = \arctan\left(\frac{B_Q(t)}{B_I(t)}\right) = \arctan\left(\frac{\sin(\Delta\phi(t) + \frac{4\pi x(t)}{\lambda} + \theta)}{\cos(\Delta\phi(t) + \frac{4\pi x(t)}{\lambda} + \theta)}\right) \quad (3.11)$$

However, quadrature channel imbalance and DC-offset act as a linear transform on the I and Q components, thus modifying (3.11) to

$$\Phi(t) = \arctan\left(\frac{B_Q(t)}{B_I(t)}\right) = \arctan\left(\frac{V_Q + A_e \sin(\Delta\phi(t) + \frac{4\pi x(t)}{\lambda} + \theta + \phi_e)}{V_I + \cos(\Delta\phi(t) + \frac{4\pi x(t)}{\lambda} + \theta)}\right) \quad (3.12)$$

Where V_I and V_Q refer to the DC offsets of each channel, and A_e and ϕ_e are the amplitude error and phase error, respectively. Impact and correction of these errors will be discussed later in this chapter. The dc offset issue is more complex, however, since the total DC signal contains DC information required for accurate demodulation. The sources of the DC offset in Doppler radar system are shown as below Figure 3.8; DC information associated with the target's position is also part of each baseband signal.

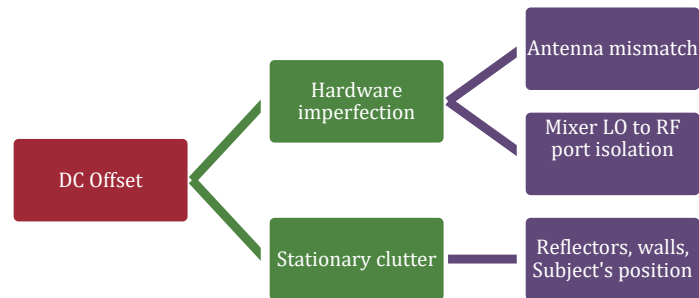


Figure 3.8 Sources of the DC offset in Doppler radar system.

The magnitude of this DC level is reliant on the target's position, such that the DC level is higher for target positions closer to the “null” case [70]. As a result, before arctangent

demodulation is performed, the DC information must be extracted from the total DC output and preserved.

3.6 Channel imbalance correction

Amplitude and phase imbalance problems in quadrature radio transceivers are obvious due to hardware imperfections [71]. The consequences of I/Q mismatch in a quadrature microwave Doppler radar have been previously documented [72]. An efficient and accurate data-based quadrature imbalance correction method that does not involve any hardware medications has been reported in [73]. A mechanical target is utilized that provides a sufficient arc length to perform the best-fit ellipse method for calibration. The imbalance coefficients determined from the best-fit ellipse method are used to carry out GS correction [74].

$$I = B_I + A_I \cos\left(\frac{4\pi x(t)}{\lambda} + \phi_I\right) \quad (3.13)$$

$$Q = B_Q + A_Q \sin\left(\frac{4\pi x(t)}{\lambda} + \phi_Q\right) \quad (3.14)$$

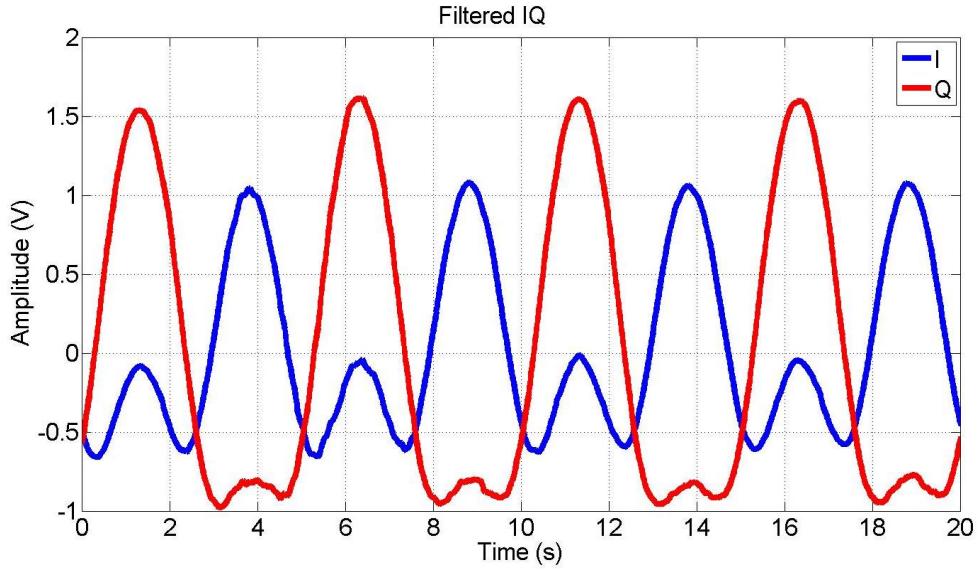
The DC offsets are represented by B_I and B_Q . The displacement of the target is $x(t)$. The signal amplitude factors for the two channels are A_I and A_Q . In ideal case, these should be equal. However, the amplitude imbalance is present because of hardware imperfection and is given by $A_e = (A_I/A_Q)$. Similarly, the phase imbalance is denoted by, $\phi_e = (\phi_I - \phi_Q)$. Now the following algebraic equation can be found after combining equation x and equation y.

$$\left(\frac{Q}{A_Q} - \frac{B_Q}{A_Q}\right)^2 + \left(\frac{I}{A_I} - \frac{B_I}{A_I}\right)^2 - 2\left(\frac{Q}{A_Q} - \frac{B_Q}{A_Q}\right)\left(\frac{I}{A_I} - \frac{B_I}{A_I}\right)\sin(\phi_e) - \cos^2(\phi_e) = 0 \quad (3.15)$$

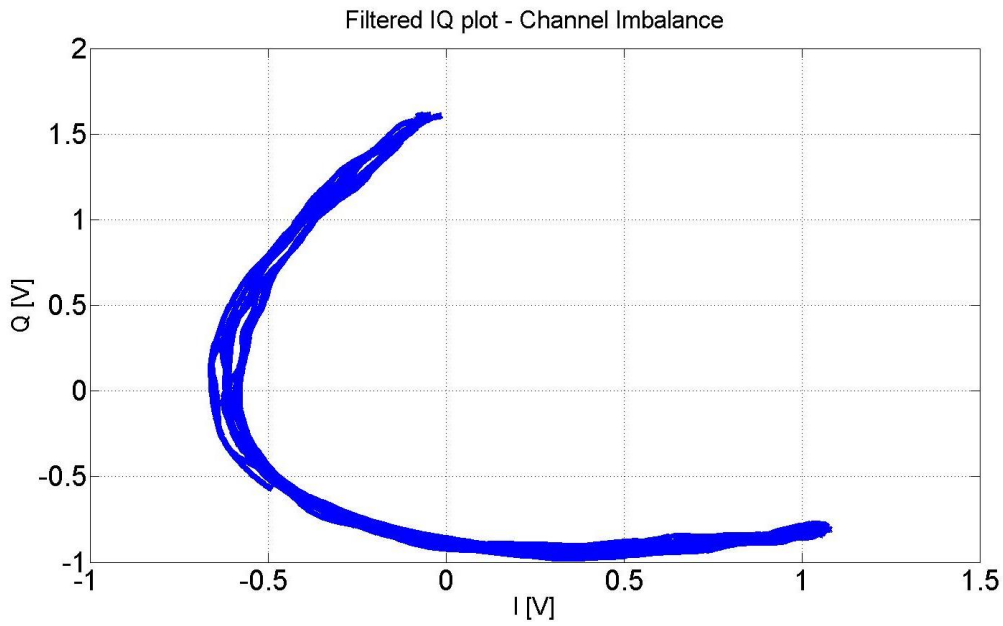
Now, this equation can be expanded, and coefficients of interested can be found by comparing and the general ellipse equation as follows [74].

$$I^2 + A * Q^2 + B * IQ + C * I + D * Q + E = 0. \quad (3.16)$$

$$A_e = \sqrt{\frac{1}{A}} \quad (3.17)$$



(a)



(b)

Figure 3.9 A reflector was moved in periodic sinusoidal motion in front of a quadrature radar, with the balanced channel the IQ plot would have been an arc of a circle. a) shows time series of I and Q channel, displacement is more than a quarter circle in IQ plane, b) IQ plot to show channel imbalance, it is evident from the elliptic shape.

$$\phi_e = \sin^{-1} \left(\frac{B}{2\sqrt{A}} \right) \quad (3.18)$$

$$A * Q_N^2 + B * I_N Q_N + C * I_N + D * Q_N + E = -I_N^2 \quad (3.19)$$

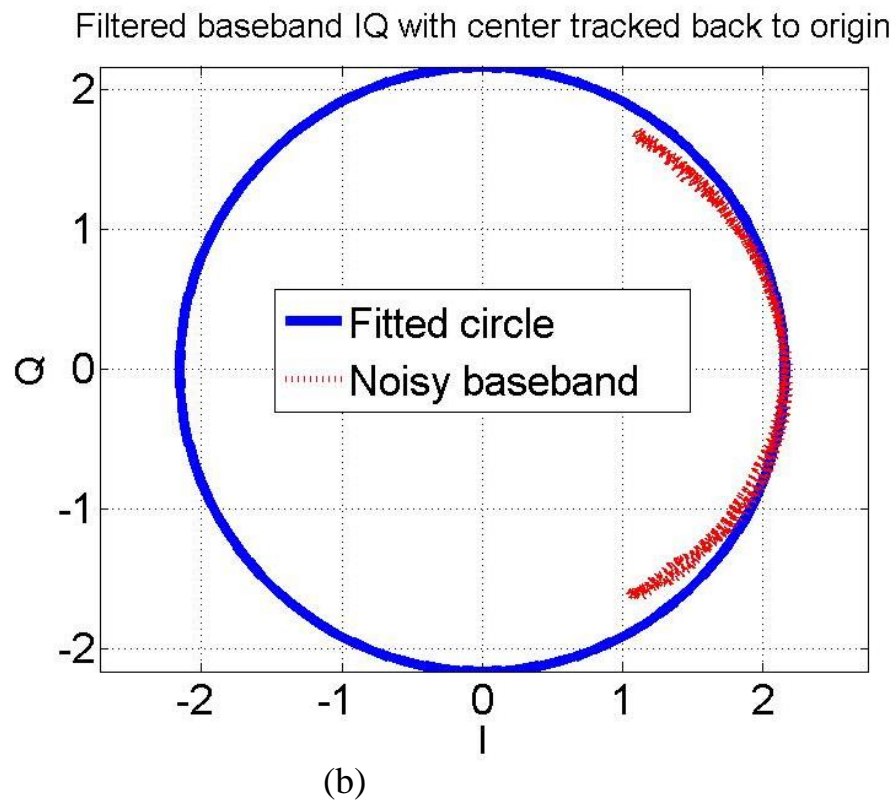
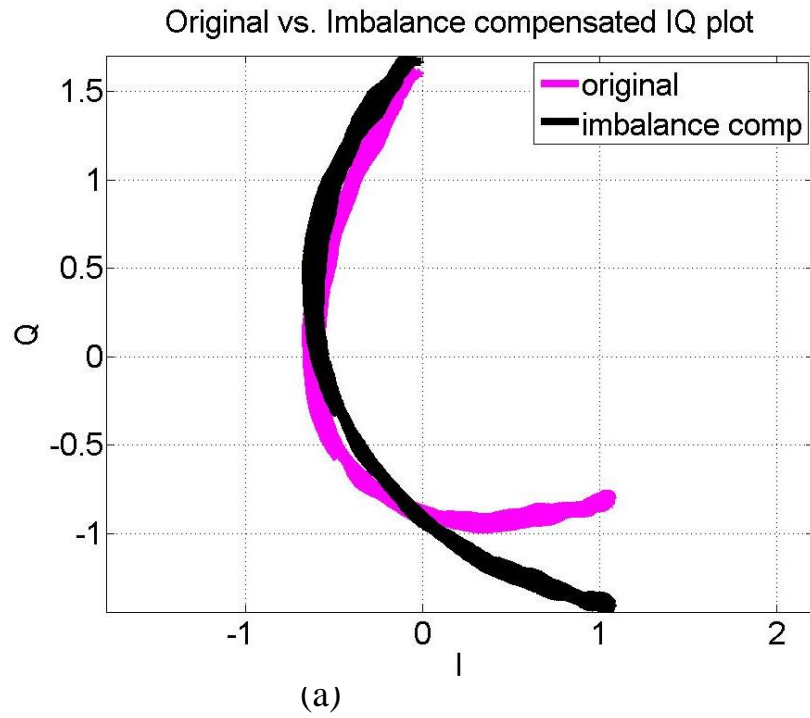


Figure 3.10 a) shows imbalance correction using the method described in this section (ellipse fit), and b) shows circle fitting using GS method.

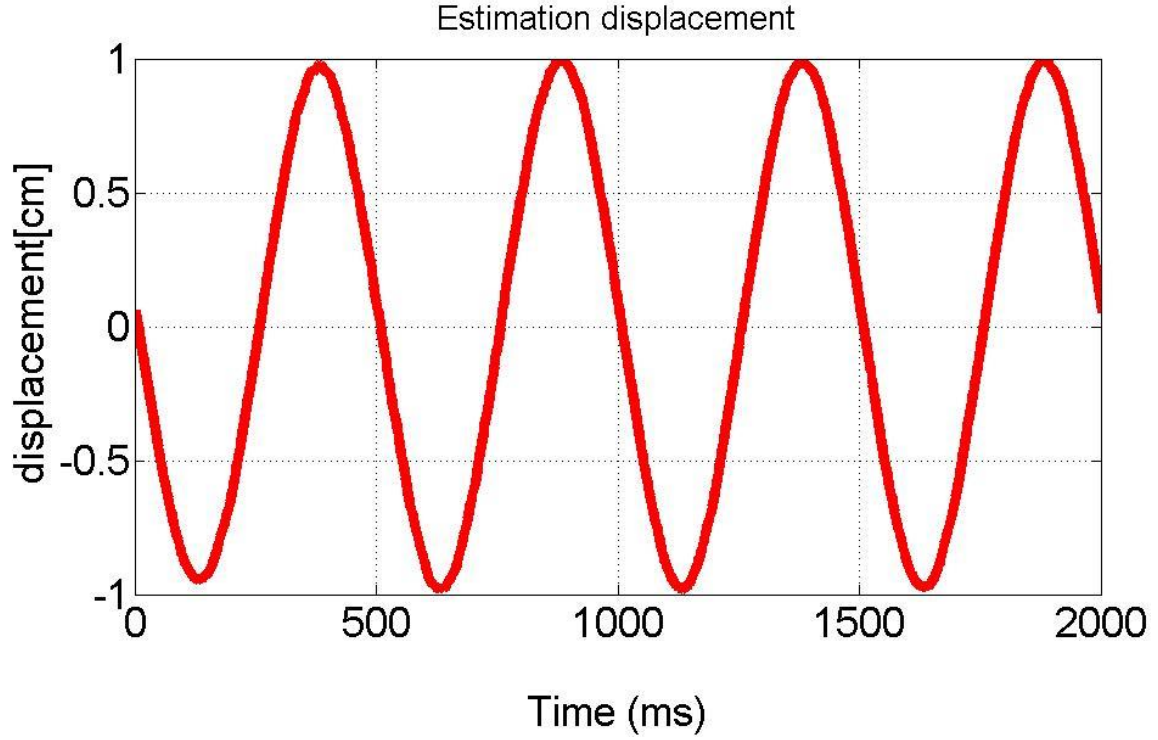


Figure 3.11 Demodulated output after imbalance correction, which resembles the sinusoidal movement.

The coefficient matrix of such linear system is given by,

$$M = \begin{bmatrix} Q_1^2 & \cdots & I_1 Q_1 & I_1 & \cdots & Q_1 & 1 \\ \vdots & \ddots & \vdots & \vdots & \ddots & \vdots & \vdots \\ Q_N^2 & \cdots & I_N Q_N & I_N & \cdots & \cdots & 1 \end{bmatrix} \quad (3.20)$$

$$b = \begin{bmatrix} -I_1^2 \\ \vdots \\ -I_N^2 \end{bmatrix} \quad (3.21)$$

The solution of such system is given by, $(M^T M)^{-1} M^T b$. After estimating the coefficients, the imbalance factors can be found. The popular Graham-Smith method can be then applied to correct the imbalance factor. The arc transcribed in the I-Q plane is a function of the transmitted frequency and displacement of the target. Figure 3.10 shows the imbalance correction results. Using the imbalance parameters ϕ_e and A_e in Equation (3.12) the phase angle and displacement relation can be obtained. Figure 3.11 shows recovered displacement.

$$\Phi(t) = \frac{4\pi x(t)}{\lambda} \quad (3.22)$$

CHAPTER 4. RADAR SIGNAL CLASSIFICATION

In the last decade, new front-end architectures, baseband signal processing methods, and system-level integration technologies have been proposed by many researchers in biomedical radar to improve detection accuracy and robustness. The advantages of non-contact detection have drawn interest for various applications, such as energy management in smart homes, baby monitoring, cardiopulmonary activity assessment, and tumor tracking. Advances in biomedical radar technology have also opened the door to many indoor activity monitoring applications, only limited by the imagination [14] [35] [34]. Beyond the measurement of heart and respiratory rate, this technology enables us to measure the effective radar cross section (ERCS) yielding information about body orientation, torso displacement, and physical characteristics of human subjects [47]. Sleep is widely understood to play a key part in physical and mental health. The quality and quantity of sleep that an individual experience can have a substantial impact on learning and memory, metabolism and weight, safety, mood, cardiovascular health, disease and immune system function [75]. Research indicates that in America alone 40 million people suffer from insomnia and chronic sleep disorders. Doppler radar technology shows a promising non-invasive way of monitoring sleep behavior with automated pattern recognition [76] [41]. This technology can potentially provide a huge cut in the cost of sleep studies. In addition to recognition, artificial neural network based automatic classifiers will be very useful in the diagnosis of diseases and physiological conditions. Radar technology may also provide a non-contact, low cost, fast, unique identification solution without the privacy concerns associated with camera-based

monitoring systems [4]. Doppler radar offers a convenient method for monitoring activity of animals as well as the recognition of various behavioral events. Using multi-radar systems provides the ability to classify motion such as walking, running, or fidgeting, which is important in animal activity monitoring of energetic cost [59]. It's a demographic fact that elderly population (older than 60 years) has been gradually increasing worldwide. This change calls for greater attention to cost-effective healthcare worldwide. Since falling represents a major risk for older adults who live independently, innovative techniques are required for long-term monitoring of human subjects [61].

4.1 Future of RF activity classification

We are at the beginning of an era in networking that has the potential to define a new phase of human existence. This era will be demarcated by the digitization and connection of everything and everyone with the goal of automating much of life, successfully creating time, by exploiting the efficiency of all we do.

The future is emerging towards a reality of big data. The new Envision is everything will be sensed, and data will be turned into knowledge [77]. Computing technology, software and an immense amount of sensing capabilities will augment human intelligence and the ability to perform more efficiently and achieve more than people could only imagine in the past. Big enterprises have already started implementing some of these concepts.

Samsung Electronics broadcasted Samsung Smart Home, a service enabling Smart TVs, home appliances, and smartphones to be linked and managed through a single integrated platform [78]. Samsung claimed Smart Home's unique functionality enables users to control and manage their home devices through a sole application. The application connects personal and consumers to connect with their devices from anywhere, anytime, device control, home view, and smart customer service [78].

This example shows that we are moving towards an internet of things (IOT) and big data. Cameras are good for a security application, unique identification, however, sometimes they are overkill depending on the application, if we only care about the information, high-resolution data might be redundant and will just add up to cost for storing or transporting. Radars can well replace some of the applications of the camera. Some features of the wearables can also be replaced by radar sensing, providing the benefits of non-invasive sensing.

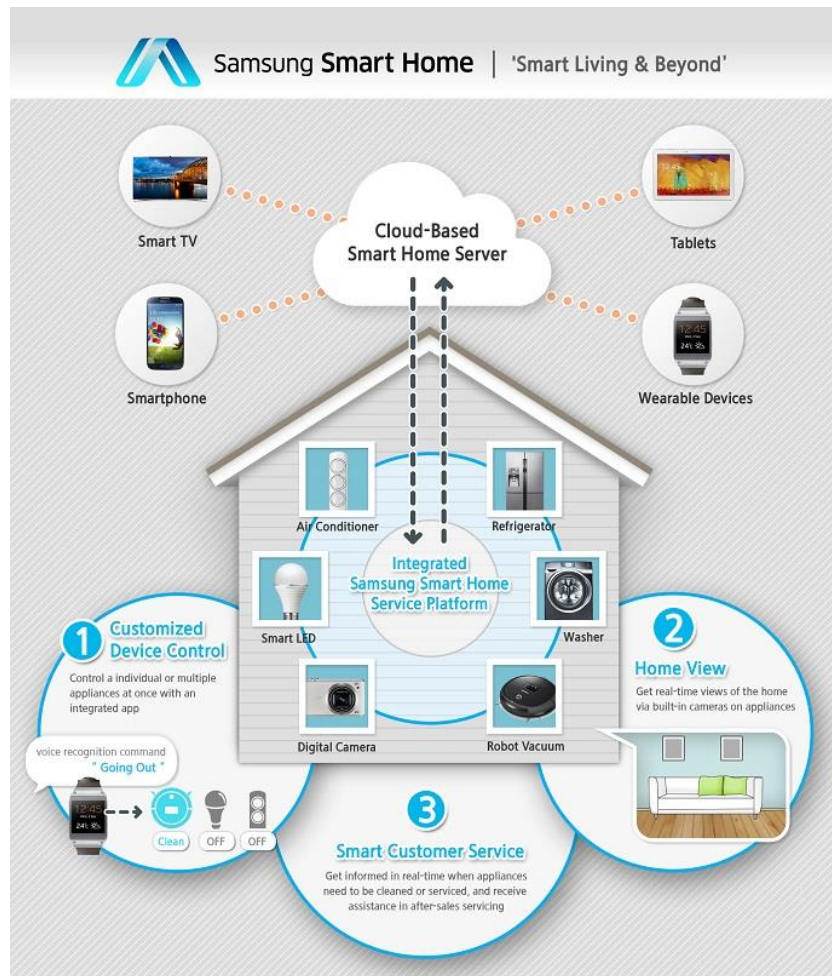


Figure 4.1 Samsung's smart home service architecture [78].

It follows that we can envision a future where RF based sensing will play a big role in indoor activity monitoring, sharing information with cloud servers. As big data technology is emerging, more and more sensing data will be sent to the cloud servers, and intelligent decisions will be made. Figure 4.2 shows some of the possible applications which have already been through several phases of research. A centralized service platform will collect useful data and communicate with cloud server for decision making.

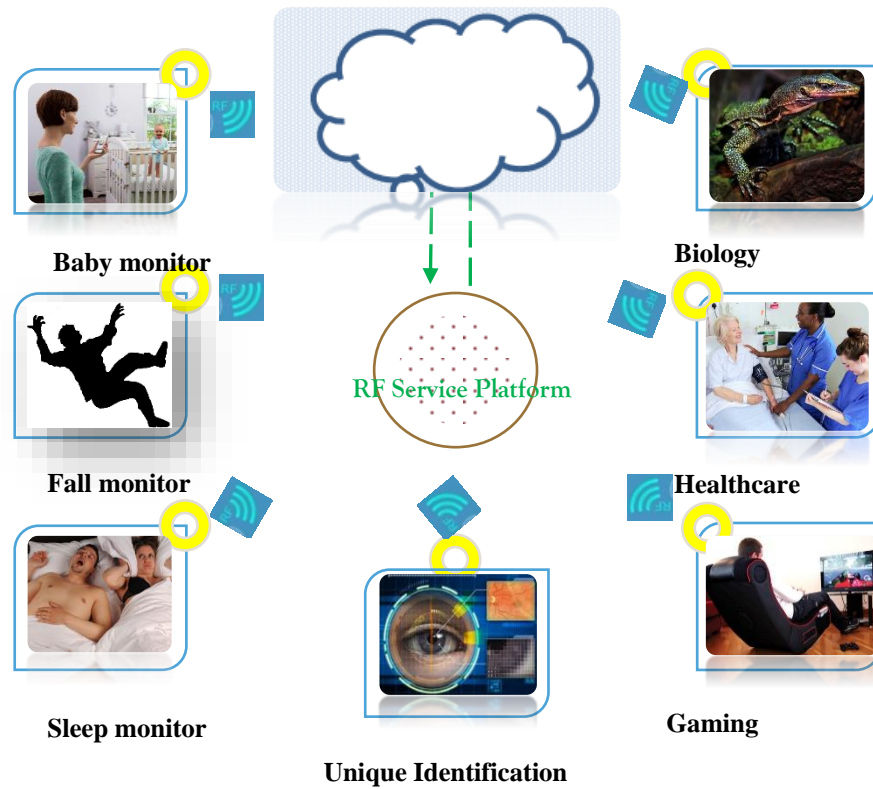


Figure 4.2 The author's vision for indoor RF activity sensing and classification [79]

4.2 Theory of RF activity classification

Using wireless technology in indoor environments for activity classification will require a comprehensive integration of multiple techniques, including RF sensing, signal processing, and artificial intelligence.

4.2.1 Sensing techniques

Researchers have reported different types of short distance radar for different applications [79] [80]. Ultra-wide band (UWB) radar, continuous wave (CW), frequency modulated continuous wave radar (FMCW), pulsed-radar to cite a few [81] [82] [46] [83]. Radars also vary based on the operating frequency (X band, K band, etc.) [82]. The directivity of sensing is also a diversity; this diversity is mainly introduced by antenna design [84] [36]. However, the sensing principle is unique regardless the type of each radar. They all

sense the backscattered signal reflected from the target. The single channel radars are limited by the inability to produce displacement sensing in all positions. However, this limitation is overcome using quadrature radar system, which in principle provides a stereo vision. The outputs of the quadrature radars are called in-phase (I) and quadrature phase (Q).

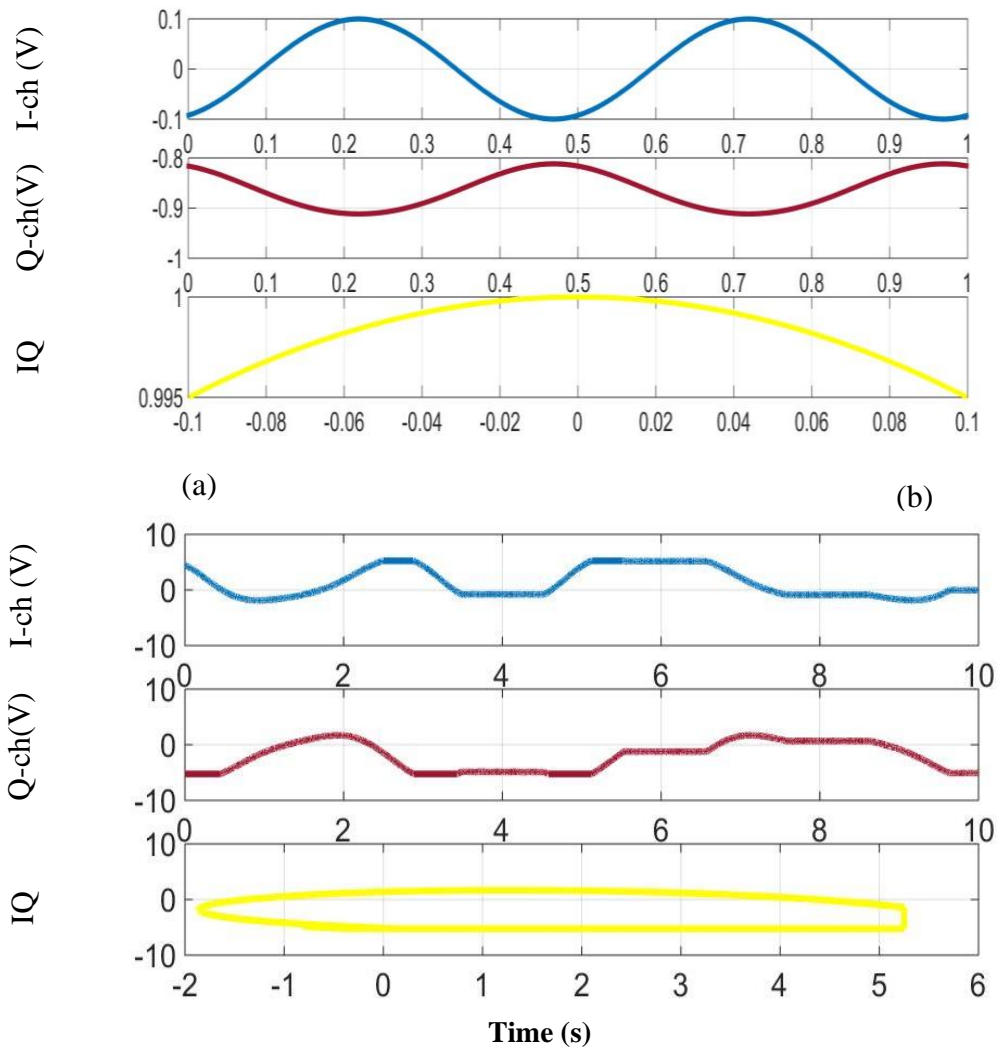


Figure 4.3 Time domain data and corresponding IQ plot, for Doppler radar measurement of sinusoidal motion in (a), and (b) shows the same for a series random linear movement [79].

The combination of I and Q can provide useful insight in characterizing targets motion. Figure 4.3 shows the experiment results of two different kinds of motion patterns of a linear moving platform. It is evident from the plots that distinguishing patterns of I and Q waves holds the information regarding the motion pattern. Additionally, IQ plots are apparently different, indicating that these could be useful parameters in RF activity classification.

4.2.2 Useful information extraction

Sensing enables us to record data; this data contains useful information about target's motion, position, or some other characteristics. However, firstly, collected data needs to be demodulated with a proper software algorithm. Upon demodulation of data summary information needs to be extracted from data and store those features in vectors or matrices. For instance, for a long time series of the sinusoidal wave we may only be interested in frequency, amplitude and phase information of the signal rather than each data points of the time series. The useful features can be statistical or multi-domain. Some of the well-known statistical features are mean, and variances. Some other common techniques applied in signal processing are listed in subsequent paragraphs.

4.2.2.1 Mean and variance

The mean is a measure of the central tendency of a given set of numbers. There are many different central tendencies including but not limited to: mean, median, mode, and range. An average or arithmetic mean is the sum of a list of numbers divided by the number of numbers in the list. Variance is the expectation of the squared deviation of a random variable from its mean. Statistical tools sometimes provide a good understanding of the data.

4.2.2.2 Frequency domain analysis

A frequency domain analysis determines the existences or extent of each given frequency band over a range of frequencies. Fourier analysis and Fourier transforms are the most common techniques of frequency domain analysis. There are many established algorithms for Fourier transforms; each one is strong in its own set of applications.

4.2.2.3 Fixed and adaptive filters

There are many different bases of categorizing filters, and they may overlap. Some notable classifications are linear and non-linear; time-invariant and time-variant; causal and non-causal. Also, filters could be classified as analog or digital, discrete-time (sampled) or continuous-time, passive or active class of continuous-time filter, infinite impulse response (IIR) or finite impulse response (FIR) type digital filter. Some filters are inherently good for removing noise, for example, Wiener filter, Kalman filter, Savitzky–Golay smoothing filter. On the other hand, adaptive filters dynamically change its coefficients over time, therefore, dynamically changes its frequency suppression properties.

4.2.2.4 Wavelet transformation

Unlike Fourier transforms wavelet transform methods provides temporal resolution, i.e., it captures both frequency and location information. The location refers to time. A discrete wavelet transforms (DWT) is any wavelet transform for which the wavelets are discretely sampled.

4.2.2.5 Spectral energy

The distribution of signal energy for each frequency can be mathematically described. Also, it can be measured for a given signal. Spectral energy distribution can provide vital information of a signal, in classification and characterization of the signal itself or the device that delivered the output.

4.2.2.6 Spectral entropy

Spectral entropy is a derived parameter. The results of Fourier transform is usually used to measure this parameter. The spectral distribution of entropy may be a good feature in classifying signals. Also, time-frequency analysis can be useful for pattern extraction [85].

4.2.2.7 Fractal Analysis

Fractal analysis is a modern method of applying non-traditional mathematics to patterns. It measures complexity using the fractal dimension. There are many versions of fractal analysis, and each has its strength and weakness. The fractal analysis assumes beforehand that a signal is fractal in nature. Algorithms for fractal dimension calculations are applied to the signal. The fractal analysis evaluates a form of the signal's complexity. Researchers have reported fractal dimension analysis can predict some patterns in sleep EEG signals [86]. Pathological insight can be found from this analysis [87] which leads the way of using radar-based vital sign data as well.

4.2.2.8 Empirical mode decomposition

The Hilbert–Huang transform (HHT) is a way to decompose a signal into intrinsic mode functions (IMF). A trend is also observed. Instantaneous frequency data is obtained alongside. This method works well with nonstationary and nonlinear data. Unlike Fourier transform, the HHT is considered as an empirical method. Empirical mode decomposition can be applied to a data set, which is little different than just a theoretical tool.

4.2.3 Turning data into knowledge

This chapter, so far, discussed the non-invasive sensing techniques and touched on some useful analytical tools that can extract useful parameters from raw data. However, this extracted knowledge can only be put to use once we know how those relate to some physical phenomenon that we care about, and it requires extensive data mining [88]. Often time these parameters change over time, we also want to relate these dynamic behaviors to the behavior of certain things. While we care about instantaneous output sometimes, some other behaviors need to be observed over a long time. For instance, we may be interested in knowing someone's heart rate at this moment, which can be measured using the current RF sensing technology. However, if we are interested in how someone's long time behavior of heart rate that relates to a certain disease, we need to have more knowledge. Acquiring more knowledge will call for long-term data collection and understanding of the disease. Artificial intelligence may help us make an intelligent decision. Systems can be trained using features extracted from raw data over a long term. Then these trained systems can be used to guide us, warn us with a collective knowledge and classifying various phenomena. Essentially, data needs to be turned into knowledge. The subsequent paragraphs mention some of the artificial intelligence techniques out of many. These techniques can be used to train and classify data.

4.2.3.1 Neural network

Artificial neural networks (ANNs) are a very common family of models in machine learning and cognitive science. ANNs are enthused by biological neural networks (the central nervous systems of animals, in the brain) which are used to estimate or approximate functions that can depend on many inputs and are unknown [89].

4.2.3.2 Probabilistic Neural Network

A probabilistic neural network (PNN) is a derived algorithm from the Bayesian network. This network is a class of feedforward neural network. D.F. Specht introduced it in the early 1990s. In a PNN, the processes are organized into a multi-layered feedforward network with four layers. These layers are input layer, hidden layer, summation layer, and the output layer [90] [89].

4.2.3.3 Support Vector Machine

Support vector machines (SVMs) are a kind of supervised learning models. Each SVM has its learning algorithms for analyzing data. SVMs are used for classification and regression analysis. Assumed a set of training instances, each is assigned to one of the two

categories, an SVM training algorithm constructs a model that assigns new examples into one category or the other. SVMs essentially follows a non-probabilistic binary linear classifier algorithm [91].

4.2.3.4 k-Nearest Neighbor

The k-Nearest Neighbors algorithm (or k-NN for short) is a non-parametric method which is one of the most common algorithms used for classification and regression. An object is classified by a popular vote of its neighbors, with the object being allocated to the class most common among its k nearest neighbors. Usually, k is a small positive integer.

4.2.3.5 Bayesian classifier

In machine learning, naive Bayes classifiers are a family of simple probabilistic classifiers based on applying Bayes' theorem. The classifier tend to have strong (naive) independence assumptions between the features. Some of the concepts of naïve Bayes classifier are explained in [92].

4.3 Doppler radar-based unique identification system

A continuous-wave (CW) Doppler radar-based unique identification system has been studied. Experiments have been performed using a neural network based classifier to uniquely identify individuals based on the variation in their breathing energy, frequency, and patterns captured by the radar [93]. Adult human breathing patterns at rest are different not only regarding tidal volume, inspiratory and expiratory duration but also in the airflow profile. Besides this diversity, in every recording of ventilation at rest in a steady-state condition, breath to breath fluctuations are observed in ventilatory variables [3]. This variability is non-random and may be explained either by a central neural mechanism or by instability in the chemical feedback loops. Beyond this variability, everyone appears to select one pattern among the infinite number of possible combination of ventilatory variables and airflow profile [3]. Inspired by some prior works [94] [94] [95] on pattern recognition in EEG signals various approach were taken at the bringing to understand the possibility and requirement. Any collection of information generated by that person's health may uniquely identify a person or a group of people which is crucial in the unique identification or creating a unique medical identity of people. Unique-identification based on the vital sign may add another dimension to the traditional fingerprint systems. Camera based unique identification can be inappropriate due to privacy concern. We propose a Doppler radar based non-contact

unique identification method which is capable of classifying people based on their vital sign parameters.

Abnormal breathings have some distinctive patterns which are indicative of specific health disorder. Breathing could be normal, Cheyene-stokes, central neurigenci-hyperventilation, ataxic-breathing, and cluster-breathing to cite some examples. Simple inspection of the respiratory cycle, rate, rhythm, inspiratory volume, and effort of breathing, are useful parameters in finding any abnormality.

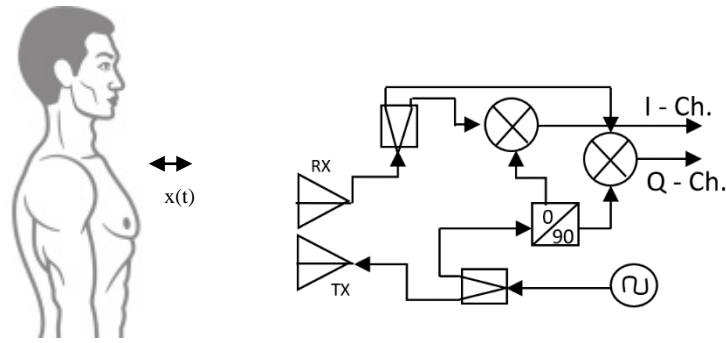


Figure 4.4 Doppler radar vital sign measurement assembly is shown. The quadrature receiver includes RF mixer and dividers.

Finding differences in normal breathing from person to person needs further careful analysis and observation which is the prime motivation of our work. However, these abnormalities are relatively easier to detect since each one shows a definitive pattern.

Useful features can be extracted, and a neural network can be trained for classifying the signals. This classification can represent a unique identification of the person or a group of persons. Recall a typical CW quadrature Doppler radar system is shown in Figure. 4.4 The output of the quadrature receiver channels is,

$$B_I(t) = V_I + \cos\left(\phi + \frac{4\pi x(t)}{\lambda}\right) \quad (4.1)$$

$$B_Q(t) = V_Q + \cos(\phi + (4\pi x(t))/\lambda) \quad (4.2)$$

where V_I , V_Q are dc offset voltages, ϕ is phase noise, λ is wavelength and $x(t)$ is chest displacement. After performing linear demodulation, the baseband output can be approximated as,

$$B(t) \approx A_B (4\pi x(t)/\lambda + \Delta\phi(t)). \quad (4.3)$$

A_B , $\Delta\phi(t)$ are baseband signal amplitude, and phase noise respectively. For each person $x(t)$ varies from person to person. For n persons in an experiment will have displacement as $x_1(t), x_2(t), x_3(t), \dots, x_n(t)$.

Artificial neural networks are usually presented as systems of interconnected units called perceptron which launch messages to each other. The connections have numeric weights that can be adjusted based on experience, making neural nets adaptive to inputs and skilled of learning. While neural networks are a system of many neurons, a single neuron's input and output can be modeled as in equation 4.4 and 4.5.

$$u_k = \sum_{j=1}^m w_{kj} z_j \quad (4.4)$$

$$y_k = \varphi(u_k + b_k) \quad (4.5)$$

where $z_1, z_2, z_3, \dots, z_m$ are the input signals or features, and $w_{k1}, w_{k2}, w_{k3}, \dots, w_{km}$ are the synaptic weights of neuron k . The variable u_k is the output generated by the linear combiner, b_k is bias vector, and y_k is the output of the neuron k . This output is achieved once the function $\varphi(.)$ is operated on the input. This function is called the squashing function. Combination of such unit neurons creates a neural network that can classify or estimate a function following the principal of minimizing error between estimated outputs to expected output for a given set of input features [89].

4.3.1 System setup

A 2.4-GHz quadrature Doppler radar system was used for the experiment. The measuring system included a signal generator and the following off-the-shelf coaxial components: transmit and receive antennas (Antenna Specialist ASPPT2988), two 0° power splitters (Mini-Circuits ZFC-2-2500), one 90° power splitter (Mini-Circuits ZX10Q-2-25-S+), and two mixers (Mini-Circuits ZFM-4212). The retrieved signal from a human subject is split and fed into two mixers. The local oscillator is connected to a quadrature power divider, providing in-phase and quadrature versions of the signal, after down conversion filtering and amplification. Finally, the data is recorded by data acquisition device for further signal

processing with MATLAB. The two channel output signals were pre-conditioned by SR560 low-noise amplifiers. Although a reasonably large dataset is recommended, as a proof of concept data from three individuals were collected for 15 minutes. There were no notable strong physiological differences among the subjects. Each person's collected data was segmented 45 sec epochs for feature extraction.

4.3.2 Feature extraction

For each person 19 windows, each containing 45 seconds of data were used for training the neural network. Three features were extracted from each window/epoch as described in the following text:

1) Peak power spectral density

Power spectral density (PSD) describes how the power of a signal or time series is distributed over the different frequencies.

$$S_x(f) = \lim_{T \rightarrow \infty} E \left\{ \frac{1}{2T} \left| \int_{-T}^T x(t) e^{-j2\pi ft} dt \right|^2 \right\} \quad (4.6)$$

where t denotes time variable, E denotes the expected value, T is a time interval, f indicates frequency, and $x(t)$ is signal component whose power spectral density is to be determined. The frequency of peak was selected as one of the features.

2) Packing density

A parameter could identify the differences in inspiratory and expiratory duration from person to person called packing density. To calculate packing density first the minimum value of the signal segment was calculated. That value was added to the signal to transform the signal window as a non-zero envelope. Integration was performed to find out the area covered. The integrated value was divided by the area of the bounding box of the signal segment.

3) Linear envelope error

By observing respiration signals, we can see that respiration cycles have slightly variable peaks. These peaks might show some patterns and will vary person to person. After determining the local maximum points, a linear fit is determined. The deviation for each peak from the fit line was summed as a distinct feature of each window.

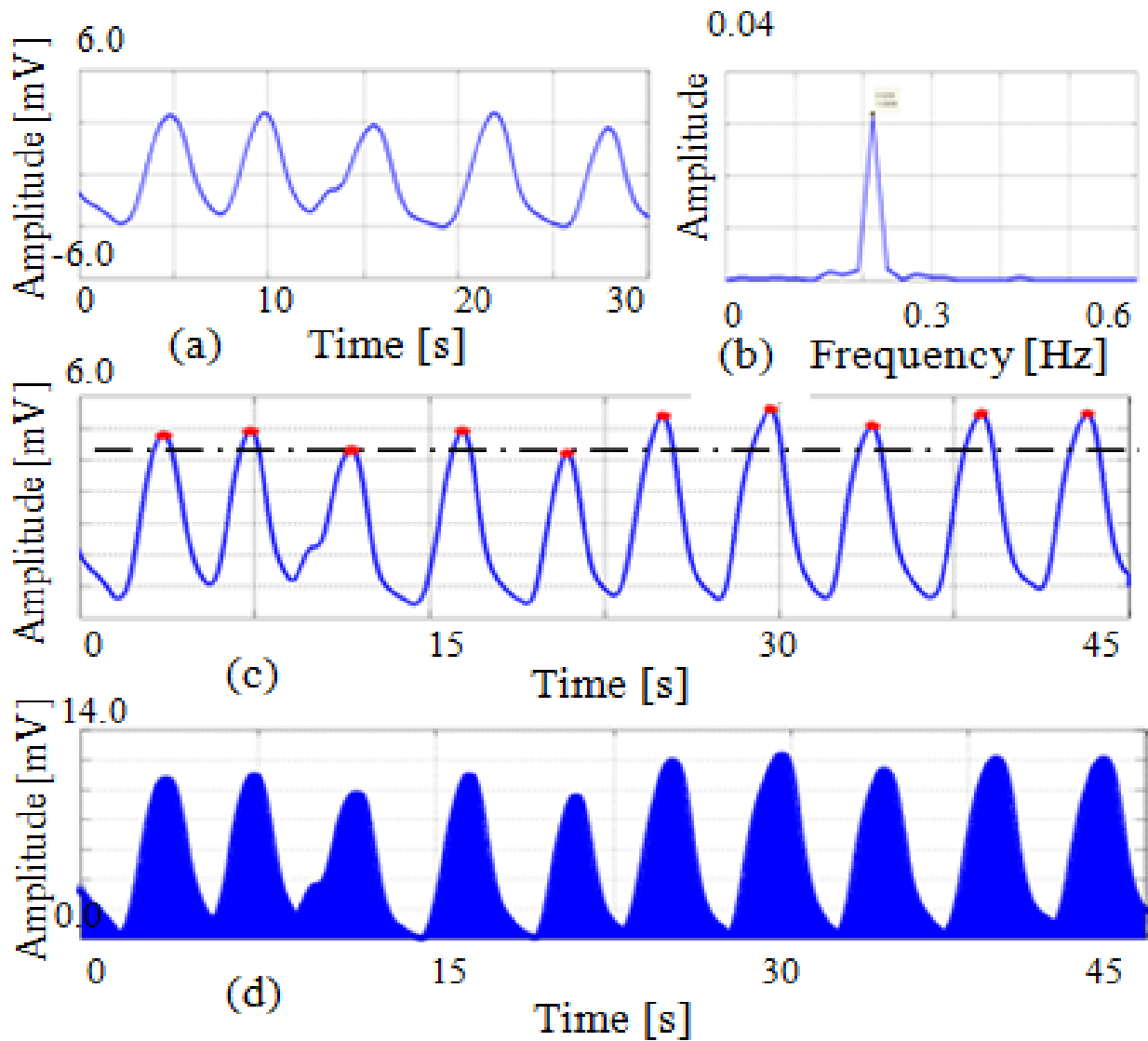


Figure 4.5 Epoch features for neural network training are illustrated. a) Time series of respiration record b) Power spectral density c) Peak line fit and error d) Packing density [4] [79].

4.3.3 Method and results

A three layer (input, output and hidden) neural network was trained using Levenberg- Marquardt back propagation algorithm in MATLAB to perform classification task. There were six neurons in the system, 3 in the input layer, 1 in output and 2 in the hidden layer. Overall regression coefficient was in neural network training was 0.954 having a potential of good classification. Training converges with six validation stops with mean squared error 0.01. For testing the performance of the trained network, a different set of data were collected at a different time. A total of 43 set of data each having 45 seconds of epoch were collected from the three persons. The saved trained network was then tested against

these new data which did not have any part in network training. A confusion matrix shows the classification performance. Person-1 and person-3 have classified accurately. However, out of 17 data from person-2, four were misclassified as person-3.

Table 4-1. Respiration segment features

Packing density	Frequency of maximum spectral power (Hz)	Linear regression error in peak fit (mV)	Person
0.521341	0.213298	0.170702	P1
0.517554	0.191968	0.038110	P1
0.406263	0.213298	0.010226	P1
.....	
0.312932	0.277287	0.019954	P2
0.369265	0.277287	0.067173	P2
0.354366	0.234627	0.090660	P2
.....	
0.499702	0.234628	0.027535	P3
0.473084	0.234628	0.019782	P3
0.4183060	0.2346208	0.0136630	P3

Table 4-2 Unique identification testing results in a confusion matrix [4]

	Person 1	Person 2	Person 3	Success
Person 1	7	0	0	100 %
Person 2	0	13	4	76.4%
Person 3	0	0	17	100%

Doppler radar is investigated as a unique human identifier with more than 90% success rate. A three-layer back propagation neural network classifier is used to identify individuals based on their breathing patterns. Peak power-spectral-density, packing density, and linear envelope-error are three parameters of the breathing used for identification purpose. In addition to recognition, artificial neural network based automatic classifiers will be very useful in the diagnosis of diseases and physiological conditions.

4.4 Conclusion

Radar technology can provide non-contact, low cost, fast, unique identification solution with no privacy violation as is in camera-based systems.

CHAPTER 5. MOBILE PLATFORM RADAR

This Chapter presents an investigation of mobile non-contact vital sign monitoring device for short range application. The radar module is mounted on a programmable linear stage, and an optical tracking system monitors precise stage movements. The motion artifacts due to radar system's mobility are removed using IIR filter and adaptive noise cancellation techniques. The system is capable of extracting respiration rate even in the presence of radar module motion. In many applications, vital sign measurement from a mobile platform will be very useful, i.e., using the unmanned vehicle as a first responder in battlefield including other military and medical applications. The experiments and theoretical techniques provide a baseline that can be potentially used to measure vital signs from any arbitrarily moving radar system.

As mentioned in earlier chapters, vital sign detection from mobile radar system is challenging due to possible aliasing, phase distortion, and occurrence of a null point [97]. These problems occur due to variable traveling distance from radar antennas and target. If tracked radar motion is simple and precisely detected, IIR filtering techniques could remove the motion artifact. However, in cases of extreme aliasing advanced noise cancellation techniques are required. Some works have been published addressing motion artifact due to hand shake for Doppler radar sensors. One way of tackling this problem is using a sensor node [6]. Empirical mode decomposition techniques were discussed for removing fidgeting interference in Doppler radar life signs monitoring devices [7]. This chapter presents further

analysis of the noise compensation not only for transmit antenna, but also the whole radar module for continuous motion of larger amplitude to use the system in vehicle mounted devices. Sensor node technique is not always feasible because it requires additional equipment nearby a subject. In EMD method intrinsic mode functions (IMFs) should be selected by the programmer which is not always achievable, and it is more computationally complex.

5.1 Platform motion compensation

In a mobile Doppler radar, received data has two motion signature one coming from radar itself and the other from the human respiratory effort. Experimentally the movement of the radar is determined using the optical tracker. Further advanced filtering techniques can be applied to filter the net effect of radar movement and extract heart rate in addition to respiration rate. The experimental assembly including radar system has been shown in Figure. 5.1. The local oscillator generates 2.4 GHz signal which is transmitted through the antenna, the reflected signal from the subject whose vital signal is to be measured is then mixed with local oscillator signals to generate quadrature outputs. The output signals $B_I(t)$ and $B_Q(t)$ of the radar system are given by [96],

$$B_I(t) = A_{BI} \cos(\theta + \frac{4\pi x(t)}{\lambda} + \Delta\phi(t - d(t)/c)) \quad (5.1)$$

$$B_Q(t) = A_{BQ} \sin(\theta + \frac{4\pi x(t)}{\lambda} + \Delta\phi(t - d(t)/c)) \quad (5.2)$$

$$x(t) = x_1(t) - x_2(t) \quad (5.3)$$

$$d(t) = |d_0 + x_1(t) - x_2(t)| \quad (5.4)$$

where θ , λ , and $\Delta\phi$ represent constant phase shift, wavelength and residual phase noise of the oscillator. Fixed phase shift depends on the nominal distance between the target and radar antenna. $x(t)$ is composed of two displacements, one coming from the human respiratory-effort and the other from radar's movement itself which are denoted by $x_1(t)$ and $x_2(t)$ respectively. $d(t)$ is the distance between target and radar at any given time, and d_0 denotes the nominal distance between the radar and target. After filtering, amplification, and performing linear demodulation the received baseband signal can be approximated by [96],

$$B(t) \approx A_B \left(\frac{4\pi x(t)}{\lambda} + \Delta\phi(t) \right). \quad (5.5)$$

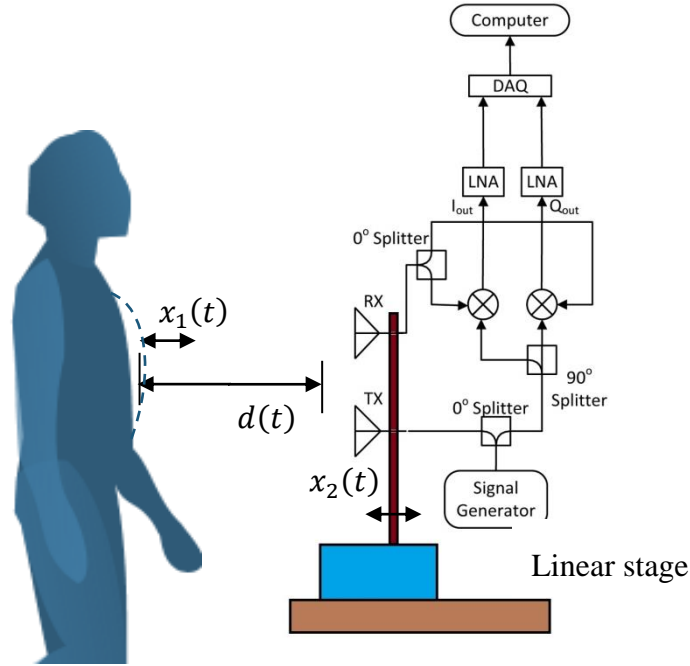


Figure 5.1 Mobile quadrature Doppler radar system. The transceiver is mounted on a linear stage which can move the radar.

5.2 Motion compensation experiment

A 2.4-GHz quadrature Doppler radar system was used for the test. The assembly included a signal generator and the following off-the-shelf coaxial components: transmit and receive antennas (Antenna Specialist ASPPT2988), two 0° power splitters (Mini-Circuits ZFC-2-2500), one 90° power splitter (Mini-Circuits ZX10Q-2-25-S+), and two mixers (Mini-Circuits ZFM-4212). The reflected back signal from a human subject is split and fed into two mixers. The local oscillator paths that are connected to mixers have 90-degree phase shift, providing in-phase and quadrature versions of the signal. Finally, the data is recorded by data acquisition device for further signal processing with MATLAB. Both DC and AC couple measurements were taken. The two channel output signals were pre-conditioned by SR560 low-noise amplifiers. Radar transceiver was mounted on a precision linear stage (Single-Axis

Series CDS-3310) from Galil that provided motion in front of the human target. The linear stage was programmed to have periodic motion with 0.2Hz, 1.2Hz and 2Hz frequencies. The amplitude of the motion was 4mm (8 mm displacement).

For capturing the motion of the radar system, an infrared camera based tracking device has been utilized. The tracking system is designed by Advanced Real-time Tracking (ART). Their images are processed to identify and calculate possible marker positions with high precision; a mean accuracy of 0.04 pixels is typical in ART tracking systems.

For testing and respiration measurement a human subject was sitting stationary in a chair and breathing normally. A conventional respiratory belt transducer (contains a piezo-electric device) is strapped around the chest to derive breathing rate. The human subject was 1 meter away from the radar transceiver reference point. The output from the Doppler radar system, optical tracking system, and respiratory belt transducer was connected to SR560 low-noise amplifier via coaxial connectors. A National Instrument data acquisition tool was used to record and synchronize data from various sensors.

While the radar was moving in 2 Hz and 1.2 Hz, IIR low pass filters showed good results in extraction of respiratory rate showing an exact match with a respiratory belt. A 4th order Butterworth filter was applied that returns the filter coefficients of low pass digital infinite impulse response (IIR) filter. The filter coefficients are generated based on the cut-off frequency approximation from the tracked motion of the radar. As shown in Figure 5.2 and Figure 5.3, the effect of the radar motion was filtered out successfully to extract respiration rate for 1.2 Hz and 2 Hz radar movements. However, with 0.2 Hz motion fixed IIR filters were not very useful due to extreme aliasing as respiration rate was roughly about the same. An adaptive noise cancellation (ANC) filter was applied to this case. Adaptive filtering results in optimal noise reduction without distorting the signals as could be the case with single-linear filtering. Least mean square algorithm is employed for ANC due to its simplicity and real-time capability with 0.008 constant step size and an order of 8. The results are shown in Figure 5.4 [5].

5.3 See-through-the-wall (STTW) life sign detection from a mobile platform

A through wall radar has many civil and military applications, for instance, in rescue missions, behind-the-wall target detection, surveillance, and reconnaissance. UWB for short-

range radar imaging has been researched for remarkably fine range resolution, high power efficiency due to low transmit duty cycle, low probability of detection, low interference to

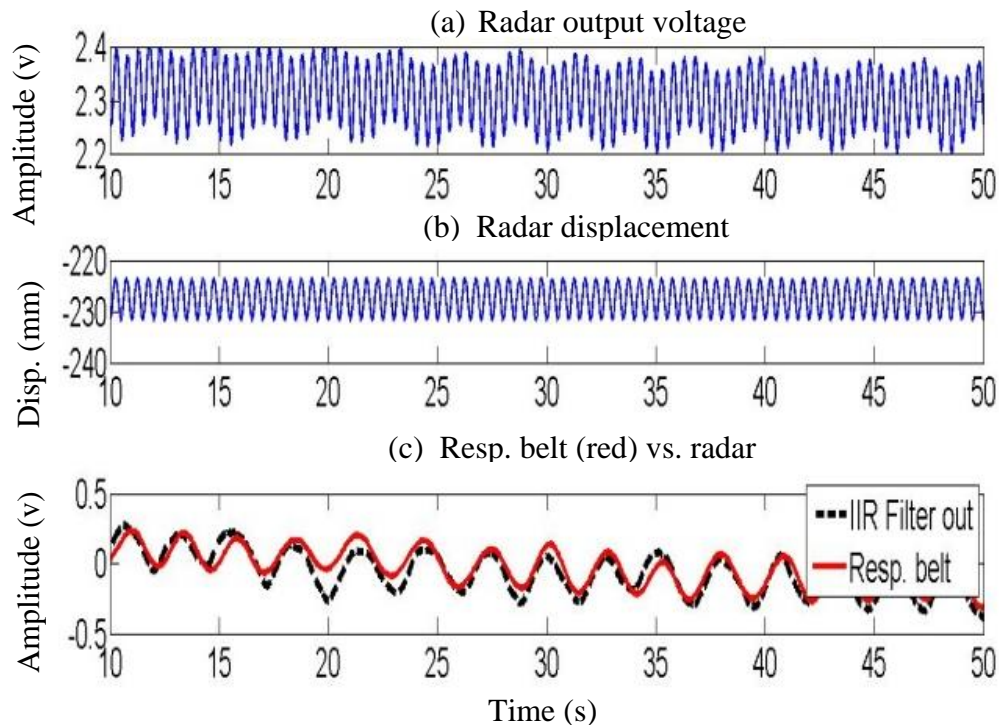


Figure 5.2 Linear stage mounted radar system moving with 2 Hz sinusoidal having 4 mm amplitude. a) Linear demodulated the signal from radar system b) radar displacement (mm) from the nominal reference position with infrared tracking system c) comparison of extracted respiration rate using IIR filter (blue) and respiratory belt transducer (red) [5].

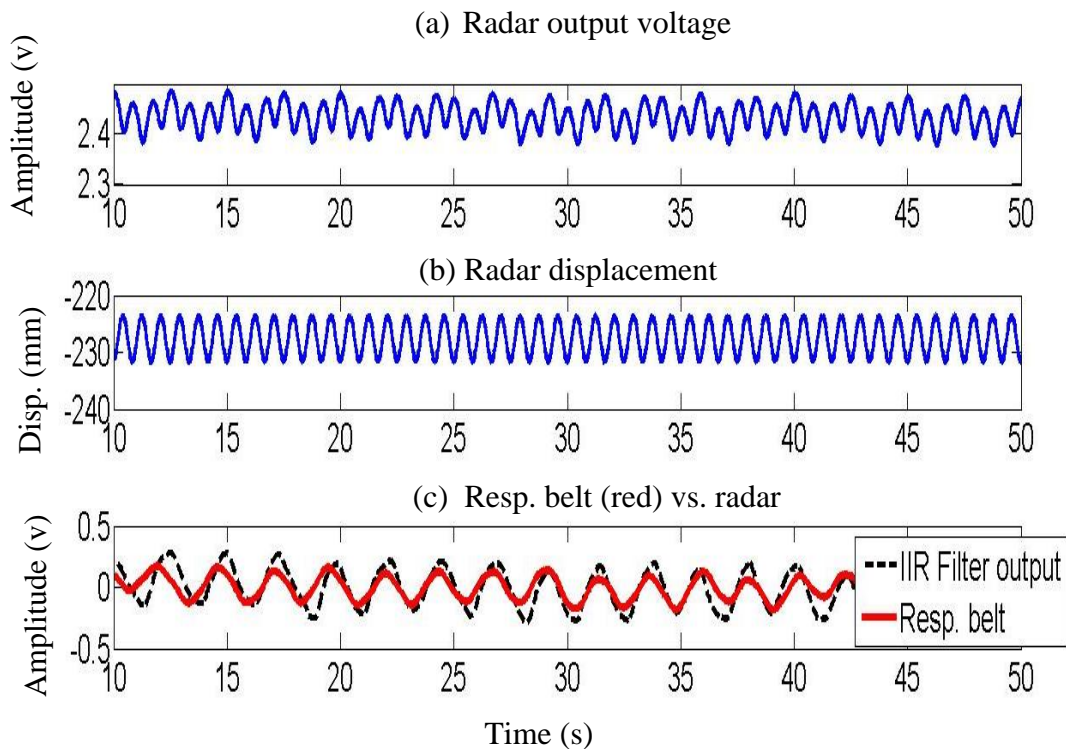


Figure 5.3 Radar system is moving with 1.2 Hz sinusoidal having 4 mm amplitude [5].

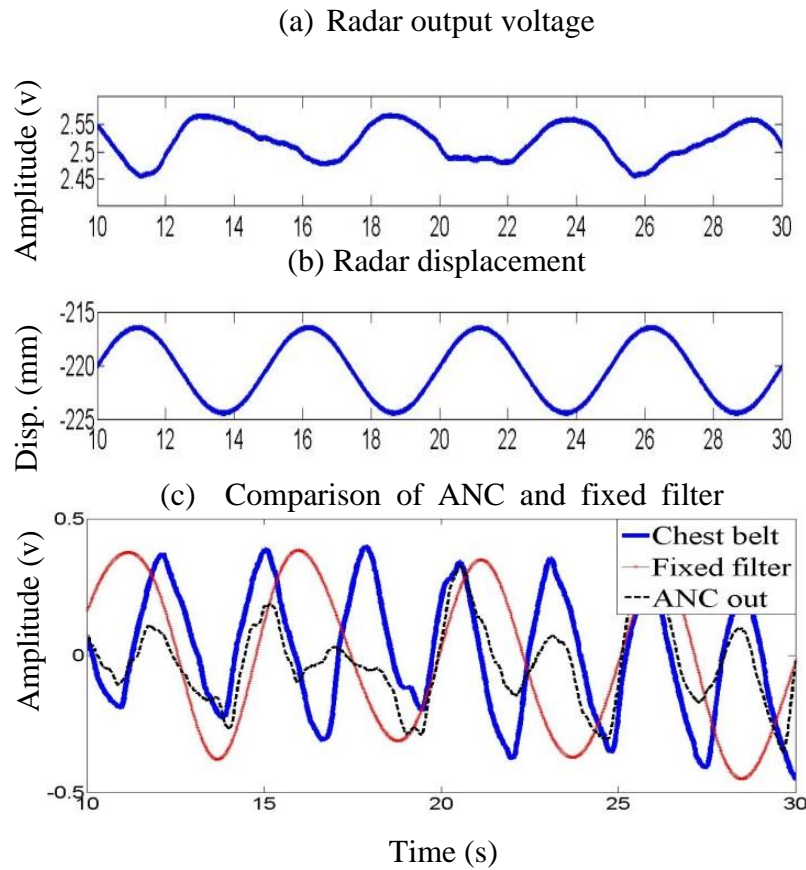


Figure 5.4 Mounted radar system running with 0.2 Hz sinusoidal having 4 mm amplitude. a) Linear demodulated the signal from radar system b) radar displacement (mm) from nominal reference position c) plot showing respiration rate from ANC (black) filter, IIR notch filter with 0.2 Hz center (red) and chest belt (blue) reference. In extreme aliasing case (0.2 Hz radar motion) ANC showed much better performance in respiration measurement [5].

legacy systems, and ability to detect moving or stationary targets [97]. Some STTW radars are reported in the literature [98]. However, none presents a mobile platform scenario.

5.3.1 Theory of mobile STTW radar

Doppler and UWB STTW radar research comprises complex propagation channel modeling based on real-world urban environment expectations and multiple wall scenarios. Advanced algorithms for real-time vital signs detection and high-resolution imaging algorithms, antenna arrays and multiple receivers for increased resolution and estimation accuracy, passive exploitation of environmental signals, and compact radio integration technologies are employed [99] [13]. Clutter and motion isolation hampers these technologies, as well as persistent wide band hardware challenges, limits the field

deployment [29] [100] [101]. Wall loss, hardware, regulations, and the probability of detection also influence the transmit power levels, frequencies, and modulation choices, ultimately limiting the effectiveness of any radar. Some other works deal with the localization problem of behind-wall stationary human that achieve human location by life-sign detection and ellipse-cross localization [97]. This part of the thesis is inspired by the fact that through wall vital sign detection may be required from a mobile platform to get a faster measurement on the go. In previous chapter vital sign detection from a mobile platform was demonstrated. High precision cameras were used to characterize platform motion, in other words, the signal components proportional to positional variation were determined. Using cameras is not a viable solution for a practical scenario. The next chapter will discuss Frequency shifting tags (low-IF tags) to extract signal components due to the unwanted motion. The tag will be placed on a side and slightly behind the human target hiding it from the field of view of target's reflection so the tag can only see platform motion. However, through wall systems cannot take advantage of tag because the tag needs to be placed physically beyond the wall. There is no optimum position where the tag only sees platform motion. The tag will be uncovered to the reflections coming through the wall from the subject [97].

Enough information about the motion artifact is required to apply adaptive filters successfully, or other motion compensating algorithms. Ultrasonic distance measurement sensors can range based on echo bounced from an obstacle. Ultrasonic sensors are inexpensive and seemingly an affordable solution to uniquely identify one-dimensional platform motion in through wall measurements from a mobile platform. The distance of wall to radar transceivers measured by these sensors provides a means to sense the positional variations of radar platform.

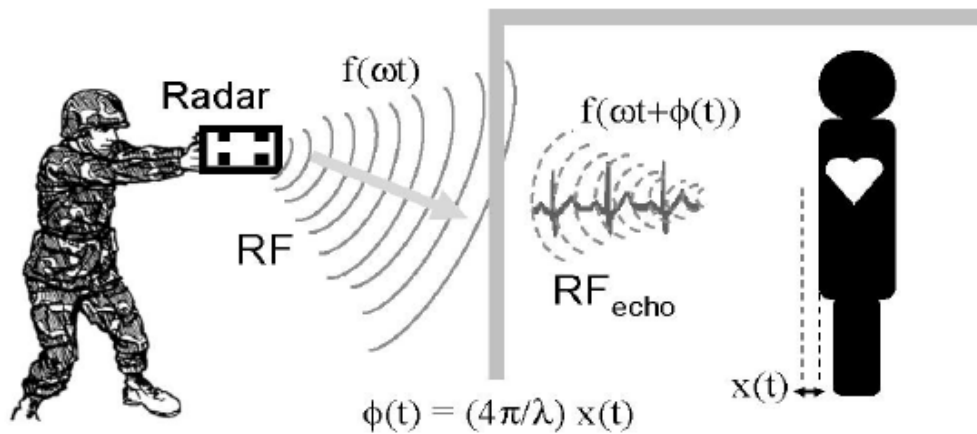


Figure 5.5 See through wall vital sign detection for a stationary human target and stationary radar using continuous wave radar [1]. Ultra-wide band (UWB) pulse radars also used for STTW applications [97].

Ultrasonic sensors can be an alternative to low-IF tag for platform motion measurements.

This work includes an ultrasonic sensor for acquiring platform's motion information. Doppler theory states that a time varying periodic motion with net zero velocity will modulate the phase of received signal.

As shown in Figure 5.5, this phase can be expressed as

$$\phi(t) = \frac{4\pi x(t)}{\lambda} \quad (5.6)$$

where λ is wavelength and $x(t)$ is the periodic movement of the target. However, the received signal can be altered with multiple sources of motions, including the motion of the radar itself. Since the experiment is carried in a place where radar is confined in walls. Signal bounced off the walls from moving radar modulates the phase in a similar manner. The received signal can be represented in a general expression as,

$$\vec{r}(t) = \sum_{i=1}^n \vec{r}_i(t) \quad (5.7)$$

The integer i is an index of moving bodies in the experiment scenario. Figure 5.6 illustrates the see-through-the-wall system. When considering a single axis movement, the total received echo can be expressed as is,

$$R_m(t) = A_s \cos \left(2\pi f_{LO}t + \theta + \frac{4\pi(x_1(t) + x_2(t))}{\lambda} + \Delta\phi \left(t - \frac{d_n(t)}{c} \right) \right)$$

$$d_n(t) = d_0 + x_1(t) - x_2(t) \quad (5.8)$$

where $x_1(t)$, $x_2(t)$, d_0 , f_{LO} are target motion, radar platform motion, nominal distance between the target and radar, and oscillator frequency respectively. However, the intensity of radiation transmitted depends on several things, the wavelength of the radiation, the intensity of the radiation hitting the barrier, the chemical composition of the barrier, the physical microstructure of the barrier, and the thickness of the barrier. Since a great deal of RF radiation is reflected and scattered by the obstacle, therefore, any through wall experiment will require more input RF power for penetration which can be controlled during experiments given the wall parameters are fixed.

A 2.45-GHz quadrature Doppler radar system was implemented for the experiment. A USB signal generator from Trinity Power Incorporated (TPI) was used along with following off-the-shelf coaxial components: transmit and receive antennas (Antenna Specialist ASPPT2988), two 0° power splitters (Mini-Circuits ZFC-2-2500), one 90° power splitter (Mini-Circuits ZX10Q-2-25-S+), and two mixers (Mini-Circuits ZFM-4212). The



56

it requires further work to calibrate the sensors to one another. Regardless the radar and ultrasonic sensor data were captured by the same DAQ. Hence, they were well synchronized.

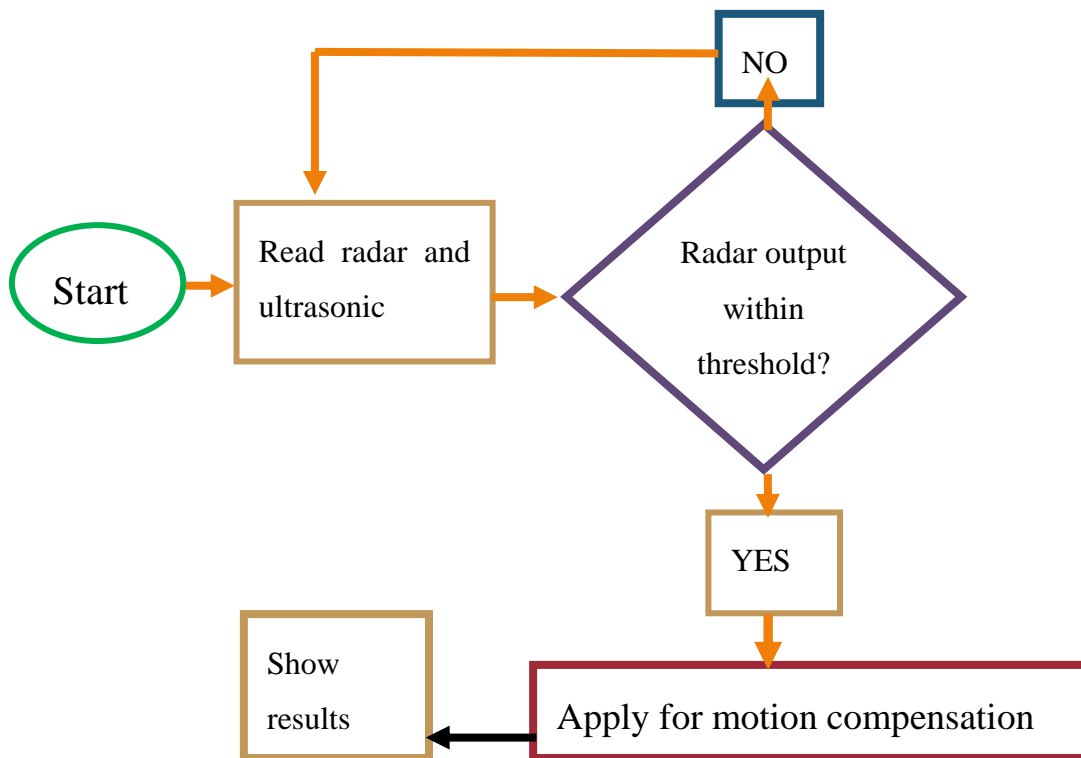


Figure 5.7 Flow chart is showing motion compensation procedure. Radar output is continuously checked against a threshold. Motion compensation is only performed on the data that is within the limit. Various motion compensation techniques are applied such as spectral filtering, adaptive noise cancellation, or sometimes fixed filtering [97].

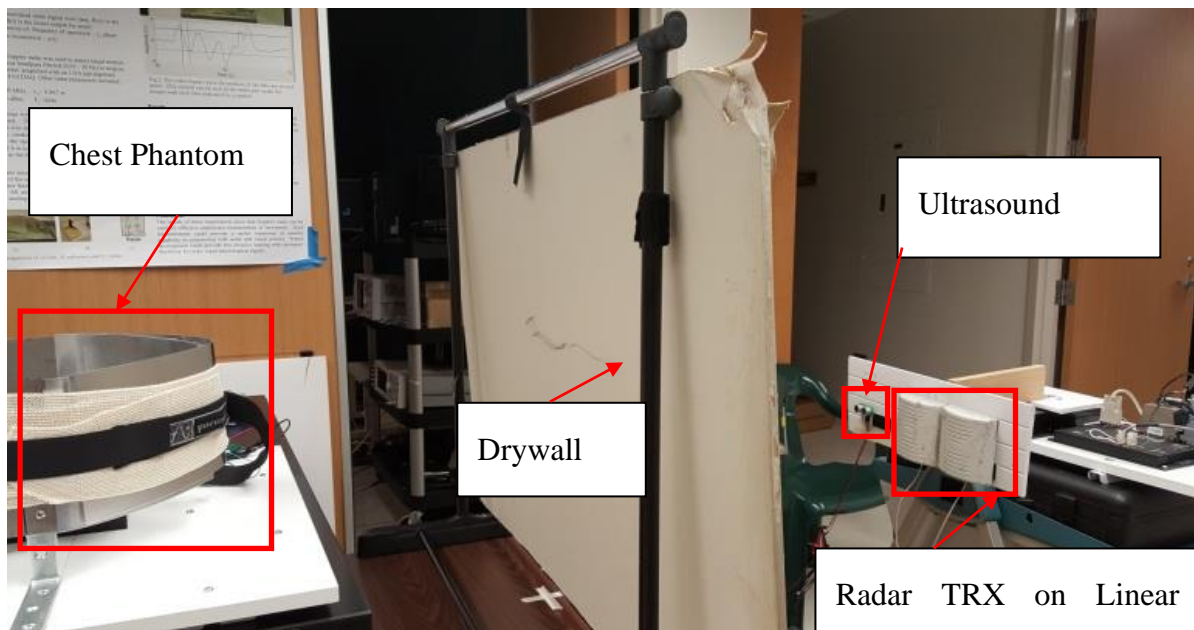


Figure 5.8 Through wall experiment in the laboratory [97].

For quick testing, it is possible to perform frequency domain processing since the output shapes are similar to platform motion. However, beyond some threshold radar signals get saturated and conventional demodulation techniques become invalid due to the non-linearity introduced. So the boundary conditions must be defined, and motion compensation can be performed within the limit of the threshold. Figure 5.7 shows the flowchart of motion compensation (MC) procedure. It is required that valid times are picked to perform filtering and discard the rest which is shown in Figure 5.9.

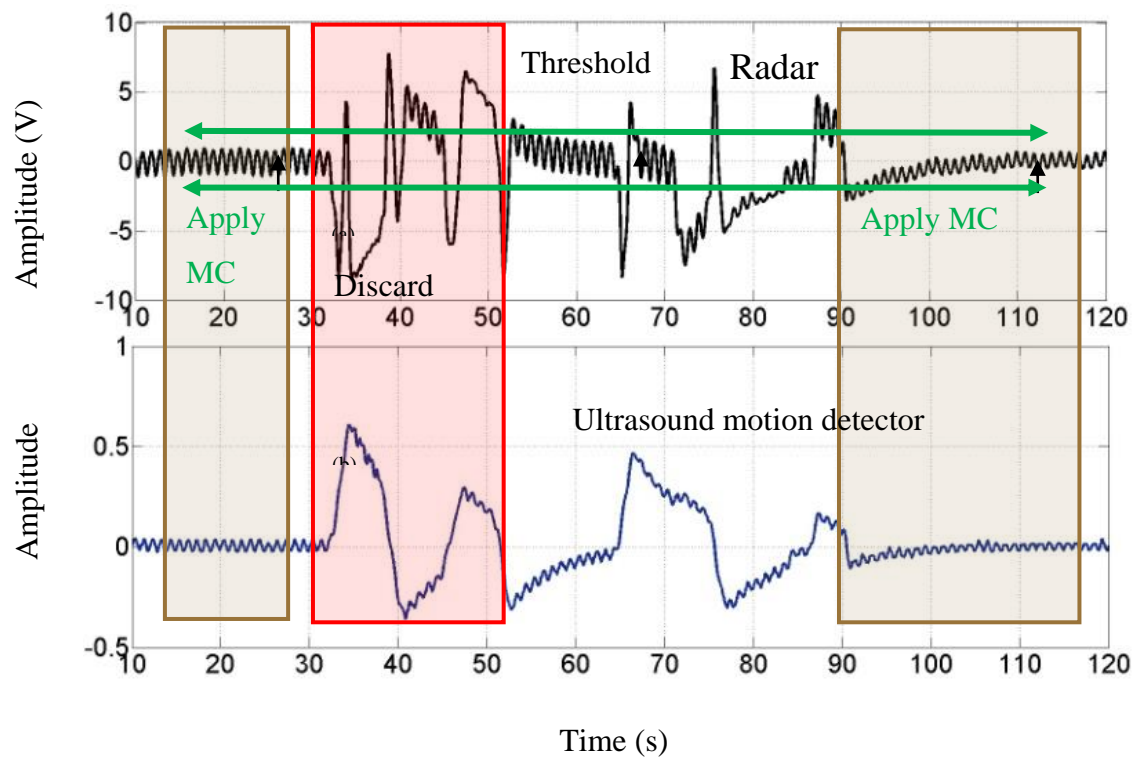


Figure 5.9 Implementation of the adaptive algorithm as shown in Fig. 5.8. Any turbulent motion causes the radar signal to be severely saturated and throws in the nonlinear region for that is not suitable for vital sign detection. The filtering only takes place when the motion is within the limit of the threshold, (a) shows the output of the radar for a two-minute span of time, (b) shows the same for ultrasound sensor.

The green marked times are suitable for processing. A segment from 100 s to 120 s in Figure 5.9 has been selected for filtering. Performing FFT on both ultrasound sensor and radar signal it is evident that a 1 Hz signal is present in both which is the base motion of the platform. On the FFT plot, a 0.2 Hz component is present with a significant amplitude which is supposedly the motion of the mechanical target since radar could see through the wall. Vital sign detection for mobile radar system has been successfully tested for various cases. These experiments lead to the conclusion that once radar motion is known, applying filtering

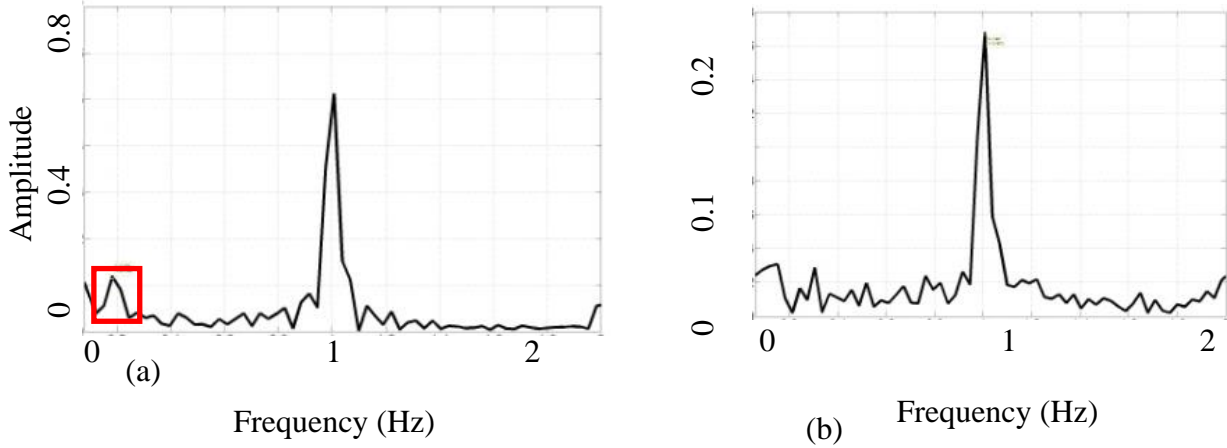


Figure 5.10 Frequency response of radar output in (a), and ultrasonic sensor's output in (b). Both outputs show that a common 1 Hz is present which is platform's motion [98].

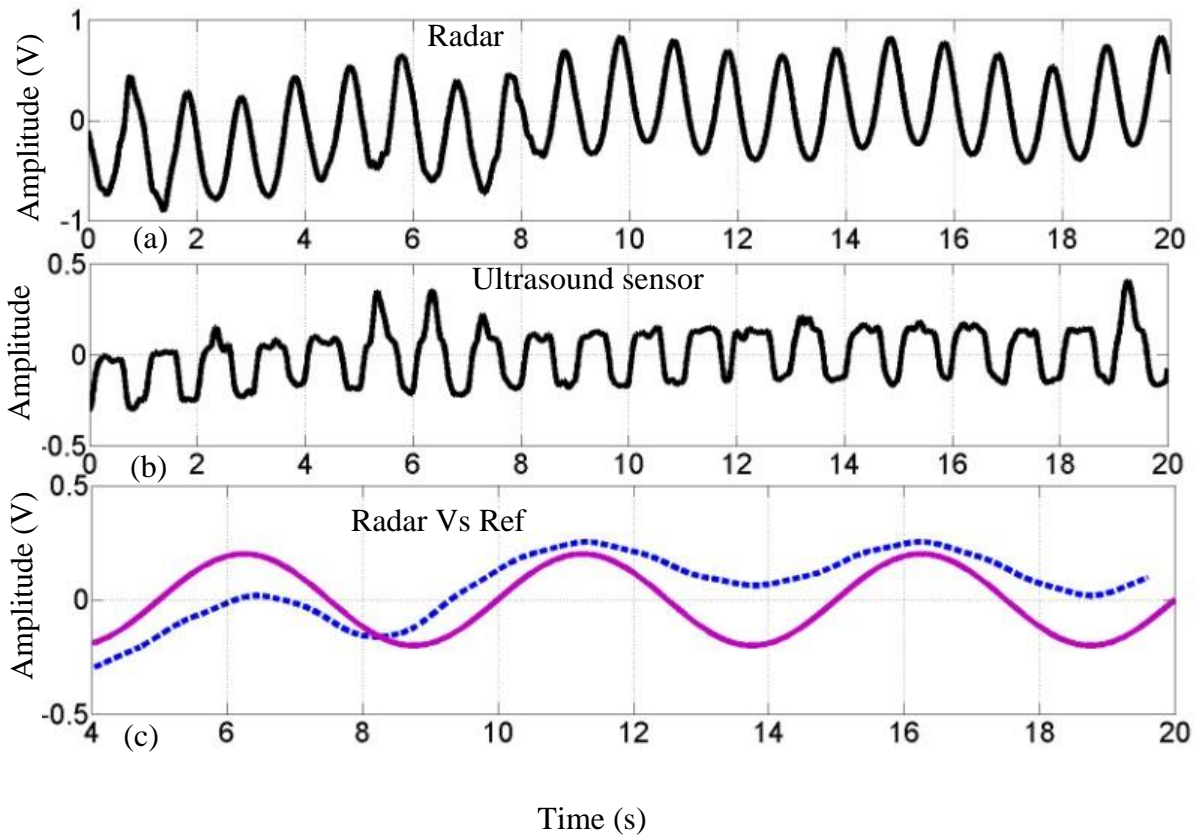


Figure 5.11 Radar output is shown in (a) which comprises voltage output due to the motion of platform and target. (b) shows the output of ultrasonic sensor capturing voltage due to platform motion, and (c) is the output of filtering of platform motion from the radar output resulting in the voltage proportional to the motion of the target which fairly compares well with the reference of the target [97].

algorithms vital signs can be detected. Butterworth IIR filter and adaptive filter are used for radar movement cancellation. The infrared tracking system is employed for tracking radar

module movements and training the adaptive filter. By applying filtering techniques desired motion signature can be traced even in the presence of unwanted radar module motions. The analysis and experiments are conducted to demonstrate the feasibility of vital sign detection through a wall when the device is in motion.

Ultrasonic distance meter sensor is used to compensate for unwanted motion simulated with a mechanical target. Adaptive noise cancellation technique enables to combine platform movement information and behind the wall radar data to cancel unwanted motion from radar data.

5.4 Conclusion

This chapter presented theory and experiments of mobile Doppler radar for vital sign measurement. Upon characterizing the platform motion it can be subtracted from composite signal (representing vector summation of chest wall motion and platform motion), and thus the motion of interest (related to vital signs) can be extracted.

CHAPTER 6. LOW-IF TAG BASED COMPENSATION

This chapter presents low intermediate frequency (IF) techniques for non-invasive detection of vital signs from a mobile short-range Doppler radar platform. Stationary continuous wave Doppler radar has been used for displacement measurement and vital signs detection. However, on mobile platform measurements become challenging due to motion artifacts induced by the platform. In an earlier chapter, it was shown that motion of the radar module was determined using cameras installed on site. However, practical mobile monitoring applications would preclude the use of such stationary cameras. In the chapter, research effort presents the development and implementation of an RF tag and a low IF radar architecture with an adaptive noise cancellation technique to extract desired vital signs motion information even in the presence of large platform motion.

6.1 Low IF Background

Previous research addressing motion artifacts due to a subject's extraneous body movement has been reported [100] [101]. Random body movement cancellation with complex signal demodulation has shown promising results [101]. The technique in [101] requires two identical radars sitting on opposite sides of the human torso which limits its usage, e.g., a subject lying on the ground. Applying this technique to a mobile platform requires two identically moving radars from opposite sides of a subject which may not be practical.

Life signs detection from a mobile platform is a new topic in literature. Researchers have investigated artifacts due to the shake of a hand-held radar sensor [6], and a sensor node architecture has been demonstrated to solve the interference problem [6]. However, this technique is not always feasible; it may result in poor SNR due to the use of an over-the-air local oscillator signal. Empirical Mode Decomposition (EMD) has been investigated as a technique for removing fidgeting interference in Doppler radar life signs monitoring devices [7]. EMD intrinsic mode functions (IMFs) were selected manually though, which is not always possible and involves a good deal of computational complexity.

This experiment focus is the analysis of noise compensation methods suitable for the motion of the whole radar system, which can be applied to large amplitude motion as would be expected in vehicle mounted applications. The original idea of this experiment is inspired by prior work [8] [9] where motion artifact cancellation for a moving target (stationary radar) was investigated via the use of a harmonic radar tag which provided a reference signal for the motion content to be canceled. The harmonic tag and receiver uniquely identified a tagged moving subject in the presence of multiple motion sources and facilitated cancellation of tag-related motion to isolate the remaining motion within the radar's view [8] [9] which was due to a second, untagged mover. Low-IF system architectures have also been investigated for CW [102] and pulse Doppler radar [103] [104]. In theory, it is possible to apply the same principle to track and cancel radar platform motion instead of the motion of the second moving target. Two distinct applications of RFID tags for motion cancellation have been shown in Figure 6.1. Figure 6.1(a) depicts a stationary radar and a stationary subject. Figure 6.1(b) illustrates a case where the tag is attached to the chest to cancel extraneous motion, but the radar is stationary. Figure 6.1(c) shows the proposed application, where the radar itself is in motion. In this case, radar platform motion compensation is performed without attaching a tag to any moving object, but instead placing it stationary near the subject (Figure 6.1(c)). While this could be done using harmonic tags, these commonly require a complex system architecture with two receivers [8], as was done when this approach was studied for the tagging of a moving target.

This thesis proposes a frequency shifting tag method that only requires one receiver [96]. The frequency shifting tag is essentially a low intermediate frequency technology. The reflection from a stationary tag can be used to isolate and track the random motion or drift information of the moving radar platform. Tags which induce a small frequency offset combined with a low IF system offers paramount flexibility as opposed to harmonic tags. With a low IF system, one front-end can be used to uniquely decode reflections from multiple

tags with distinct offsets which theoretically leads to the identification and measurement of multiple sources of motions. In a harmonic tag system, multiple receiving antennas and circuits are required, and feasible measurements can likely only be made up to a few harmonics. Using low IF tags, multiple subject isolation or tracking of a specific motion (i.e., radar motion) can be done by each tag shifting and reflecting the incident frequency by a unique amount. Decoding of all sources of motion can be done using multiple IF band pass filters that lead to unique identification and measurement of each motion source [9].

Low intermediate frequency (IF) methods have been used for dc offset management, and flicker noise reduction [105] [9] [102]. Some results investigating multiple-target motion compensation techniques for vital signs detection have been published [8]. When platform motion data (i.e., displacement, acceleration) is known, vital signs can be detected by filtering out the components introduced due to radar motion. This subtraction can be direct, spectral, or achieved through adaptive filtering [8] techniques or a combination of these methods. It has been demonstrated that if radar motion is simple and precisely tracked, filtering techniques could remove the motion artifact [97].

However, in cases of extreme aliasing, advanced noise cancellation techniques are required [5]. An adaptive filtering technique was employed in one of the test cases. In [5] high precision infrared cameras were used in a lab environment to measure the motion of the mobile radar platform. However, in practical applications, a system is needed that can determine the motion or vibration of the mobile platform on the fly. Practical applications for the work proposed here include vital signs radars mounted on unmanned aerial vehicles to measure vital signs in search and rescue operations or for monitoring wildlife activities, where arranged precision cameras would be impractical. Real-time onboard processing will also be crucial for such systems.

This chapter introduces a low IF tag (small, portable RF device) based method for platform motion assessment and cancellation in life signs detection from mobile radar systems. The use of simple scattered tags (disposable) promotes the possibility of life signs measurement from radar mounted on a vehicle. Tags can be made very small, lightweight, portable, and wireless providing a practical solution for field applications.

Radar transceiver movement will modulate the received signal, just as the target motion will. If the movement is small in displacement, and thus phase, small angle approximation can be applied for demodulation [5]. This approximation is valid in simple cases where the motion is one-dimensional [5]. Even the experiment is demonstrated for a linear one-dimensional scenario. However, the analysis can be extended to a spherical

coordinate system for multiple dimensions.

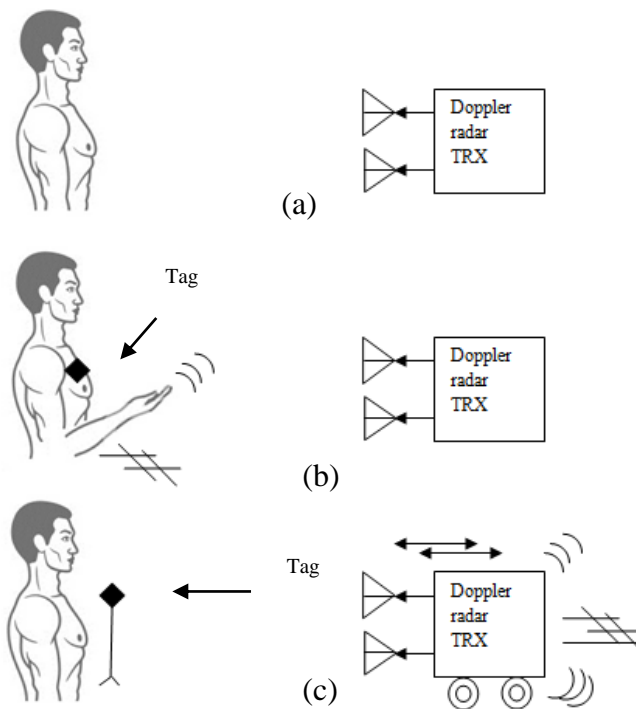


Figure 6.1 Application of RFID tagging in Doppler radar motion sensing. A stationary radar and subject, (a), a subject tagged to cancel (ignore) unwanted hand movement, (b), and the proposed system where the radar itself is in movement, (c), are shown. In (c), the stationary tag is used to find the radar motion and cancel it from another motion measurement [97].

A complex vector model can be designed to map physical motion and electrical signal strength for three-dimensional cases since received signal strength is a function of effective radar cross section [5].

6.2 Theory of operation of low-IF motion compensation tag

Figure. 6.2 gives an illustration of life signs detection from a mobile radar platform. The null distortion problem in the Doppler radar receiver can be addressed by using a quadrature receiver [68]. Linear and arctangent demodulation combine two channels and select the optimum channel at any given instance. Linear demodulation is a straightforward procedure of projecting the two-dimensional baseband data to a single dimension through linear combination, maximizing variance in the data and suppressing redundant information [4] [9]. With the linear demodulation technique, the small signal approximation is valid for the received data that will directly relate motion that modulates the phase. However, the received radar signal has two components: one coming from the radar itself and the other

from human target's cardiorespiratory effort. After detecting the modulation component due to the radar platform displacement or vibration, advanced filtering techniques can be applied to filter the net effect of radar movement, thus allowing extraction of heart or respiratory rate.

The local oscillator generates an RF signal which is transmitted through the antenna; the reflected signal from the subject whose vital signs are to be measured is then mixed with local oscillator signals to generate quadrature outputs. The output baseband signals $B_I(t)$ and $B_Q(t)$ of the radar system are given by,

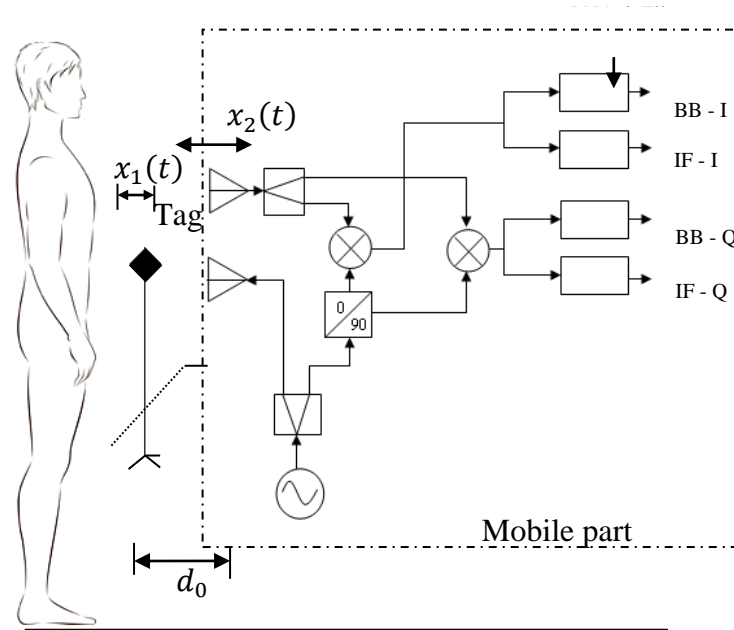


Figure 6.2 Mobile quadrature Doppler radar system. The transceiver is mounted on a linear stage which can move the radar. BB refers to baseband [96].

$$B_I(t) \approx A_{BI} \cos \left(\theta + \frac{4\pi x(t)}{\lambda} + \Delta\phi \left(t - \frac{d(t)}{c} \right) \right) \quad (6.1)$$

$$B_Q(t) \approx A_{BQ} \sin \left(\theta + \frac{4\pi x(t)}{\lambda} + \Delta\phi \left(t - \frac{d(t)}{c} \right) \right) \quad (6.2)$$

$$x(t) = x_1(t) - x_2(t) \quad (6.3)$$

$$d(t) = d_0 + x_1(t) - x_2(t). \quad (6.4)$$

where θ , λ and $\Delta\phi$ represent constant phase shift, wavelength and residual phase noise of the

oscillator. A_{BI} and A_{BQ} are the baseband amplitude of quadrature channels which are functions of receiver gain and mixer conversion losses [2]. Steady phase shift depends on the nominal distance between the target and the radar antenna. $x(t)$ is a composition of two displacements, one coming from the human torso displacement due to respiratory effort, and the other from radar's movement itself, which are denoted by $x_1(t)$ and $x_2(t)$ respectively, while $d(t)$ is the distance between target and radar at any given time, and d_0 denotes the nominal distance between the radar and target [5]. After filtering, amplification, and performing linear demodulation the received baseband signal can be approximated by,

$$B(t) \approx A_B \left(\frac{4\pi x(t)}{\lambda} + \Delta\phi(t) \right). \quad (6.5)$$

A_B is the baseband gain of demodulated signal. While $x(t)$ is the resultant of two motions, once the radar's motion is identified the other (respiratory) motion can be determined using fixed or adaptive filtering techniques.

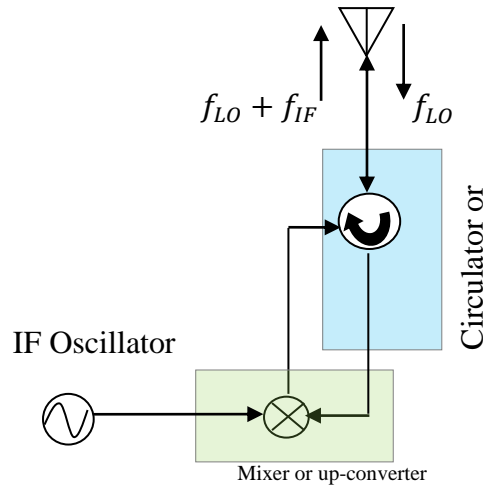


Figure 6.3 RF tag device includes a mixer, an on-board oscillator, and an antenna [96].

A new RF-based method using an RF tag can be used to track platform motion. The RF tag is essentially a lightweight, a small device that can be dropped or set in the field of view of the radar on a mobile platform, but the tag is unaffected by the motion of the subject being measured. The device can be a passive or active node that is coherent with the local oscillator (with frequency f_{LO}) and able to shift the local oscillator frequency to an

intermediate extent. The tag antenna will receive the transmitted signal and mix it with a generated IF signal (with frequency f_{IF}).

The output of the mixer will then be transmitted back to the receiver. When the tag is stationary, the down-converted signal should contain the IF signal which is modulated only by the motion of the mobile platform. The proposed tag circuit is shown in Figure 6.3. Figure 6.2 shows the complete system architecture with the tag. Note that the tag is placed beside the subject, so that reflected signal from the human torso poses minimal interference to the tag signal. The total received signal in the radar receiver has essentially two components, one up-converted signal coming from the tag and the other baseband signal reflected from the human torso. When the RF signal is mixed with a local oscillator and filtered, we can separate both baseband data and intermediate frequency components. The mathematical analysis is shown in following equations. The IF component includes only the motion of radar platform. Signal reflected of human torso can be modeled as [97],

$$R_s(t) = A_s \cos \left(2\pi f_{LO} t + \theta + \frac{4\pi(x_1(t) + x_2(t))}{\lambda} + \Delta\phi \left(t - \frac{d_1(t)}{c} \right) \right) \quad (6.6)$$

$$d_1(t) = d_0 + x_1(t) - x_2(t) \quad (6.7)$$

where $x_1(t)$ and $x_2(t)$ are the human torso displacement due to respiratory effort and platform motion respectively. Quantities d_0 and $d_1(t)$ are the nominal distance and variable distance between the radar receiver and human torso. A_s is the amplitude of the torso reflected signal, and c is speed of light. Frequency f_{LO} is RF local oscillator frequency and f_{IF} is the low IF frequency. Reflected signals from the tag can be modeled as [97],

$$R_{IF+}(t) = A_{IF} \cos \left(2\pi(f_{LO} + f_{IF})t + \theta + \frac{4\pi x_2(t)}{\lambda} + \Delta\phi \left(t - \frac{d_2(t)}{c} \right) \right) \quad (6.8)$$

$$R_{IF-}(t) = A_{IF} \cos \left(2\pi(f_{LO} - f_{IF})t + \theta + \frac{4\pi x_2(t)}{\lambda} + \Delta\phi \left(t - \frac{d_2(t)}{c} \right) \right) \quad (6.9)$$

$$d_2(t) = d_0 - x_2(t) \quad (6.10)$$

d_0 and $d_2(t)$ are the nominal distance and variable distance with radar receiver and tag. A_{IF} is the amplitude of the tag reflected signal. Total superimposed received signal in radar receiver antenna is,

$$R(t) = R_{IF+}(t) + R_{IF-} + R_s(t). \quad (6.11)$$

After mixing and filtering the baseband output of the quadrature radar is given by [97],

$$B_I(t) \approx A_{BI} \cos \left(\theta + \frac{4\pi(x_1(t) + x_2(t))}{\lambda} + \Delta\phi \left(t - \frac{d_1(t)}{c} \right) \right) \quad (6.12)$$

and

$$B_Q(t) \approx A_{BQ} \sin \left(\theta + \frac{4\pi(x_1(t) + x_2(t))}{\lambda} + \Delta\phi \left(t - \frac{d_1(t)}{c} \right) \right). \quad (6.13)$$

A_{BI} and A_{BQ} are the baseband amplitude of quadrature channels which are functions of receiver gain and mixer conversion loss [2]. Using linear demodulation and small signal approximation on B_I , B_Q the baseband output will be like (6.5).

The output of the IF filters is [97]:

$$\begin{aligned} IF_I(t) \approx \frac{A_{IFI}}{2} & \left[\cos \left(2\pi f_{IF} t + \theta + \frac{4\pi x_2(t)}{\lambda} + \Delta\phi(t) \right) \right. \\ & \left. + \cos \left(2\pi f_{IF} t - \theta - \frac{4\pi x_2(t)}{\lambda} - \Delta\phi(t) \right) \right] \end{aligned} \quad (6.14)$$

and

$$\begin{aligned} IF_Q(t) \approx \frac{A_{IFQ}}{2} & \left[\sin \left(2\pi f_{IF} t + \theta + \frac{4\pi x_2(t)}{\lambda} + \Delta\phi(t) \right) \right. \\ & \left. + \sin \left(2\pi f_{IF} t - \theta - \frac{4\pi x_2(t)}{\lambda} - \Delta\phi(t) \right) \right]. \end{aligned} \quad (6.15)$$

A_{IFI} and A_{IFQ} are doubled the amplitude of filtered and mixed components of IF inphase and quadrature phase signals. If with DC coupling, (6.1) through (6.15) will require some

modifications.

It is interesting to note; the IF signal does not contain $x_1(t)$ component since the tag is stationary and placed beyond the field of view of the torso reflected signal. We can view these equations as standard amplitude modulation with a carrier frequency of IF. The signal component due to platform motion $x_2(t)$ can be determined using envelop detection. The hypothetical frequency domain plot is shown in Fig. 6.4.

Now, $x_2(t)$ can be measured by mixing the IF signal with a coherent IF LO with the exact same frequency and performing low pass filtering. This method is usually known as down conversion. With small angle approximation, the filtered output will be proportional to displacement. Since the tag is a remote device the only option is creating a software based mixing. Another way to find $x_2(t)$ is to see the effect of motion on the low-IF signal. Traditionally, the received continuous wave signal is phase modulated which is demodulated by quadrature mixing with the LO signal [10] [106]. The modeling of CW radar system includes a stationary transmitter and receiver and a moving target with a zero net velocity. However, with a low-IF tag system, the net velocity of the target would be zero only from a frame of reference of an observer [107] [9]. From radar point of view, due to the presence of an IF beyond DC region, the

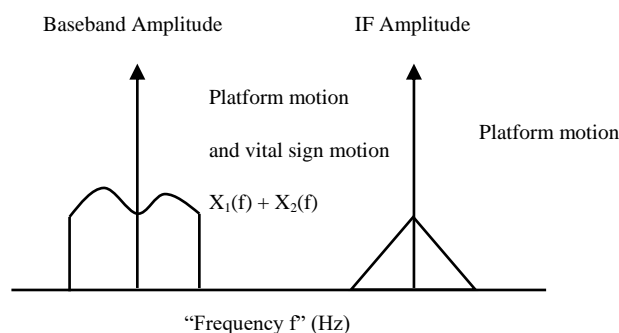


Figure 6.4 Theoretical frequency domain response of the demodulated RF signal [96].

radar is effectively looking at an object traveling radially at a speed corresponding to the IF. The challenge is to model this behavior and predict the resulting signal correctly. Fortunately, this behavior does resemble radar scattering by flying airplanes that have been studied and referred to as "jet engine modulation" [84] [9]. Reference [84] explains that moving or rotating surfaces on a moving target will have the same Doppler shift as the moving target, but will also impose amplitude modulation (AM) on the Doppler shifted return [84].

Amplitude demodulation techniques can then be applied to the obtained Doppler

shifted return to obtain information about the moving surface. In radar signal, the amplitude appears as a voltage which is proportional to the displacement within the limit of small signal approximation [4]. For our work, we have only focused on the frequency components of the platform motion. Voltage to displacement conversion remains as our future work. Few assumptions were made for this work. One assumption is linear one-dimensional platform motion with frequency range much smaller than IF. In such a scenario, squaring the signal followed by low pass filtering (LPF) results in a signal proportional to radar motion. This method is called envelope detection throughout this paper.

$$\begin{aligned}
 IF_I^2 &\xrightarrow{\text{LPF}} k_I A_{IF_I} \cos\left(\frac{4\pi x_2(t)}{\lambda} + \phi'(t)\right) = MC_I \\
 IF_Q^2 &\xrightarrow{\text{LPF}} k_Q A_{IF_Q} \sin\left(\frac{4\pi x_2(t)}{\lambda} + \phi'(t)\right) = MC_Q
 \end{aligned}$$

where k_I and k_Q are the amplification factors relating to signal conditioning such as amplification and digital filtering. One can perform arctangent demodulation of MC_I and MC_Q to find out $x_2(t)$. However, this work used linear demodulation method to record a voltage proportional to displacement. Applying linear demodulation and small signal approximation we can find out the motion compensation signal as,

$$MC_{sig} \simeq \left(\frac{4\pi x_2(t)}{\lambda} + \phi'(t) \right). \quad (6.16)$$

Note that the assumption in Fig. 6.4 is that the frequency component of the platform motion is band limited.

A prototype of a RFID tag was simulated and fabricated to measure the motion of the setup. The circuit was made as shown in Figure 6.5. An oscillator from linear technology (LTC6900) was chosen to generate intermediate frequency LO signal and configured to generate 1515 Hz. For mixing, a Schottky diode from Avago Technologies (HSMS-286Y) was used. A small size 2.4 GHz dielectric antenna from TOKO was selected (part No. DAC2450CT1T) [96]. The free-running oscillator of the tag generates 1531 Hz signal. The tag was placed 30 cm away from the radar transceivers for characterization. Typical DC power consumption of the tag was 3 mW, Transmitted power through the 8dBi radar antenna

was -11 dBm; the tag reflected received power at IF frequency with 8 dBi gain antenna was -65 dBm. The power efficiency of the tag is low and long-distance operation might not be possible with this prototype. However, the described architecture in Figure 6.3 has a dedicated directional coupler. A well-matched circuit with the directional coupler and balanced mixing is expected to provide much stronger up-converted signal in IF band suitable for long distance operation.

6.3 Experiment and results

A 2.4-GHz quadrature Doppler radar system was used for the tests. The assembly incorporated a signal generator (HP83640B) and subsequent off-the-shelf coaxial components: transmit and receive antennas (Antenna Specialist ASPPT2988), two 0° power splitters (Mini-Circuits ZFC-2-2500), one 90° power splitter (Mini-Circuits ZX10Q-2-25-S+), and two mixers (Mini-Circuits ZFM-4212). The received signal reflected from human subject and tag is split and fed into two mixers. The local oscillator paths that are coupled to mixers have 90-degree phase shift, providing in-phase and quadrature versions of the signal [5]. After down conversion, filtering and amplification are performed using SR560 LNA. Finally, the data is recorded by NI data acquisition device for additional signal processing with MATLAB. Radar transceiver is installed on a precision linear stage (Single-Axis Series CDS-3310) from Galil that provides various motion patterns. In [5], the linear stage was programmed to have periodic motion with 8 mm 1.2 Hz frequency. Same setup parameters are used in this work for a fair comparison. A human subject was sitting stationary (1 m away) on a chair and breathing normally for respiration tests. A standard respiratory belt transducer (contains a piezo-electric device) is strapped around the chest for breathing reference rate. RF tag is placed about the same height of subject's chest.

In experiments, I and Q outputs of the receiver are branched out to 4 amplifier and filter channels. Each channel is connected to one band pass filter with 300 Hz - 3 kHz to filter IF, and a baseband low pass filter having 30 Hz corner frequency to capture baseband signal. This setup required four SR560 LNAs for amplification and filtering. The band pass filters are used to record the IF data. It is assumed that bandwidth of radar movements are limited to 30 Hz. Since the induced platform motion was less than 2 Hz, the prominent frequency components would lie well under 30 Hz. The low pass filter configuration records baseband data. The sampling rate is set to 12 kHz to avoid aliasing when capturing IF data. The tag is set in a position that minimizes the reflected signal interference, but it sees the transmit signal. For our experiment, optimally this position is side by side with the subject

(considering signal scattering and antenna directivity). The tag can be viewed as a coherent device because LO signal from radar transmitter is incident on the tag, following mixing with IF signal and retransmitting of shifted signal through the same antenna. Hence range correlation benefits are achieved in tag signal demodulation [9].

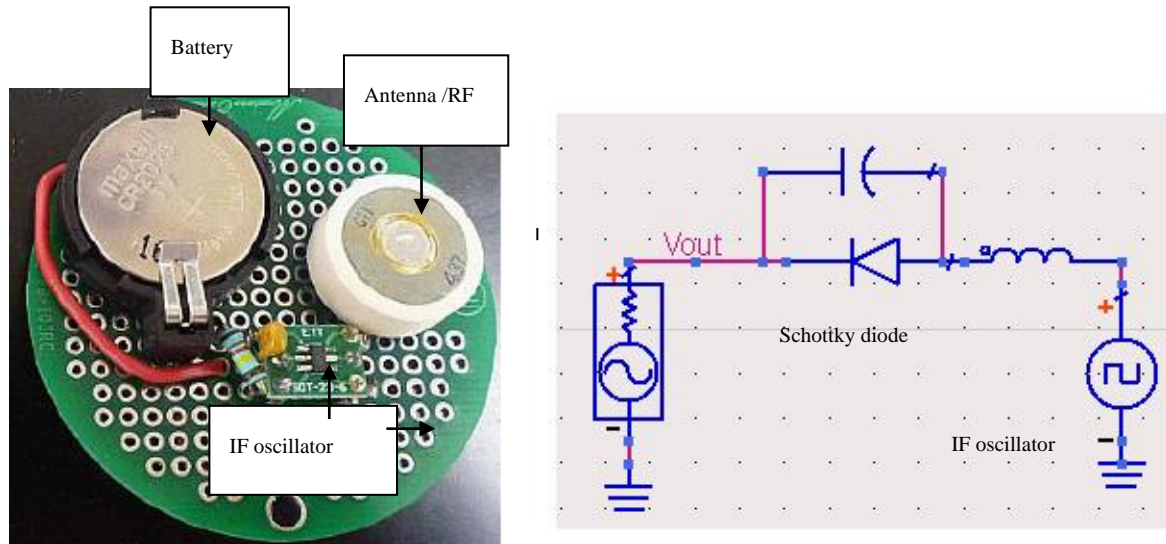


Figure 6.5 Fabricated IF tag and ADS simulation circuit [96].

The IF bandpass output data are processed and plotted in Figure 6.6 and Figure 6.7. The time series of I and Q channels are sketched on the top, and corresponding IF envelopes are plotted on the bottom in Figure 6.6(c) and Figure 6.7(c). As expected and explained in theory the IF time-series in Figure 6.6(a) and Figure 6.7(a) appears like an amplitude modulated the carrier. Since platform motion modulates the IF, it preserves the platform motion information. Performing FFT on data of Figure 6.6(a) and Figure 6.7(a) shows the presence of IF frequency at 1531 Hz in Figure 6.6(b) and Figure 6.7(b). It is suggested for low-IF quadrature systems that I and Q data be combined after envelope-detection [15] [18]. The linear demodulation of these two envelopes is plotted in Figure 6.8(b). The linear stage is programmed to move in 1.2 Hz sinusoidal motion with 8 mm displacement which apparently shows that tag can successfully reproduce a voltage proportional to platform motion. In Figure 6.8(a) filtered baseband data is plotted which should contain two displacement components. Upon IIR filtering the tag signal (platform motion) from baseband signal respiration signal is retrieved.

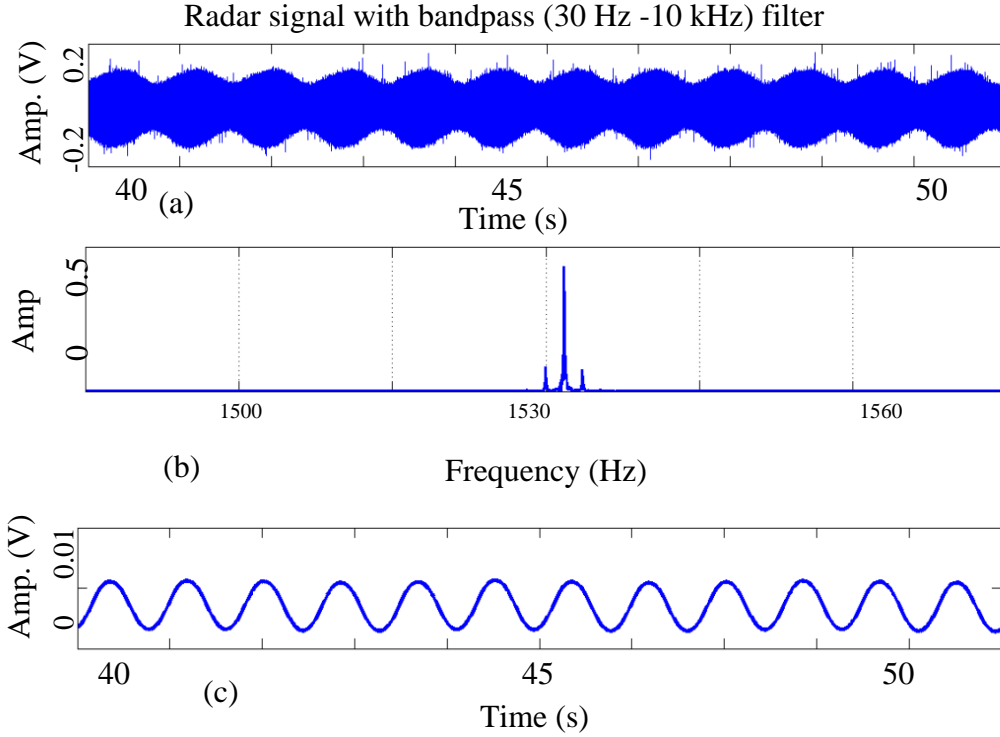


Figure 6.6 Platform motion detection using IF tag. The radar-carrying linear stage was programmed to move in 1.2 Hz with 8mm displacement. The IF filter output from I channel, (a), the Fourier transform of the 1531 Hz IF signal amplitude modulated by the motion of radar module, (b), and the IF demodulated signal which is proportional to the displacement, (c), are shown. It is evident that 1.2 Hz sinusoidal motion is detected [96].

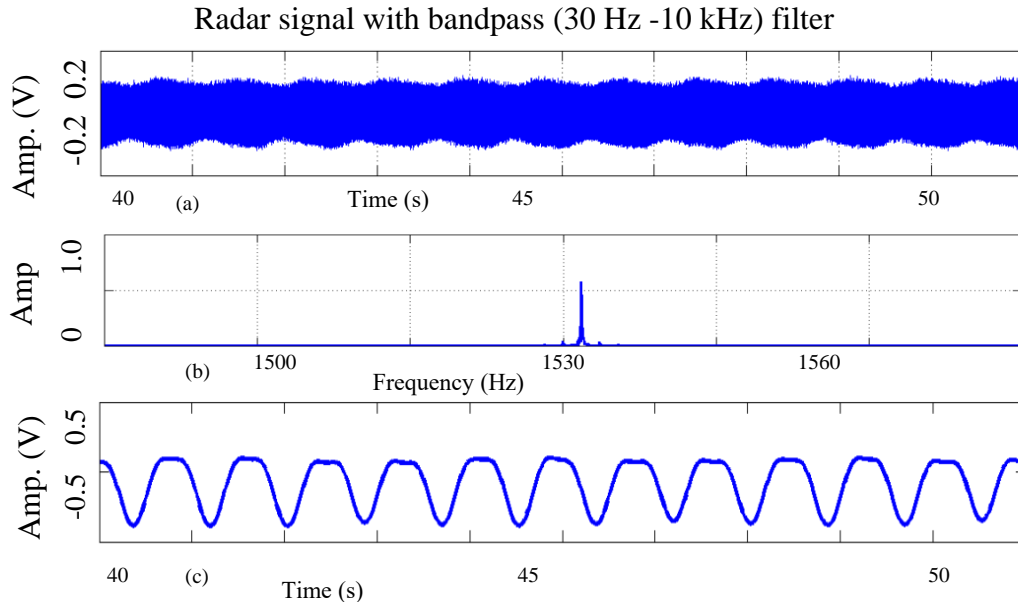


Figure 6.7 Similar plots are shown for Q channel. To avoid the null problem both I and Q channels are required. Therefore, both I and Q measurements are taken to perform linear demodulation [96].

The result summary is shown in Figure 6.8. Figure 6.8(a) shows the baseband signal comprised of the radar motion and respiration motion. Figure 6.8(b) shows the voltage

demodulated from the IF envelope. This retrieved signal is compared with chest band output and plotted. Linear scaling (10 times) is performed on the radar data for better comparison with a chest belt. In Figure 6.8(c) result shows a

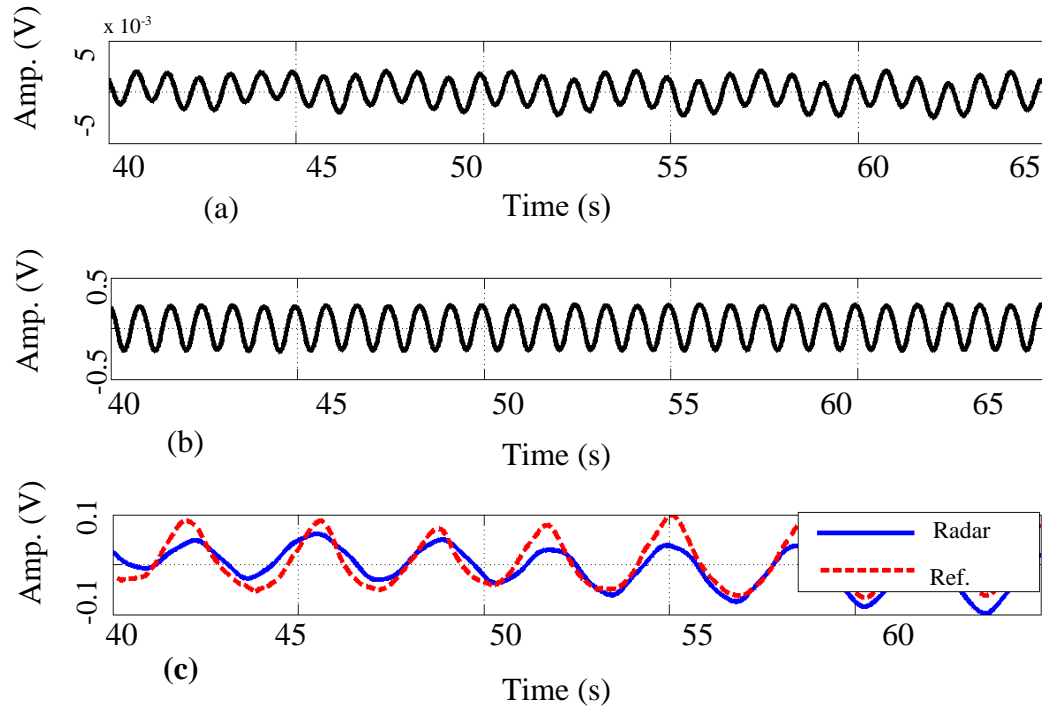


Figure 6.8 Tag performance for motion compensation. Radar output is showing baseband data comprised of (a) voltage proportional to) platform motion and respiratory effort, (a); demodulated IF signal representing the voltage proportional to platform motion. The platform motion is filtered out from baseband data to retrieve respiration signal, (b); and a comparison of motion compensated radar result and reference chest belt, (c), are shown. The results are comparable to the infrared camera tracker system (8 mm, 1.2 Hz motion of the platform) [5].

good agreement between standard chest belt reference and radar-based signal. An experiment was also conducted when there are multiple harmonics in IF received signal due to complex motion of the platform. The linear stage was programmed to move the platform in a square wave fashion; move forward with constant velocity, stop then go backward with constant velocity, stop, and repeat the motion. The system is DC coupled, so a pause in motion shows a constant voltage, constant velocity of radar platform extending and retracting represents the voltage traces having positive and negative slopes. A human subject was also in the experiment.

The radar output voltage is linearly related to the position. However, the voltage and displacement linearity only holds until a certain limit with linear demodulation. The redundant voltage component in the baseband signal can be removed by subtracting the voltage found through IF demodulation. However, direct subtraction is not possible as a proper scaling factor is not well determined. To get around this problem an adaptive filter

with normalized least mean square (step size .08) was applied to retrieve respiration information from baseband data. The output of the filter compares well with standard chest belt reference as shown in Figure 6.9(c). Side and front view of the experimental setup are illustrated in Figure 6.10. A vital signs detection technique has been explored for a mobile Doppler radar platform using low IF tags.

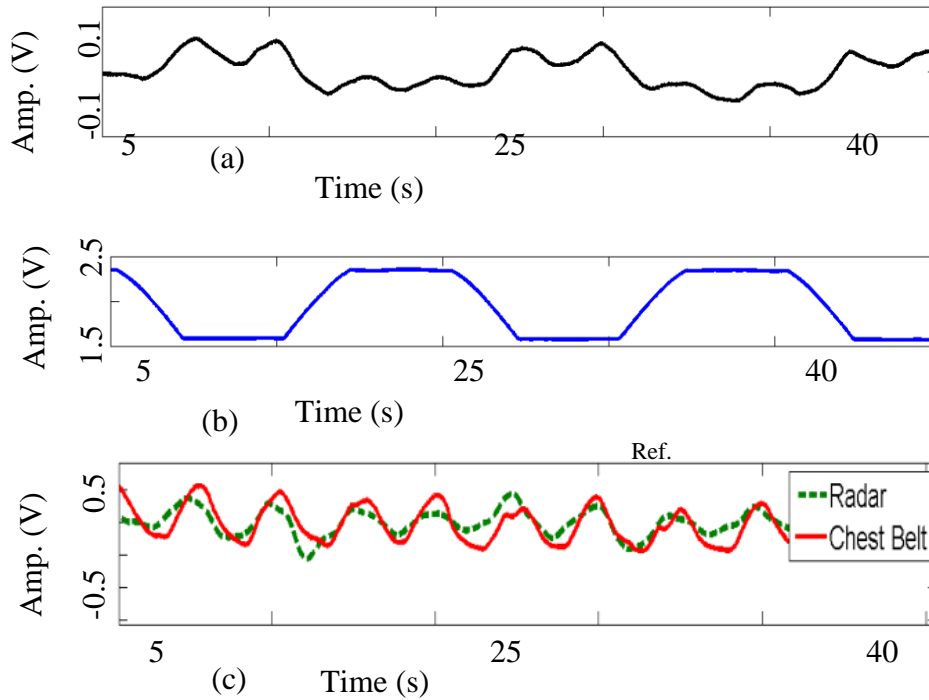


Figure 6.9 Respiration signal retrieved using adaptive filters. Radar output showing baseband data comprising (a voltage proportional to) platform motion and respiratory effort, (a), demodulated IF signal representing the voltage proportional to platform motion, (b), and a comparison of the motion compensated radar result and chest belt reference, (c), is shown [96].

A small, portable, and wireless tag can be used to produce a reference signal for platform motion compensation. A single receiver architecture has been proposed to be used with frequency-shifting low IF tags. Signal processing methods such as adaptive filtering techniques have been applied for motion compensation. A 1531 Hz IF tag was fabricated and tested for the proposed architecture. The retrieved signal was in good agreement with a standard chest band reference for two experimental cases of platform motions of 8 mm at 1.2-Hz sinusoidal motion and square-wave motion with 12-mm displacement. This experiment results may have an impact in the development of search and rescue unmanned vehicles or autonomous wildlife monitoring systems.

With the advancement of inertial measurements units and FPGA and computing technology, tiny unmanned aerial vehicles are now easy to fabricate, and public consumers are

very interested in these products. Radars with low-IF tag compensation can be used with UAVs for various purposes.

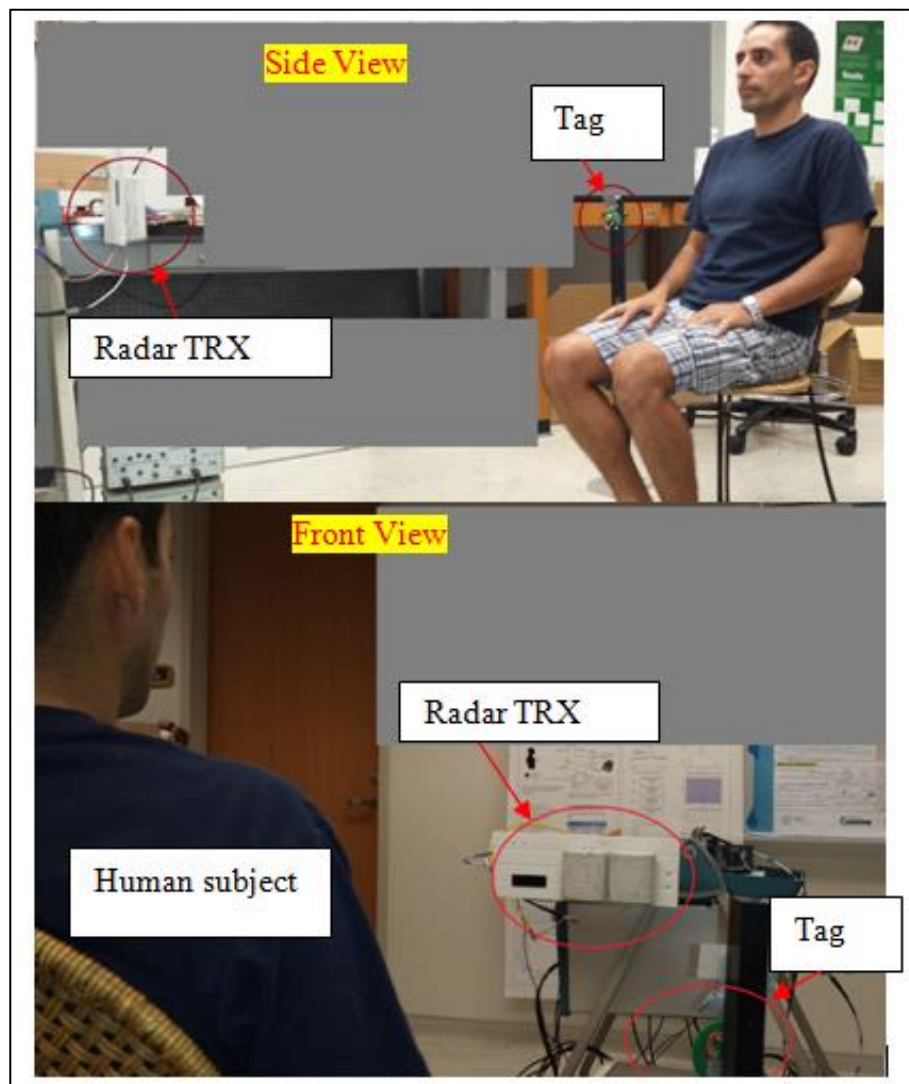


Figure 6.10 Experiment setup in the laboratory. Front view and a side view shows the placement of radar, RF tag, and human subject [96].

CHAPTER 7. SUBJECT IDENTIFICATION

7.1 System requirement

In Chapter 4 some results on unique identification were presented. Respiration signal has good potential to be used as biometric [108] [109] [110]. Owing to the simple structure and validity, 2.4 GHz direct conversion systems are frequently used for vital signs detection applications. In such system, the portion of DC offset caused by system imperfections, internal DC offset, and the external environment, clutter, is problematic. However, the DC offset added from the subject is critical for accurate displacement measurement.

This thesis proposed a system to make measurements of time-varying signals which preserve useful DC contributions while eliminating non-essential DC contributions which would otherwise undermine the use of appropriate gain and resolution. The diagnostics and analysis of sleep-disorder, unique identification involving respiration markers required high-precision displacement measurement and managed DC components. AC coupled system may offer high gain system, but AC distortion is undesirable for high precision respiration characterization.

Figure 7.1 illustrates the AC distortion problem with a mechanical experiment. Accurate displacement measurement depends on the accuracy of radius finding and proper arc fitting in arctangent demodulation. With a 2.4 GHz system, a small arc is produced with normal human breathing. Circle fitting and radius finding are core part of accurate displacement measurement. For circle fitting a small arc is less reliable. Figure. 7.2 demonstrates such an occurrence of overestimation when fitted circle has a much bigger

radius than the correct value and a biased center. With higher SNR/DR and gain the arc is magnified with the circle radius which improves the performance of LM algorithm.

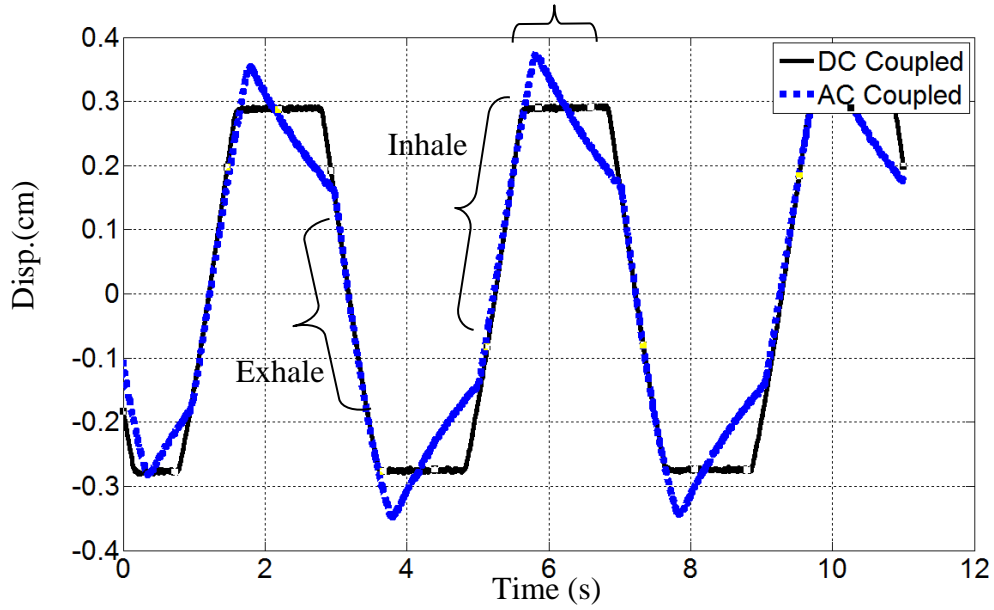


Figure 7.1 Radar output of displacement of a very simplified mechanical breathing simulator. Both AC coupled, and DC coupled measurements are presented. When a rest in between inhale and exhale is simulated, DC coupling preserves the state in its displacement measurement. However, AC coupled measurement is distorted [111].

7.2 System improvement

A 2.4-GHz quadrature Doppler direct-conversion radar system was initially used for the experiment. Major components of the system are (Antenna Specialist ASPPT2988), two 0° power splitters (Mini-Circuits ZFC-2-2500), one 90° power splitter (Mini-Circuits ZX10Q-2-25-S+), and two mixers (Mini-Circuits ZFM-4212). The local oscillator utilizes a quadrature power divider, providing in-phase and quadrature versions of the signal. Following the down conversion, filtering (DC-30 Hz) and amplification are performed. The NI-DAQ recorded the data and processed further using MATLAB. The two channel output signals were pre-conditioned by SR560 low-noise amplifiers. Multiple sets of experiments were performed using both traditional and proposed systems. Two subjects (S1, S2) with known similar breathing rate were selected for the experiment. The purpose of the experiments was to identify the subjects uniquely just by analyzing respiration data. Feature, for example, power spectral density (PSD) describes how the power of a signal or time series is distributed over the different frequencies and given by (7.1)

$$S_x(f) = \lim_{T \rightarrow \infty} E \left\{ \frac{1}{2T} \left| \int_{-T}^T x(t) e^{-j2\pi ft} dt \right|^2 \right\} \quad (7.1)$$

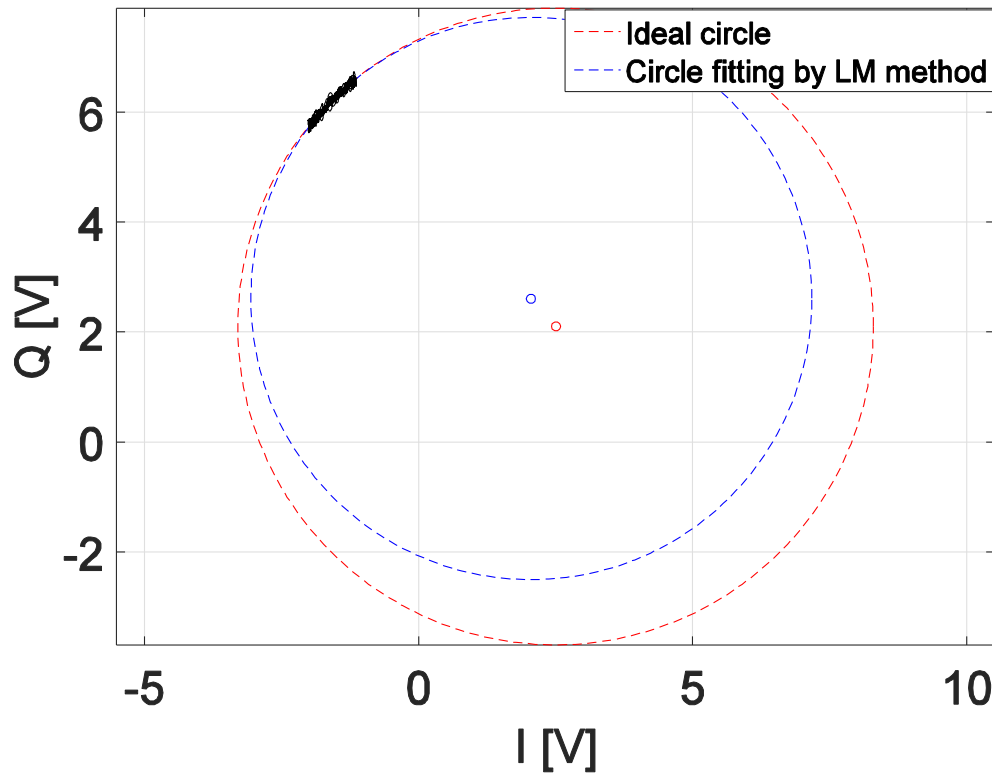


Figure 7.2 Replication of Levenberg-Marquardt method based circle fitting on the very short arc. The operating frequency is 2.4GHz. The nominal displacement simulated is 2 mm, which is equivalent to 3.2% of a full circle. A 30dB white Gaussian noise (AWGN) was added to baseband signals [111].

Some other features including the feature terms in [4] are presented in Table 7.1. Most of these features were reported in the literature for vital signal classification. In the first phase, 20 sets of data were taken in different days and beginning part of the data was saved for training. Seven sets of data from each subject were tested using a Bayesian classifier, and the results are shown in a confusion matrix in Table 7.2 showing the false detection.

Table 7.2 indicates that there is a need for hardware improvement so that additional features such as fractal or complexity analysis can be used. Poor signal to noise may undermine the presence of distinguishable patterns in different episodes of breathing cycle. The transition periods of exhaling and inhale contain important information about the breathing dynamics. To preserve this information the system needs to be low noise and high gain. These two-subject's data were collected in multiple days. The breathing rate and depth were very similar in values. The summation of feature values was overlapping. So the algorithm could not distinguish the subjects based on the features listed in Table 7.1. A

proposed DC management and DR improvement technique are presented in Figure 7.3. Programmable National Instruments (NI) data acquisition (DAQ) NI USB6009 is used in this topology. The same device is used for recording data. So, the additional voltage source is not required. The DAQ output can be used as an automatic gain control and DC offset removal. However, implementation of this topology requires voltage subtraction capability or a difference amplifier in the baseband circuit.

Table 7-1 Features for unique identification

Breathing Frequency	$Mean (1/BC_i)$ BC_i : The i th breathing cycle
Power spectral density	E denotes the expected value, T is a time interval, f indicates frequency, and x(t) is signal component whose power spectral density is to be determined. The frequency of peak was selected as one of the features.
Rate variability	$Variance (1/BC_i)$ BC_i : The i th breathing cycle
Breathing Depth	$Mean (D_{mx} - D_{mn})$ D_{mx}, D_{mn} : Inhale peak, Exhale nadir

Table 7-2 Unique identification without gain improvement for close pairs subjects

	S1	S2	% False
S1	4	3	42
S2	2	5	28

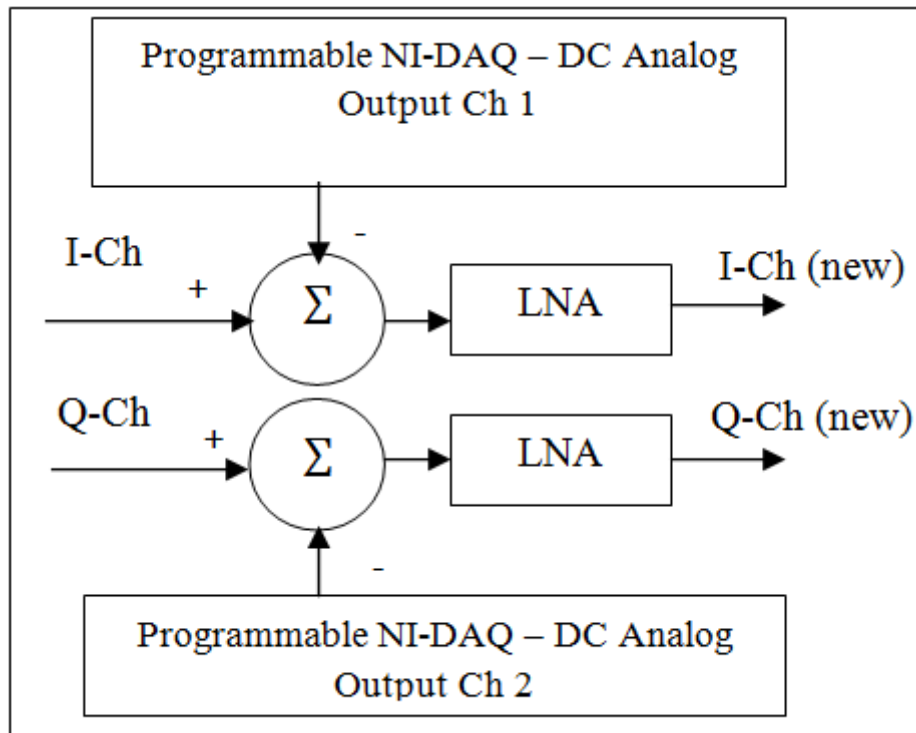


Figure 7.3 Proposed method for dynamic range improvement. Required DC offset cancellation margin is calculated in the beginning and subtracted/added from the down-conversion output which enhances the margin of amplification without saturating LNA with lower gain. Table III shows some gain improvement in two different target distances [111].

Table 7-3 Gain improvement with proposed DC-offset cancellation

Distance	Gain	Gain (new)	Improvement
.7 m	5	200	195
1 m	10	500	490

By enabling magnification of signal at a scale of 200-minute variations and features in a fraction of seconds (which are not degraded by noise) were recorded using the high DR system (Figure 7.3). The fractions of the breathing cycle were analyzed using wavelet

complexity measurement on 14 sets of data from the same subjects. The results are in Table 7.4.

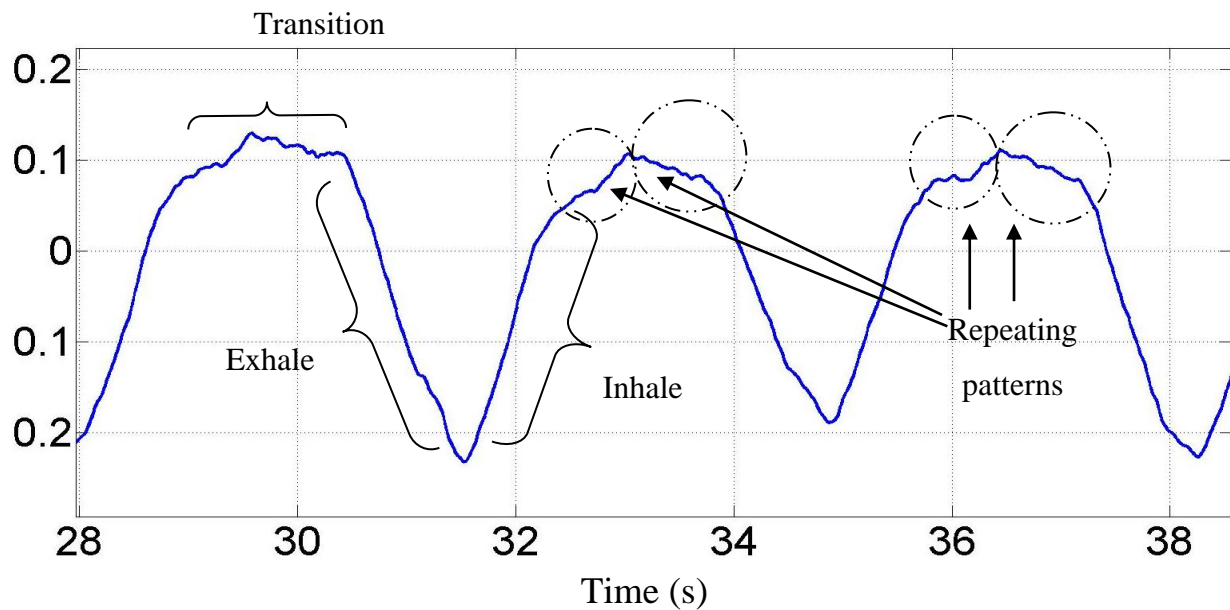


Figure 7.4 4 cycles of respiration signal from subject 1 measured using the proposed system in Fig.4. This high DR system allows zooming in the fractions of breathing cycle without distorting useful patterns. The intactness of these patterns produces good unique identification accuracy while using wavelet complexity analysis [111].

Table 7-4 Unique identification with gain improvement for close pairs subjects

	S1	S2	% False
S1	7	0	0
S2	0	7	0

7.3 Enhanced system and new algorithm

The subsequent sections do a detailed analysis of features that were discovered and studied for unique identification of a complex problem. The set consists of 6 people; some prior knowledge was taken into consideration that the subjects have similar or equal breathing frequency. A search for a distinct pattern rather than relying on rate or rate

variability or depth of breathing was required. The features were categorized in different domains called feature spaces.

7.4 Feature space 1:

7.4.1 Breathing Rate

An organism with lungs performs ventilation; this method is usually called breathing which includes inhalation and exhalation. This process is called respiration. The breaths occurring rate is usually calculated in breaths per minute. Breathing rate can be found by observation of some breathing cycle in a given amount of time. On the other hand, digital signal processing can also be used as shown in Figure 7.5 that FFT is used to find respiration rate.

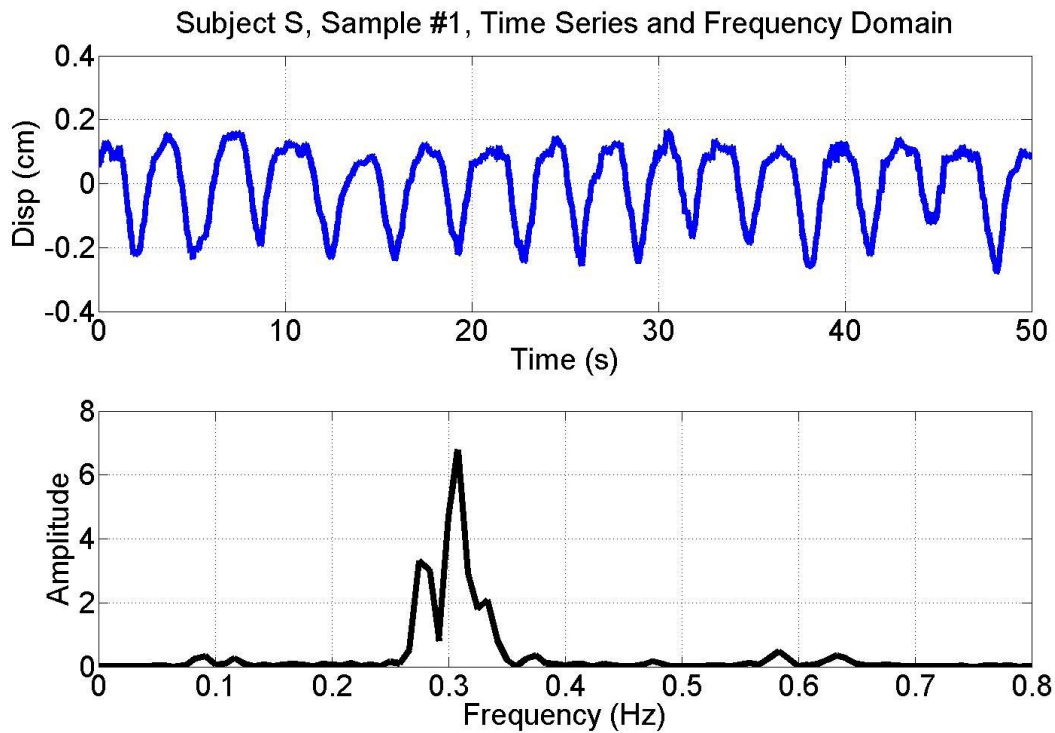


Figure 7.5 Finding the respiration rate using FFT

7.4.2 Average exhale-start cycle period T_{ex} :

During a breathing cycle, human subject inhales and take air inside the lung, when the subject feels lung volume is full he/she stops and prepares for exhaling. The point of this transitions can be found by detecting the displacement peak in Doppler radar signal. Let us assume in a data record there are N breathing cycles, and the transition peaks are denoted as p_{xi} , therefore, the set of such points will be,

$$P_{ex} = [p_{x1} \ p_{x2} \ p_{x3} \ p_{x4} \ \dots \ \dots \ p_{xN}] \quad (7.2)$$

The corresponding time stamp is denoted by tp_{xi} , therefore, exhale-start time period (time between two successive exhale start peak)

$$T_{exi} = tp_{x(i+1)} - tp_{x(i)} \quad (7.3)$$

The average exhale-start period is -

$$T_{ex} = \left(\frac{1}{N}\right) * \sum_i^N T_{exi} \quad (7.4)$$

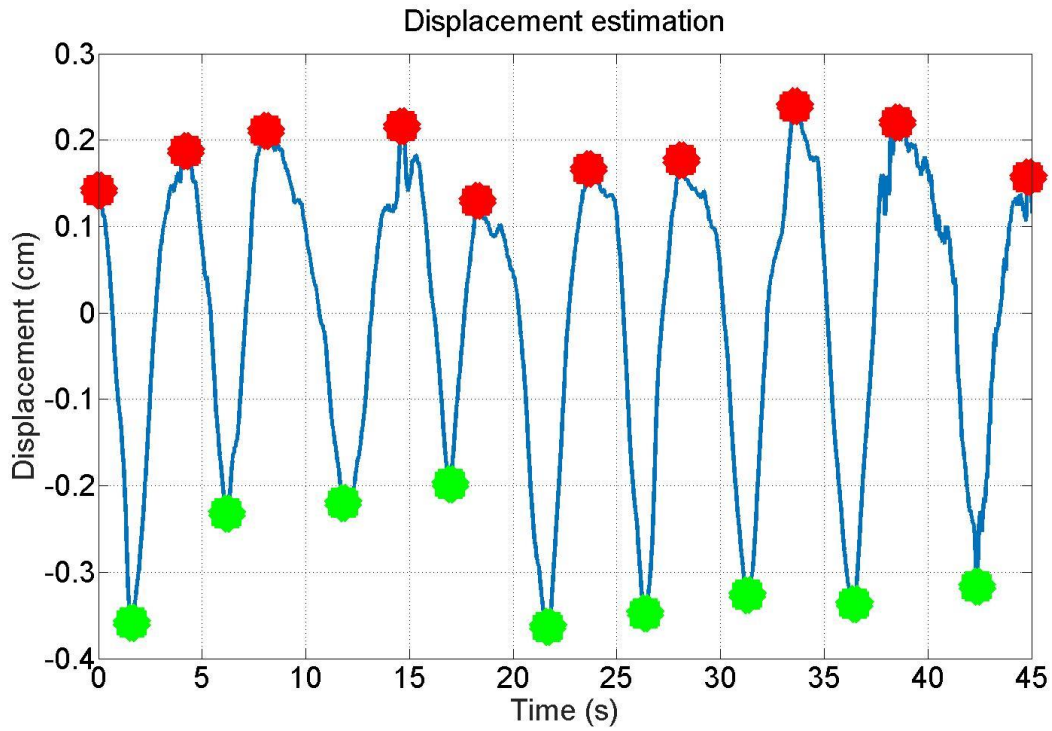


Figure 7.6 Breathing depth estimation after peak searching.

7.4.3 Standard deviation of exhaling-start period over N cycles

The standard deviation is a measure to quantify the amount of deviation or dispersion of a set of data values. A low standard deviation indicates that the data points tend to be close to the mean (also called the expected value) of the set, whereas a high standard deviation specifies that the data points are spread out over a wider range of values.

$$S_{T_{ex}} = \sqrt{\sum_{i=1}^N \frac{1}{N} (T_{exi} - T_{ex})^2} \quad (7.5)$$

7.4.4 Average inhale-start cycle period T_{in} :

The average inhales period can be defined as the average time required reaching two successive apexes in breathing curve. The apexes are defined as the transition points of exhaling and inhale.

For a record of N successive apexes, the average inhale cycle period can be defined as-

$$N_{in} = [n_{x1} \ n_{x2} \ n_{x3} \ n_{x4} \ \dots \ \dots \ \dots n_{xN}] \quad (7.6)$$

The corresponding time stamp is denoted by tn_{xi} , therefore, exhale-start time period (time between two successive exhale start peak)

$$T_{ini} = tn_{x(i+1)} - tn_{x(i)} \quad (7.7)$$

$$T_{in} = \left(\frac{1}{N}\right) * \sum_i^N T_{ini} \quad (7.8)$$

7.4.5 Standard deviation of T_{in} over N cycles

$$S_{T_{in}} = \sqrt{\sum_{i=1}^N \frac{1}{N} (T_{ini} - T_{in})^2} \quad (7.9)$$

7.4.6 Speed of exhaling

The quantized velocity of inhaling can be computed by quantizing and measuring the rate of displacement. The breathing mechanism may not resemble a constant inhale speed in its segments. However, an approximate average value can be measured by the following formulae.

The speed of exhaling = [Displacement measured successive apex to nadir] / Time required for exhaling.

$$v_{exi} = \frac{p_{x(i+1)} - p_{x(i)}}{tp_{x(i+1)} - tp_{x(i)}}$$

In N breathing cycles, the i^{th} transition peak is denoted as $p_{x(i)}$, and $tp_{x(i)}$ is corresponding time axis value. v_{exi} the speed of exhale.

7.4.7 Speed of inhaling

Like the speed of exhaling, inhale velocity can be approximated by quantizing and measuring the rate of displacement of course where the breathing curve is moving from nadir to apex. The following formulae can measure an approximate average value.

Speed of exhale = [Displacement measured successive nadir to apex] / Time required for inhaling.

$$v_{ini} = \frac{n_{x(i+1)} - n_{x(i)}}{tn_{x(i+1)} - tn_{x(i)}} \quad (7.11)$$

7.5 Feature space 2:

7.5.1 Ratio of [inhale – exhale] area to [exhale-inhale area], Inhale-exhale-trapezium / Exhale-inhale-trapezium

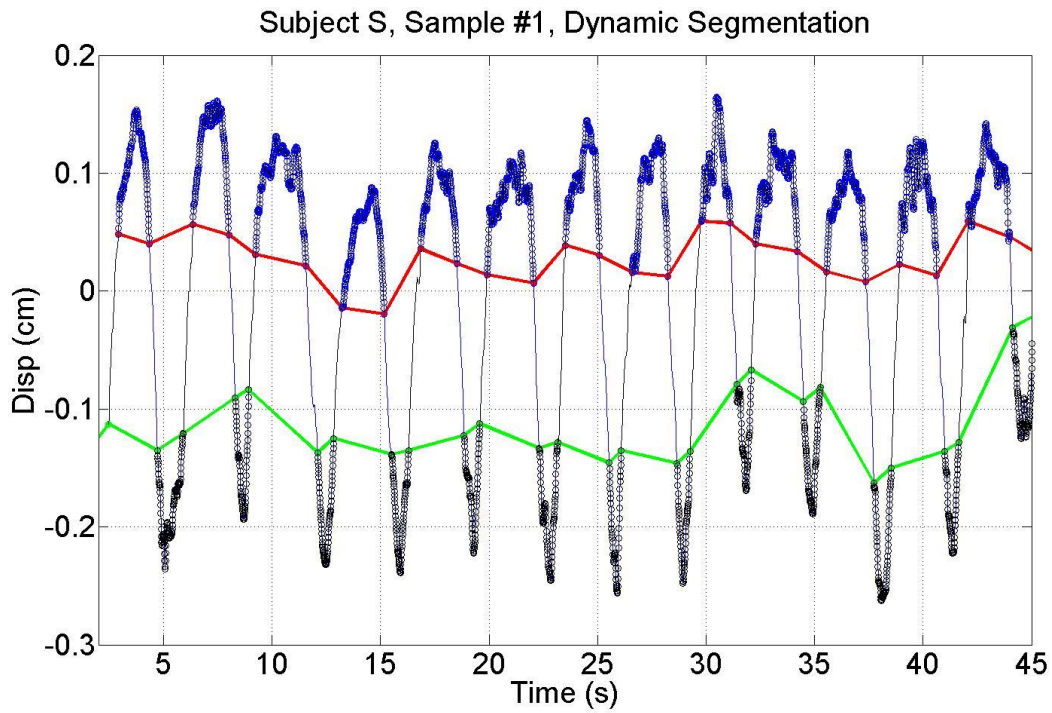


Figure 7.7 Dynamic segmentation of [30%-70%] displacement in each breathing cycle.

By dynamically evaluating the displacement and identifying points in the range of 30%-70% of both exhale and inhale episode will give four boundary points of a trapezium. Two sets of trapezia can be identified as shown in Figure 7.8.

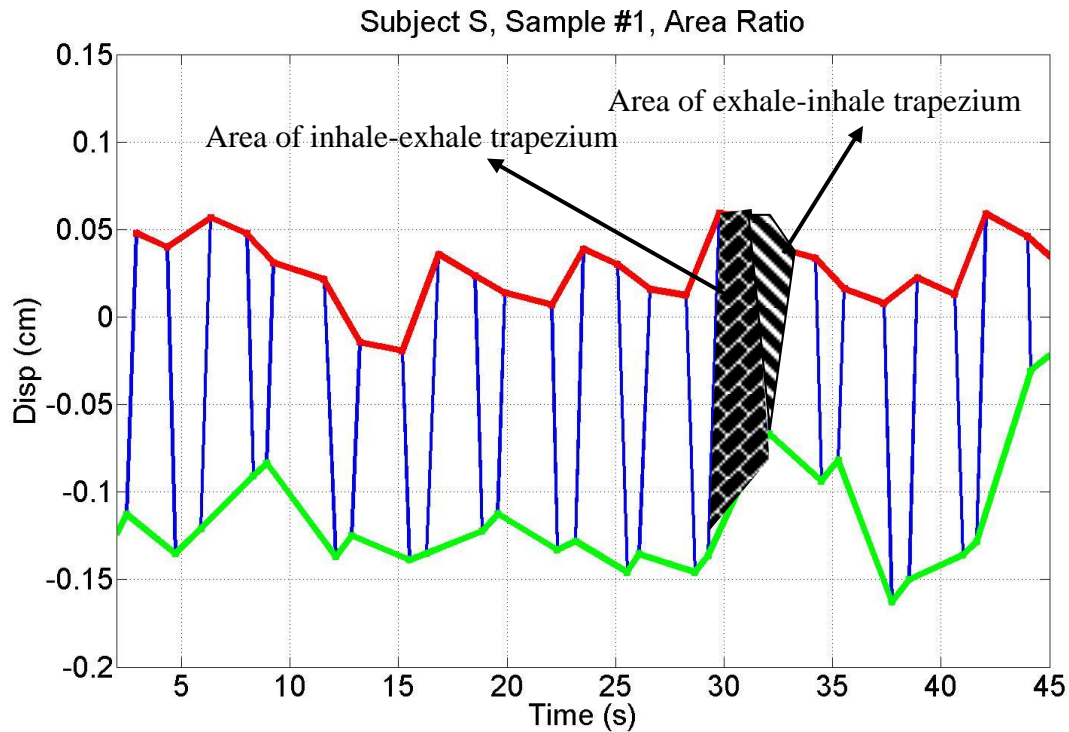


Figure 7.8 Dynamic segmentation of [30%-70%] displacement in each breathing cycle, and area ratio calculation, [inhale-exhale]/[exhale-inhale]

The algorithm for finding this ratio is described as below-

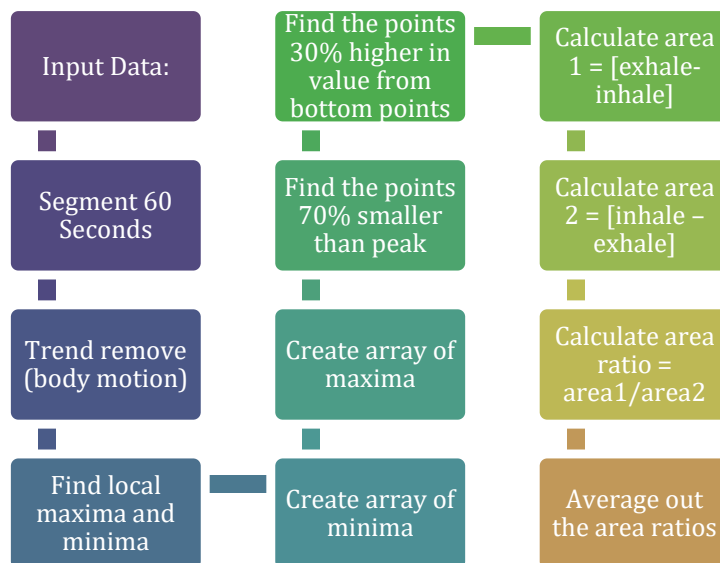


Figure 7.9 The summary of the algorithm (flow chart) of determining the ratio feature

Now the ratio of these two areas can be a useful feature because this feature relates a mechanism of how fast someone starts the next cycle of inhaling.

$$R = \frac{\text{Area Inhale} - \text{exhale} - \text{trapezium}}{\text{Area exhale} - \text{inhale} - \text{trapezium}} \quad (7.12)$$

$$r1 = \left(\frac{1}{N}\right) * \sum_i^N (A_{ex_i}/A_{in_i})$$

The R is an important feature that indicates how soon one starts inhaling after finishing exhalation. The feature R may correlate to the oxygen requirement of someone's body. Figure 7.8 shows the dynamic segmentation and area selection concept and Figure 7.9 illustrates the algorithm for ration calculation.

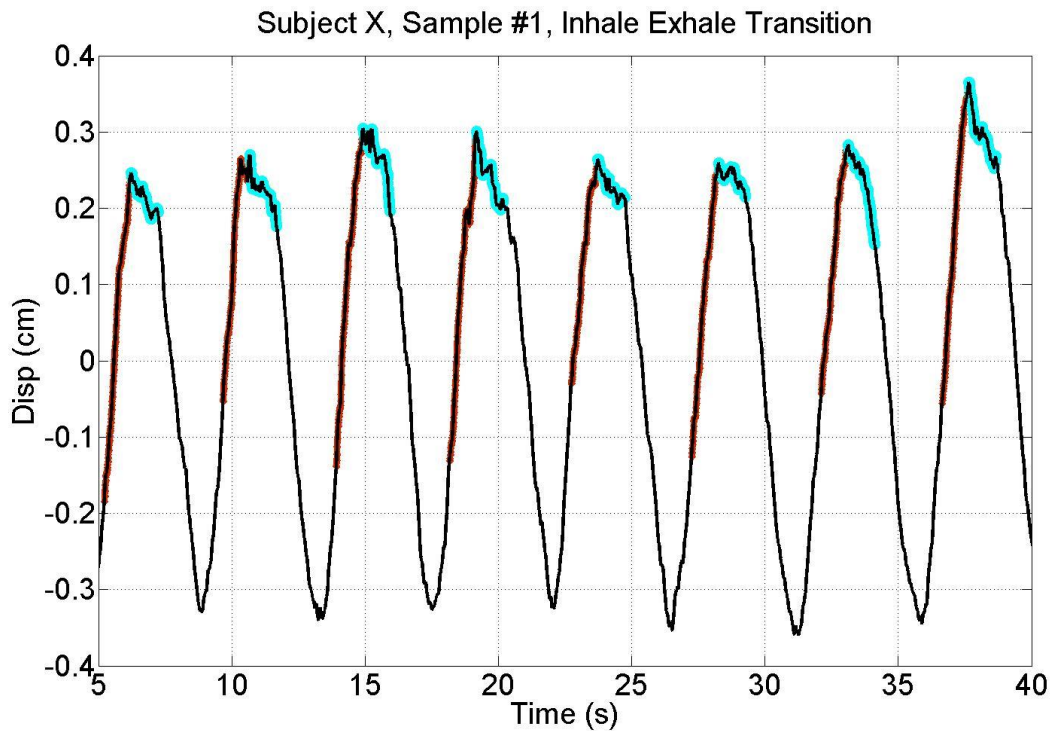


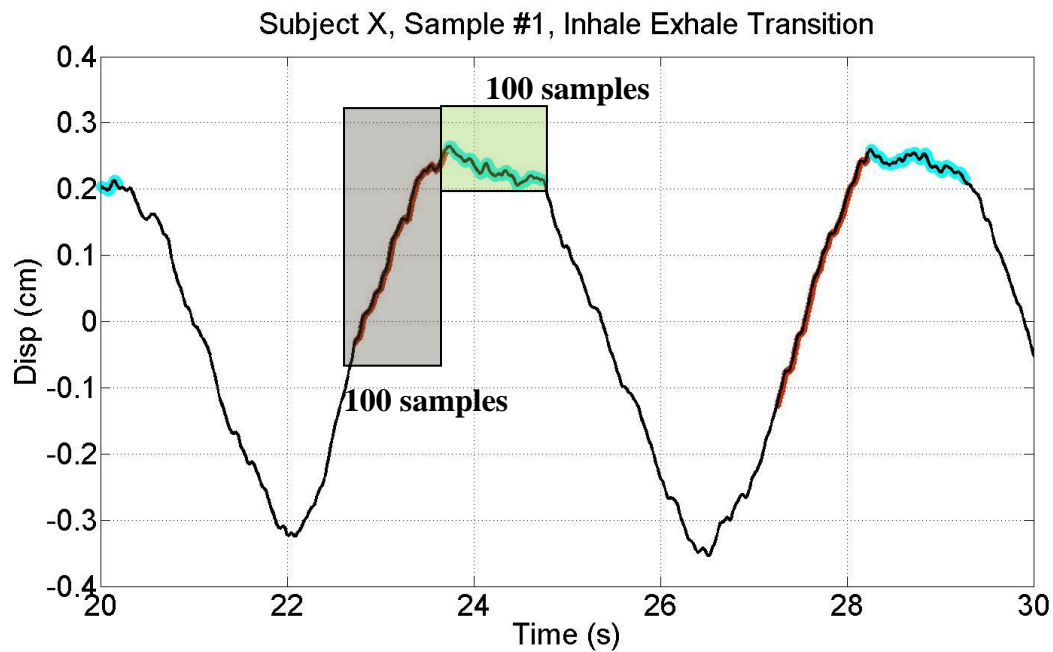
Figure 7.10 Signal pattern which relates to the dynamics of breathing near the points where exhale- inhale transition occurs.

7.6 Feature space 3:

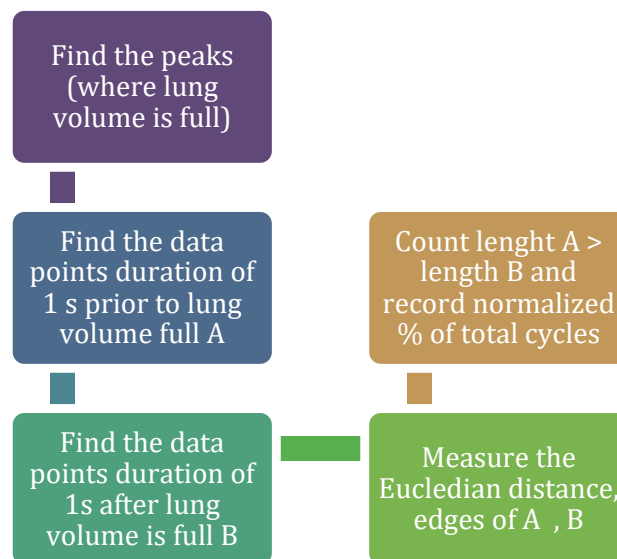
7.6.1 Signal complexity prior and after lung volume full

By observation on multiple data from multiple people, it was significant that some subject shows some unique patterns. By carefully studying the breathing mechanism right

after and before the apex (full-lung-volume) yields some interesting result. Some subjects tend to rest longer than others.



(a)



(b)

Figure 7.11 a) shows the color coded 100 samples prior and after the apex occurs. This apex is considered as the full lung volume; exhalation starts from apex; **b)** depicts the summary of the algorithm (flow chart) of determining the signal feature near breathing transition (exhale-inhale handover)

The resting behavior is slightly different as well. This behavior can be characterized in many ways. A very simple way is to use Euclidian distance as follows-

$$r2 = \left(\frac{1}{N}\right) * \sum_i^N (da_i/dp_i) < 1 \quad (7.13)$$

where da is Euclidian distance from apex to the point 100 samples (1 second) after, dp is distance from apex to the point 100 samples prior, $r2$ is the feature. This feature is unit less and averaged on N cycles in a respiration data sample.

7.7 Identify one person out of a group of people

One possible application of unique identification is identifying one single person out of many. The idea is presented in the following figure. If a group of person is tested can one single person (C) be found out from the group using prior knowledge?

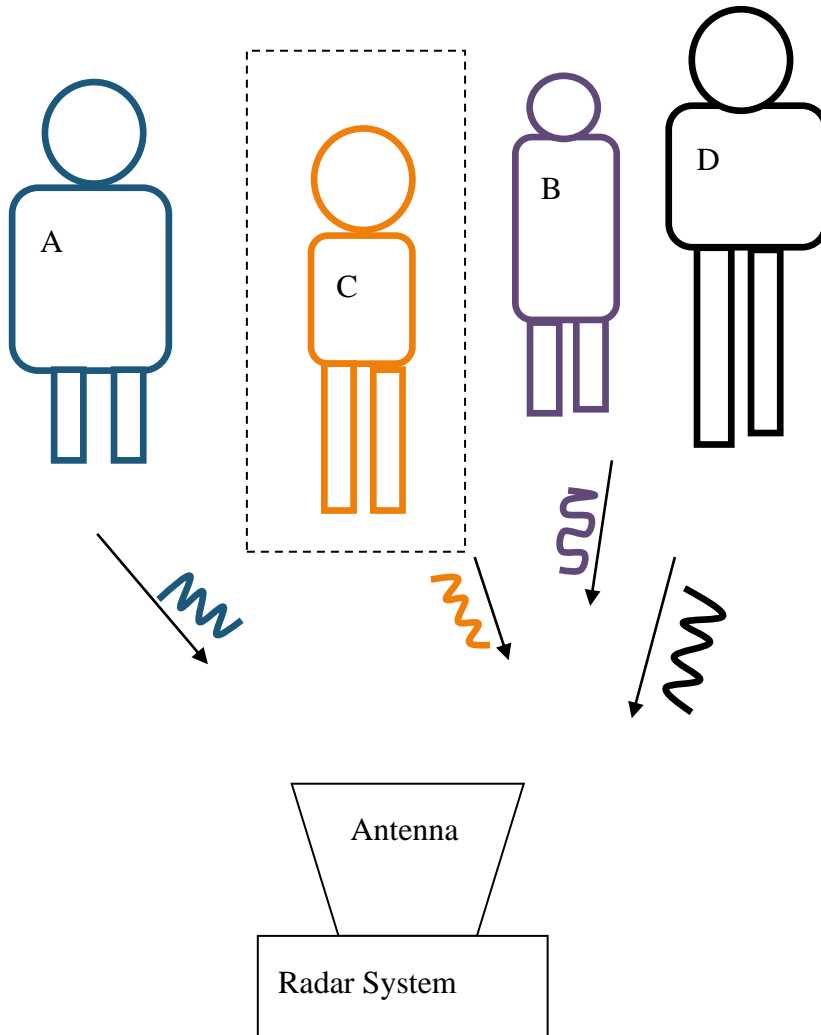


Figure 7.12 Hypothetical setup of a system where one individual is identified out of a group.

There are some distinct patterns in one individual that single out the individual from many. For example, Figure 7.13 shows individual who is very special in having $da < dp$ 100%

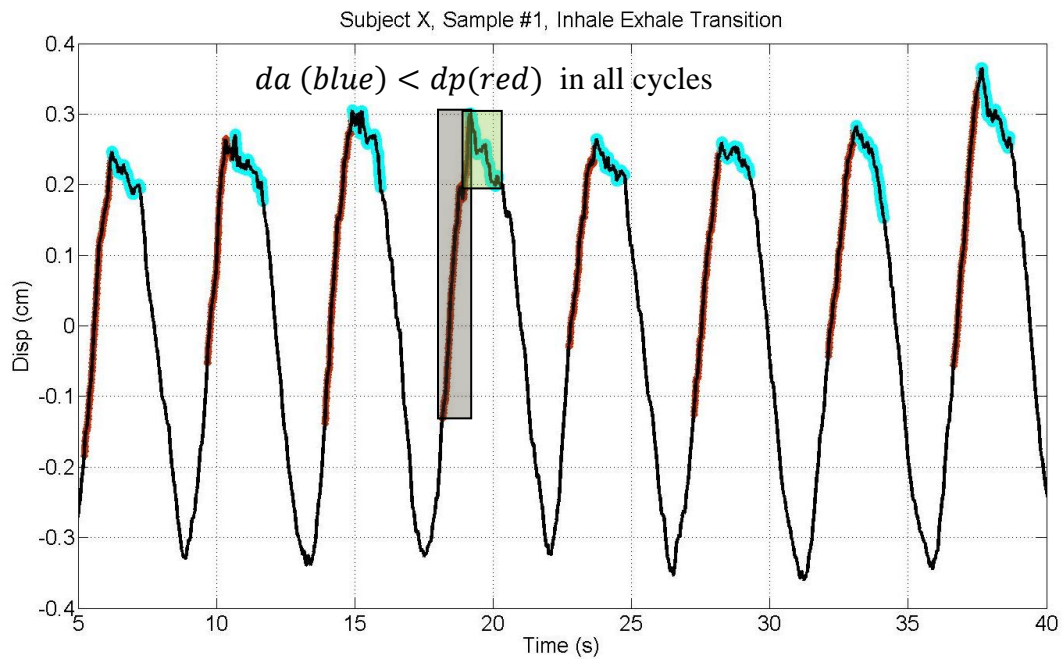


Figure 7.13 Signal pattern which relates to the dynamics of breathing near the points where exhale- inhale transition occurs. This subject shows a constant pattern of slow-down in transition.

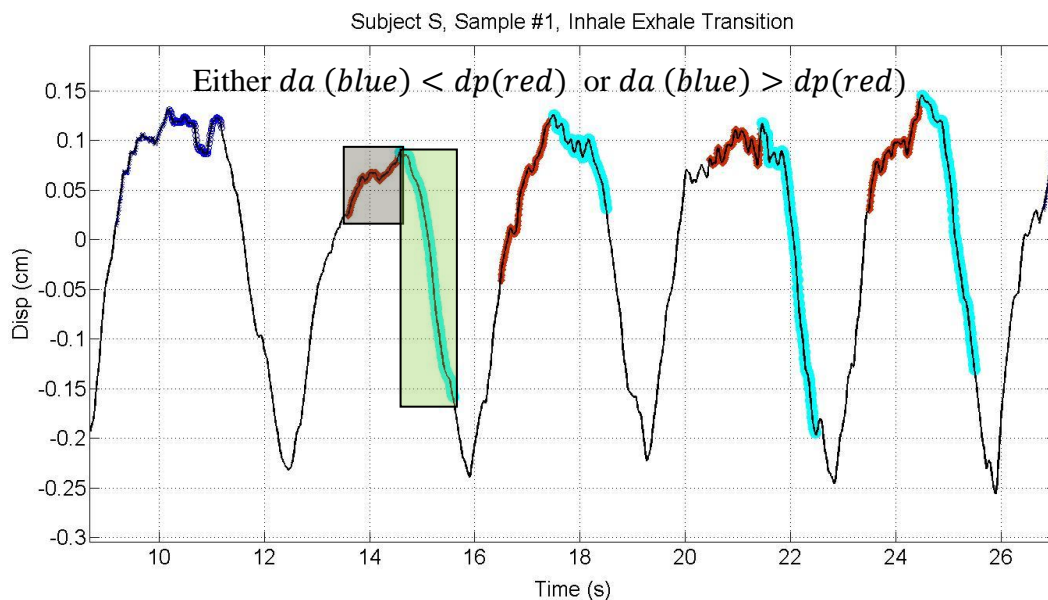


Figure 7.14 There is no fixed pattern; rather the subject shows variable nature, slow or fast either.

of the cycles, whereas, subject S (and other subjects) shows the random relation of da , dp . This feature uniquely distinguish subject X from others.

7.8 Identify a group of people from many

A group of people can be identified based on a specific feature value. For instance, the ratio of the inhale-exhale area to exhale-inhale area is tabulated for some data in Table 7-5, and the corresponding range is found. Depending on this range value we can find a group of people out of many. For instance, a value of 1.79 would give us S3/S4/S5 out of six subjects.

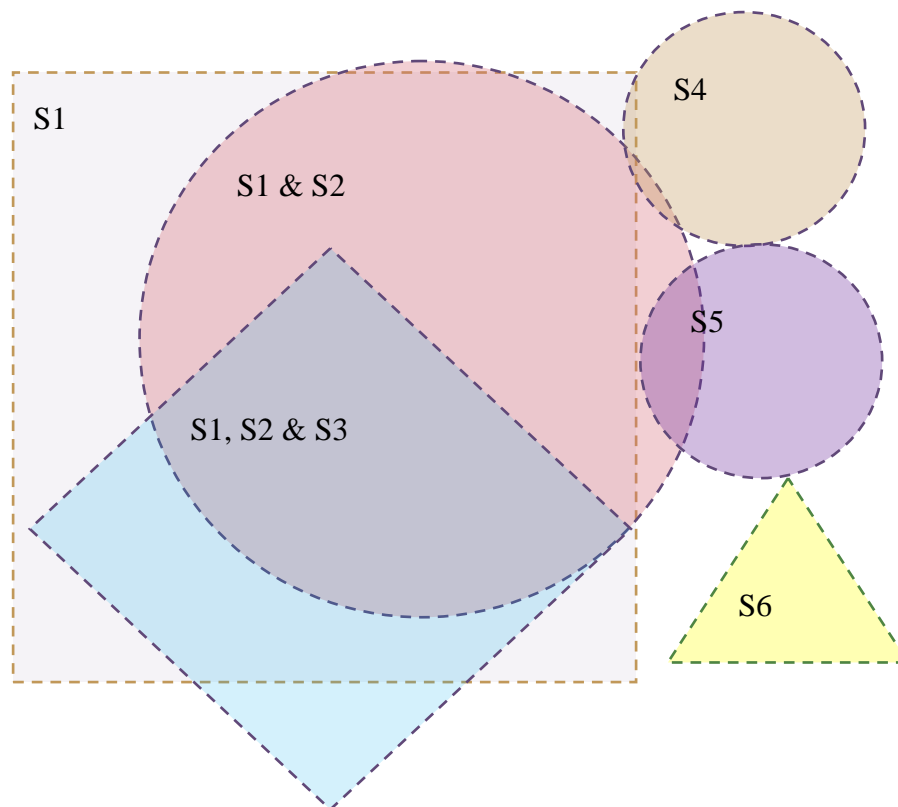


Figure 7.15 shows hypothetical class boundaries of subjects S1 through S6. These boundaries have been found by training data and fusing some features and taking a weighted average. The ranges of the feature values overlap which means we can identify a group of people (if not an individual) from a larger set.

Evaluating any recorded data and listing the feature value can be compared to previously saved range values. A group of people may represent the same value.

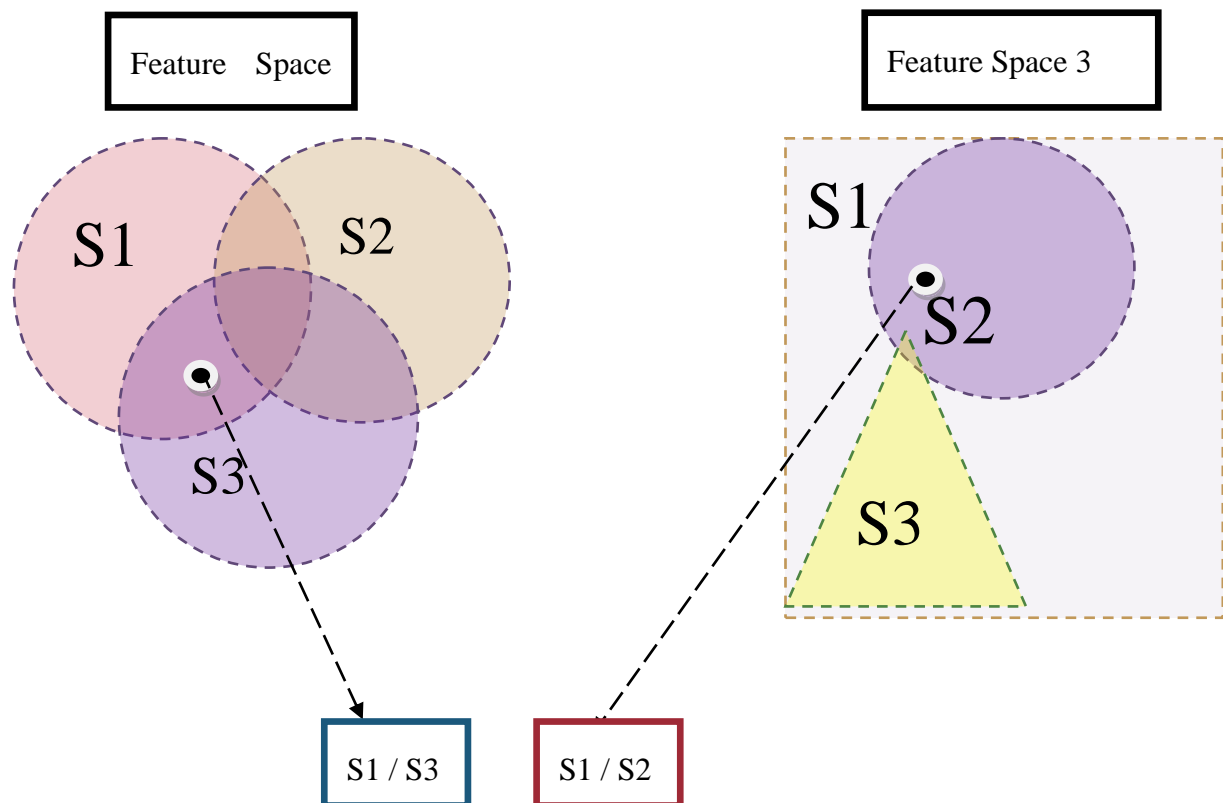
Table 7-5 Ratio of [inhale – exhale] area to [exhale-inhale area] – Feature space 2

S1	S2	S3	S4	S5	S6
1.1- 1.45	1.20 – 1.40	1.60 – 2.20	1.72 – 2.10	1.4 - 2.0	0.95 – 1.35

For example, in Figure 7.15 a feature value in the common area for S1/S2/S3 may indicate that the group has been found out of many.

7.9 Uniquely identify everyone

Majority vote criteria can be used to shrink down the groups to find out a specific person from a group.

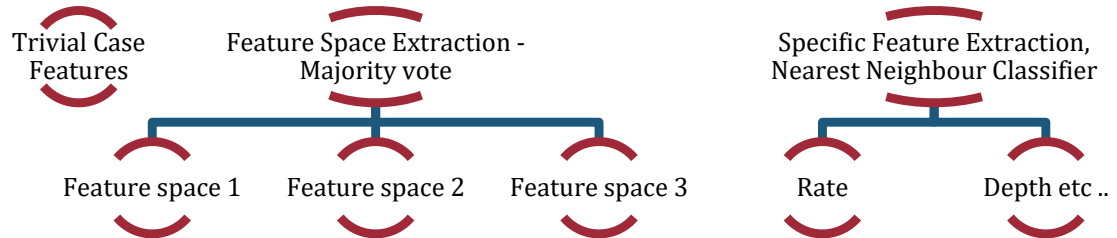


Decision: Majority common vote: S1

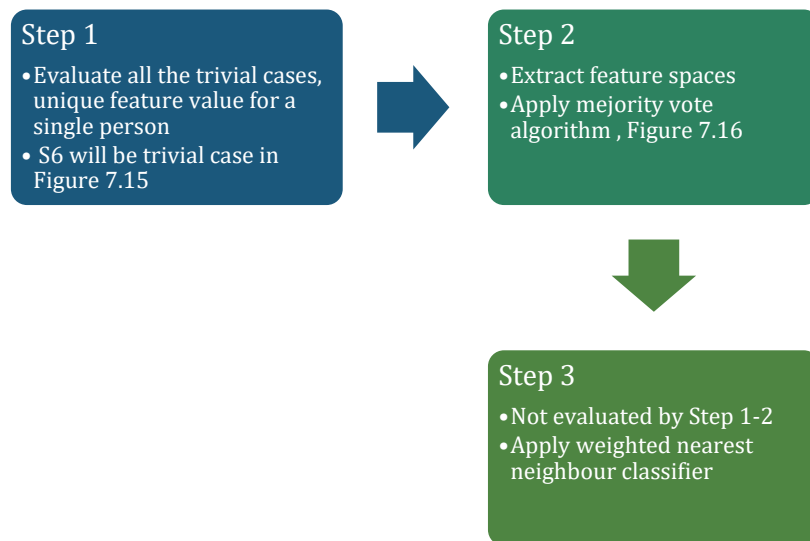
Figure 7.16 Majority vote concept from multiple feature space is illustrated. A test data evaluates to the class of S1/S3 in feature space 2. However, same test data evaluates to S1/S2 in feature space 3. Now, the majority vote goes to S1. The decision is made based on most likely probability.

Table 7-6 Fraction of times inhale-exhale transition speed is greater than unity – Feature space 3

S1	S2	S3	S4	S5	S6
0.25 – 0.60	0.75-0.95	0.50 – 0.80	0.3-0.6	0.1-0.7	0.4 – 0.6



(a)



(b)

Figure 7.17 a) shows the stages of feature extraction for identifying one person trivially from a group, a group of people from many, and uniquely identifying an individual from a group of people, b) shows steps to evaluate identification. The average value of each feature was calculated and saved in the database in the training process. Table 7-7 shows the collection of training data.

Table 7-6 lists range of values of six subjects in feature space 3. Table 7-5 indicates of feature space 2. By taking intersection set of smaller groups will make the identified group even smaller (maybe one single person). If required in next step nearest neighbor classifier can be used using the summation features in space 1, such as rate, the speed of exhaling, etc.

Table 7-7 Training data collection from subjects – October 10 – October 20, 2016

	S1	S2	S3	S4	S5	S6
Day-1	1	0	0	0	0	0
Day -2	1	0	1	0	0	0
Day -3	1	1	1	0	0	0
Day -4	1	1	0	1	0	0
Day -5	0	0	1	1	1	1
Day -6	0	0	0	0	1	1
Total	4	2	3	2	2	2

Total training data = 15 sets of 60 seconds.

Once training data were collected and features were evaluated and saved, the testing process began. In the testing process, 85 data value from multiple subjects were taken, and the system was evaluated for its performance.

Table 7-8 Training data collection from subjects – October 21 – November 20, 2016

	S1	S2	S3	S4	S5	S6	%
S1 (20)	14	0	0	0	4	2	70%
S2 (14)	0	14	0	0	0	0	100%
S3 (13)	0	0	13	0	0	0	100%
S4 (15)	0	0	0	15	0	0	100%
S5 (7)	0	0	0	0	7	0	100%
S6 (5)	0	0	0	0	0	5	100%

The confusion matrix table in Table 7.8 shows the results and success of the system.

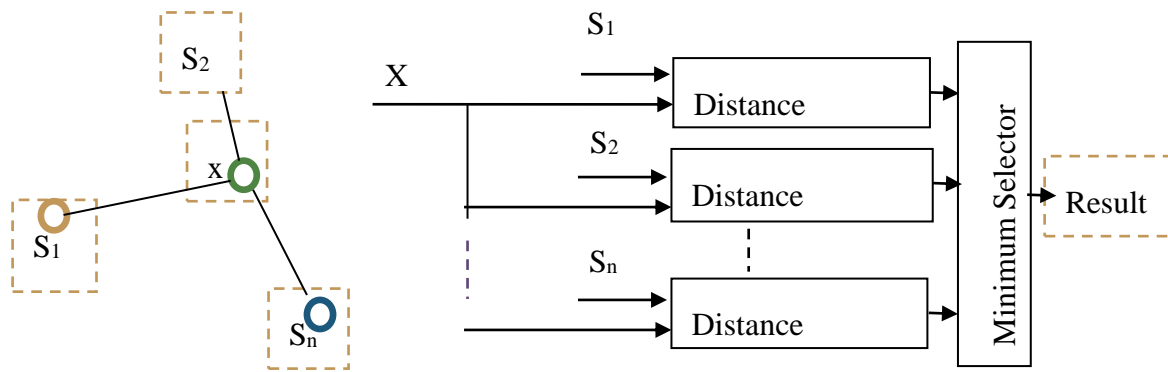


Figure 7.18 A minimum distance classifier was used if the testing data did not identify the person in stage 1 and 2. In this figure S_1 through S_n are the sum of the feature values in feature space 1 and the each point value indicates individuals in the database system. The data point is evaluated on the same feature space, and Euclidian distance is calculated to find the minimum and make decision whoever is the closest match. S_2 is closest, in this case; the identification result will be subject #2.

7.10 Conclusion:

The results prove that there is good promise in radar-based unique identification. The challenges remain in the fact that there might be overlapping feature values and the current algorithm may produce an error. However, this does not limit the system's use in local identification system rather than a global fingerprint. The advantages of such systems are many, including low complexity system. Since the unique identification is made based on vital signs, this system provides health information alongside.

CHAPTER 8. RF UNIQUE IDENTIFICATION CHALLENGES AND FUTURE WORK

8.1 Introduction

The proposed Doppler radar-based unique identification system is subject to further improvements. The critical reviewers often wonder what will be the efficiency and accuracy of such system. Another concern is minimum detection time. Is there a fundamental breaking limit of the proposed algorithm? What future measures can be taken to improve the accuracy of the system? This chapter presents some insights on the investigation of some of these crucial questions.

8.2 Accuracy Vs. detection time

Experiments were done to see how the unique identification accuracy is affected as sample time is varied. The results varied person to person showing a common trend. Many experiments may lead to a conclusion. However, there were some important findings. The lower limit of sample time is approximately 20 seconds. Having a 20-second sample size yields different success rate for a different person. However, with increasing time the accuracy tends to increase.

The experiment results are presented in subsequent figures.

Table 8-1 Accuracy and breakdown testing with varied testing time on subject #2

Time(s)	# Trial	# Success	% Success
60	8	8	100
50	8	8	100
45	8	8	100
40	8	8	100
35	8	7	87.5
30	8	7	87.5
25	8	7	87.5
20	8	7	87.5

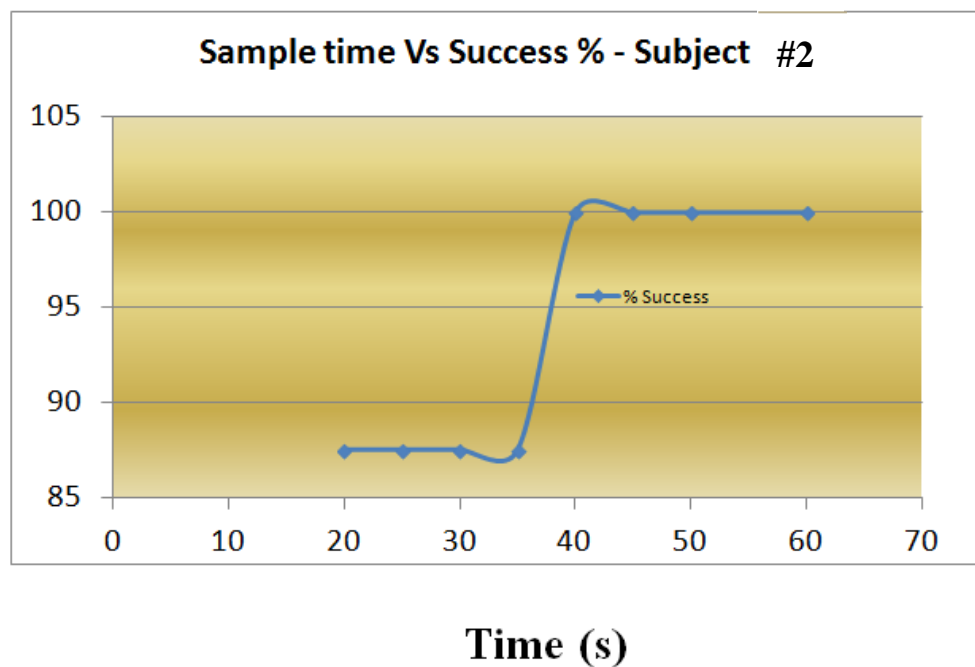


Figure 8.1 Plot of the data in Table 8.1 shows sample-time versus detection accuracy curve for subject #1. Algorithm fails to run if sample time is less than 20 s.

Table 8-2 Accuracy and breakdown testing with varied testing time on subject #3

Time(s)	# Trial	# Success	% Success
60	6	6	100
50	6	6	100
45	6	6	100
40	6	5	83.33
35	6	5	83.33
30	6	5	83.33
25	6	5	83.33
20	8	Fail	NA

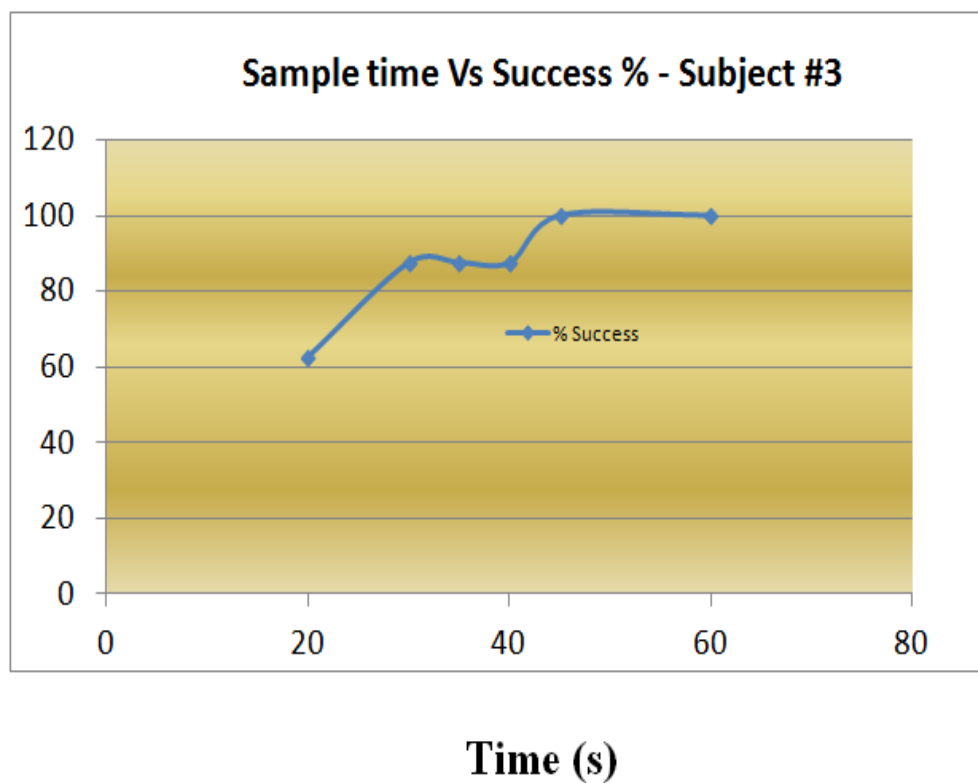






Figure 8.2 Plot of the data in Table 8.2 shows sample-time versus detection accuracy curve for subject #3

8.3 Low success rate subject

Some results of one of the subject showed lower detection rate. From accuracy versus detection time, it was logical to think that with increased sampling period accuracy will increase. The identification results for Subject #1 showed poor performance. Longer sample time was taken to examine if the results improve. With sample time 2 minutes and 3 minutes, the results were improved. However, one test with 4 minutes rather failed.

Table 8-3 Longer sample-time experiment for low success-rate subject

Trials	3	1	2	1
Success/Fail				
Time (s)	60	120	180	240

This table shows that even longer sample size does not guarantee perfect identification. So, no conclusion can be drawn for this subject, and increased sample time may not necessarily increase success rate which raises the question whether the unique patterns hold. In most cases, the answer is yes. One subject was tested six months later, and the system could identify the subject. The search for unique features should never put to an end. This dissertation further did some studies on the minor component analysis of higher frequency components. Since respiration signal is very strong, that part is filtered out using a proper set of filters. More investigation was performed on the data. This subject is often misclassified with another subject. This dissertation mainly focused on the features that can be described by some physical phenomena or patterns apparent in time domain signals. However, high-frequency components may also have unique signatures. Two-dimensional principal component analyses tend to give some new information which may be visible in the frequency domain.

8.3.1 Frequency analysis of minor components.

Two-dimensional principal component analyses give major and minor components. The variation in minor components may relate to radar cross section and high-frequency components of respiration-heart signal modulation. The steps are described here-

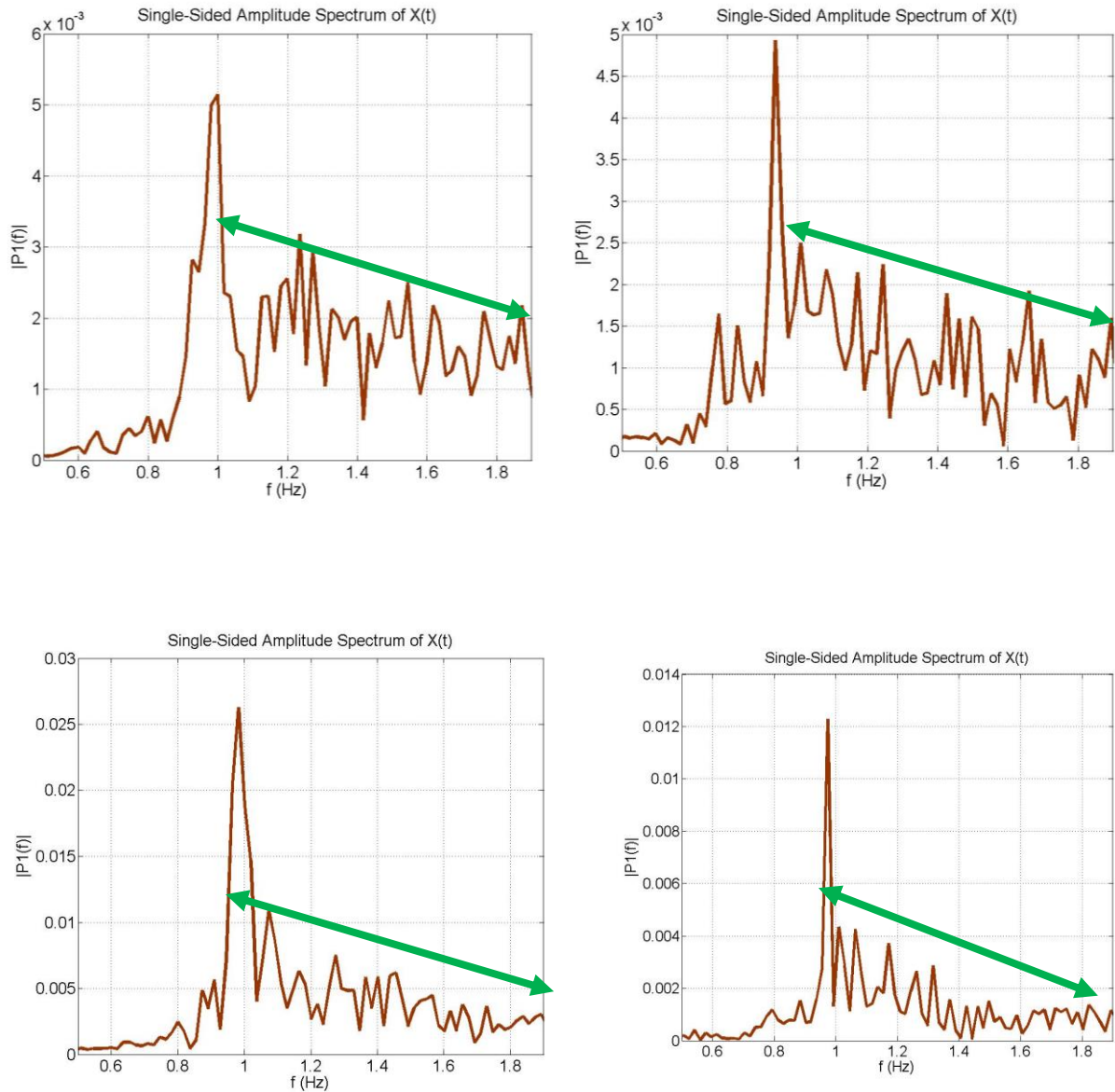


Figure 8.3 This figure shows frequency domain analysis of minor components for subject #1. There is a definite pattern visible. The data peaks at 1 Hz which is well contrasted with other frequency components.

Step 1: DC cancellation and respiration filtering

The mean value of both I and Q signals are calculated in post-processing, the low-frequency respiration component is filtered.

Step 2: Covariance matrix

The covariance matrix of the I and Q signals is created from the data points. The covariance matrix generalizes the notion of variance to multiple dimensions.

Step 3: Eigenvectors and eigenvalues

Upon finding the covariance matrix the eigenvectors and eigenvalues are found.

Step 4: Largest variance

The Eigenvectors are multiplied with data, and the output with the smallest variance is picked.

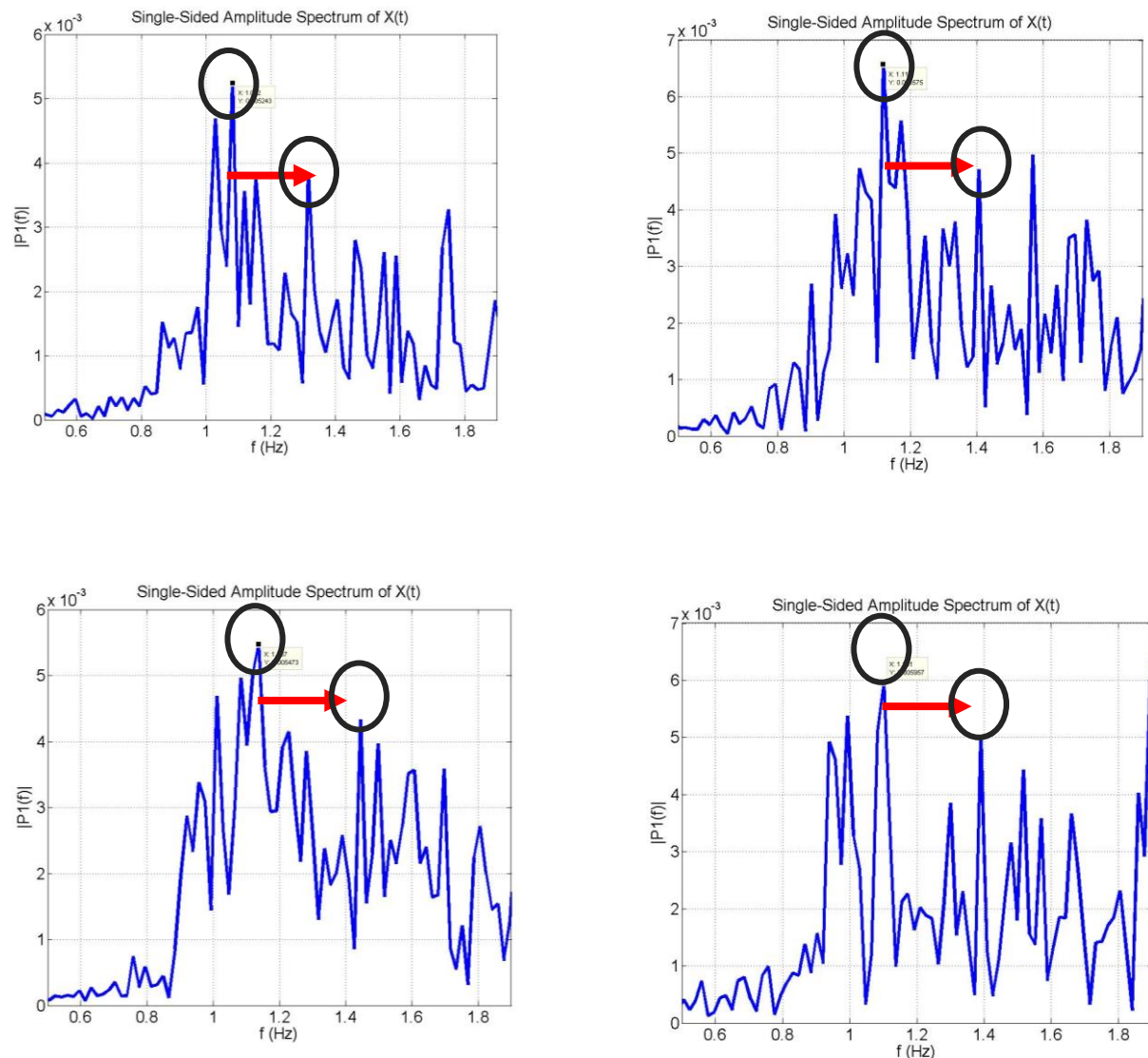


Figure 8.4 This figure shows frequency domain analysis of minor components for subject #4. If this data is compared to subject #1, a clear difference is visible. The data peak is at nearly 1.1 Hz. The other frequency components are relatively much more dominant than the subject #1. Also, there a second peak noticed almost same distance for all the four samples.

8.3.2 Algorithm for minor component feature for unique identification

The simplified algorithm is presented in the following flow chart.

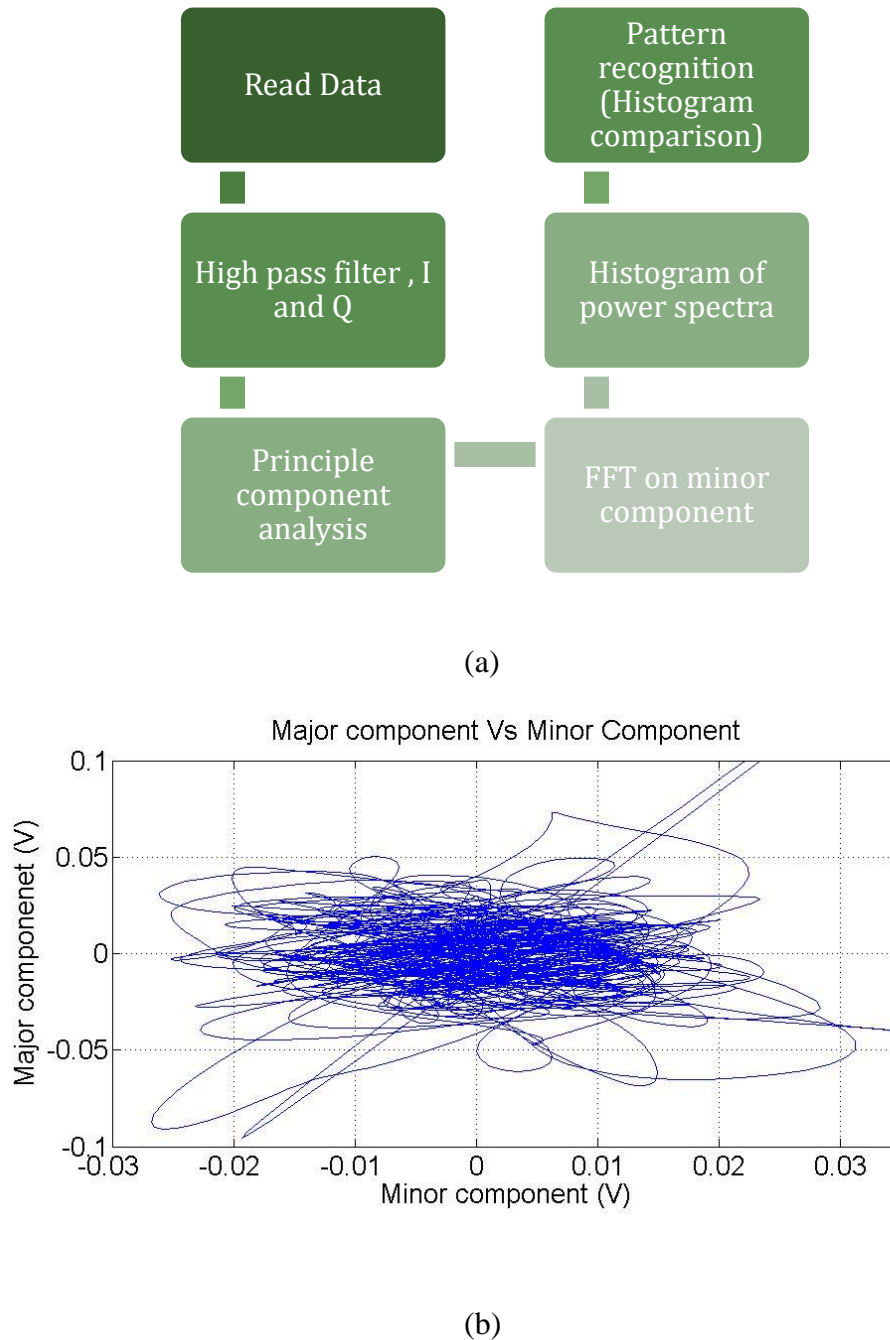


Figure 8.5 In (a) the algorithm of using minor component of demodulated high passed IQ data is presented for unique identification, (b) shows the plot of major versus minor components of high passed demodulated radar data for one of the subjects in the experiment.

Other biometric capabilities combine with those – gait analysis and others; radar cross section may be fused with radar information to enhance the success rate and make the system applicable to larger data set.

8.3.3 Biometric feature summary

Table 8-4 Biometric features [112]

No.	Feature	Technology	Description
1	DNA Matching	Chemical Biometric	The identification of an individual using the analysis of segments of DNA
2	Ear	Visual Biometric	The identification of an individual using the shape of the ear
3	Eyes - Iris Recognition	Visual Biometric	The use of the features found in the iris to identify an individual
4	Eyes - Retina Recognition	Visual Biometric	The use of patterns of veins in the back of the eye to accomplish recognition.
5	Face Recognition	Visual Biometric	The analysis of facial features or patterns for the authentication or recognition of an individual's identity. Most face recognition systems either use Eigenfaces or local feature analysis
6	Fingerprint Recognition	Visual Biometric	The use of the ridges and valleys (minutiae) found on the surface tips of a human finger to identify an individual
7	Finger Geometry Recognition	Visual/Spatial Biometric	The use of 3D geometry of the finger to determine identity
8	Gait	Behavioural Biometric	The use of an individual's walking style or gait to determine identity.

Table 8-5 Biometric features continued [112]

No.	Feature	Technology	Description
9	Hand Geometry Recognition	Visual/Spatial Biometric	The use of the geometric features of the hand such as the lengths of fingers and the width of the hand to identify an individual
10	Odor	Olfactory Biometric	The use of an individual's odor to determine identity.
11	Signature Recognition	Visual/Behavioural Biometric	The authentication of an individual by the analysis of handwriting style, in particular, the signature
12	Typing Recognition	Behavioural Biometric	The use of the unique characteristics of a person's typing for establishing identity
13	Vein Recognition		Vein recognition is a type of biometrics that can be used to identify individuals based on the vein patterns in the human finger or palm.
14	Voice / Speaker Recognition	Auditory Biometric	

8.3.4 Feature fusion topology

Additional features may help to achieve better performance than that with a single one. Different features can represent different characteristics of human uniqueness, and utilizing different features will have a constructive effect. Meanwhile, the advances of

algorithms in image processing (for instance, sparse coding) enable us to develop various recognition methods to cooperate with multiple features.

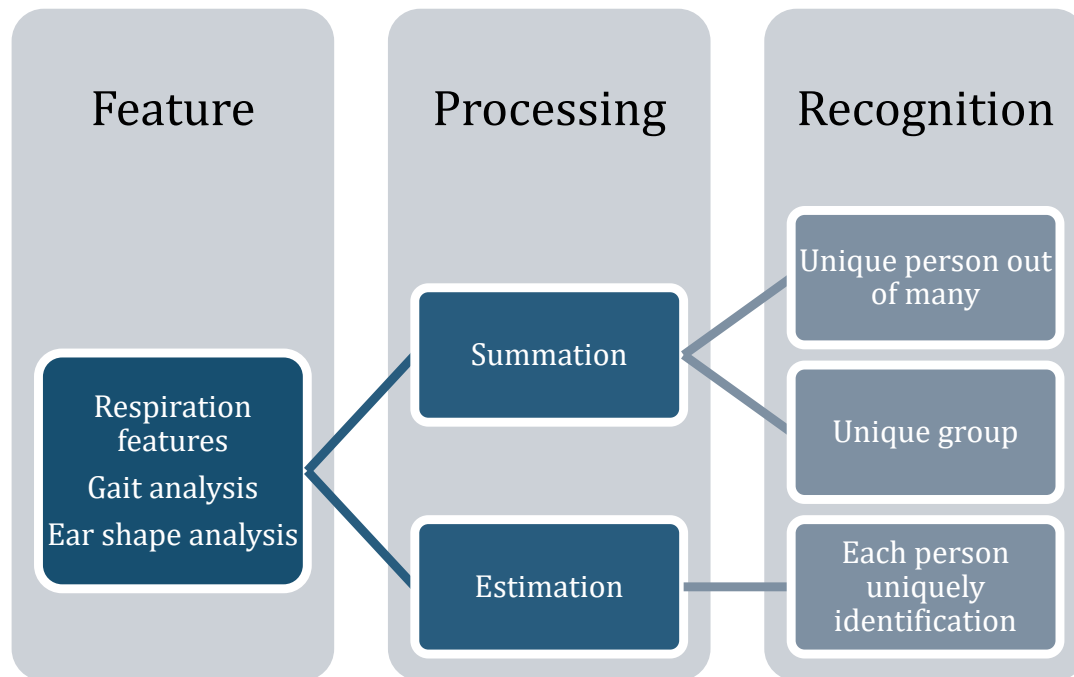


Figure 8.6 Algorithm shows the prospective feature fusion method that can be used to enhance the performance of radar-based unique identification

8.4 Conclusion

With the advancement of electronics technology and microwave communication, it is now possible to make cheap hardware, and we can process much data with low cost. Data have values because we can learn many physical phenomena by studying data. This dissertation presents hardware and algorithm development for a system that can collect human vital sign information and extract unique markers to identify patterns to recognize any specific illness or a specific person. 5G is emerging with the potential of making everything connected. Long-term data can be collected from human subjects, and further study can be done to learn a lot about human physiology. From an application point of view, this can be used to identify people for security reasons. The subject can artificially trick many biometric markers. However, the ones that are unique to people and has less control on those can be

used for unique identification. Continuous monitoring of human subject and collecting long-term data is possible using such system.

Artificial intelligence can be employed to perform analytics, optimization and extract knowledge from data. Long-term data can be useful for predictors of possible physiological change. Health can be monitored much well than ever without even going to hospitals and clinic. The radar offers many advantages over other systems. For example, identifying person beyond the wall is very lucrative. Radar measurement is non-invasive, and the subject does not have to be in a controlled environment which mitigates measurement bias. Direction to high SNR system design has been proposed in this work. Various features were identified to distinguish patterns among individuals. More study and more data collection will lead to finding more features. Intelligently fusing many features will make the system more robust and fault tolerant.

REFERENCES

- [1] J. C. Lin, "Microwave sensing of physiological movement and volume change: A review," *Bioelectromagnetics*, vol. 13, pp. 557- 565, 1992.
- [2] A. Droitcour, Non-contact Measurement of Heart and Respiration Rates With a Single-Chip Microwave Doppler Radar, Stanford: Stanford University, 2006.
- [3] G. Benchetrit, "Breathing pattern in humans: diversity and individuality," *Respiration Physiology*, vol. 122, pp. 123-129, 2000.
- [4] A. Rahman, E. Yavari, V. M. Lubecke and O. Boric-Lubecke, "Noncontact Doppler radar unique identification system using neural network classifier on life signs," in *IEEE Topical Conference on Biomedical Wireless Technologies, Networks, and Sensing Systems (BioWireleSS)*, Austin, TX, 2016.
- [5] A. Rahman, E. Yavari, X. Gao, V. Lubecke and L. Olga-Boric, "Signal Processing Techniques for Vital Sign Monitoring Using Mobile Short Range Doppler Radar," in *IEEE Radio Wireless Week*, San Diego, 2015.
- [6] I. Mostafanezhad, B.-K. Park, O. Boric-Lubecke, V. Lubecke and A. Host-Madsen, "Sensor Nodes for Doppler Radar Measurements of Life Signs," in *Microwave Symposium*, Honolulu, 2007.
- [7] I. Mostafanezhad, O. B. Lubecke, V. Lubecke and D. Mandic, "Application of empirical mode decomposition in removing fidgeting interference in Doppler radar life signs monitoring devices," in *Engineering in Medicine and Biology Society*, Minneapolis, 2009.
- [8] A. Singh and V. Lubecke, "Adaptive Noise Cancellation for Two Frequency Radar Using Frequency Doubling Passive RF Tags," *IEEE Transactions on Microwave Theory and Techniques*, vol. 61, no. 8, pp. 2975-2981, 2013.
- [9] A. Singh, *Subject Isolation and Non-stationary Clutter Rejection Using RF Backscatter – Tag Radar*, Honolulu: University of Hawaii at Manoa, 2012.
- [10] D. K. Barton, C. E. Cook and P. Hamilton, *Radar Evaluation Handbook*, Norwood, MA: Artech House, Inc., 1991.
- [11] M. I. Skolnik, "Radar," *Encyclopedia Britannica*.
- [12] C. Gu, "Short-Range Noncontact Sensors for Healthcare and Other Emerging Applications: A Review," *Sensors*, vol. 16, no. 8, 2016.
- [13] C. Li, V. Lubecke, O. Boric-Lubecke and J. Lin, "A Review on Recent Advances in Doppler Radar Sensors for Noncontact Healthcare Monitoring," *Microwave Theory and Techniques, IEEE Transactions*, vol. 61, no. 5, pp. 2046 - 2060, 2013.
- [14] A. Droitcour, V. Lubecke, J. Lin and O. Boric-Lubecke, "A microwave radio for Doppler radar sensing of vital signs," in *Microwave Symposium Digest, 2001 IEEE MTT-S International*, Phoenix, 2001.
- [15] "Doppler radar," Wikipedia, [Online]. Available: https://en.wikipedia.org/wiki/Doppler_radar. [Accessed

10 May 2017].

- [16] P. N. Pathirana, S. C. K. Herath and A. V. Savkin, "Multitarget tracking via space transformations using a single frequency continuous wave radar," *IEEE Trans. Signal Process.*, vol. 60, no. 10, p. 5217–5229, 2012.
- [17] M. Muragaki, S. Okumura, T. Sakamoto and T. Sato, "Non-contact respiration measurement using ultra-wideband array radar with adaptive beamforming technique for cancer radiotherapy," in *International Symposium on Antennas and Propagation (ISAP)*, 2016.
- [18] D. Matsumoto and Y. Kuwahara, "Heartbeat and respiratory monitoring using standing wave radar and independent component analysis," in *International Symposium on Antennas and Propagation (ISAP)*, 2016.
- [19] V. M. Lubecke, *Continuous Non-Contact Sensor Technology for Sleep Monitoring*, Manoa, 2013.
- [20] P. H. Martin and D. M. Unwin, "A Microwave Doppler Radar Activity Monitor," *Behavior Research Methods Instrumentation*, vol. 12, no. 5, pp. 517-520, 1980.
- [21] L. Ren, M. S. Hasan, S. K. Islam, A. E. Fathy and R. A. Fathy, "UWB baby and sleep apnea monitor," in *IEEE International Symposium on Antennas and Propagation & USNC/URSI National Radio Science Meeting*, San Diego, California, July 2015.
- [22] H. Ren, J. Shao, B. Arigong, H. Zhang, C. Gu and C. Li, "Application of phased array antenna for radar respiration measurement," in *Proceedings of the 2012 IEEE International Symposium on Antennas and Propagation*, 2012.
- [23] Z. Peng, J. M. Muñoz-Ferreras, Y. Tang, C. Liu, R. Gómez-García, L. Ran and C. Li, "A Portable FMCW Interferometry Radar With Programmable Low-IF Architecture for Localization, ISAR Imaging, and Vital Sign Tracking," *IEEE Transactions on Microwave Theory and Techniques*, vol. 65, no. 4, pp. 1334 - 1344, 2017.
- [24] J.-H. Oum, D.-W. Kim and S. Hong, "Two frequency radar sensor for non-contact vital signal monitor," in *IEEE Int. Microwave Symp. Dig.*, 2008.
- [25] D. Obeid, S. Sadek, G. Zaharia and G. El Zein, "Touch-less heartbeat detection and cardiopulmonary modeling," in *Int. Symp. Appl. Sci. Biomed. Commun. Technol. (ISABEL)*, 2009, 2009.
- [26] X. Gao and O. Boric-Lubecke, "AC Coupled Quadrature Doppler Radar Displacement Estimation," in *Microwave Symposium (IMS), 2015 IEEE MTT-S International*, Phoenix, AZ, 2015.
- [27] A. D. Droitcour, O. Boric-Lubecke, V. M. Lubecke, J. Lin and G. T. A. Kovacs, "Correlation Effect on ISM Band I/Q CMOS Radar for Non-Contact Sensing of Vital Signs," *IEEE MTT-S IMS2003 Digest*, vol. 3, pp. 1945-1948, 2003.
- [28] A. D. Droitcour, O. Boric-Lubecke and G. T. A. Kovacs, "Signal-to-noise ratio in Doppler radar system for heart and respiratory rate measurements," *IEEE Trans. Microw. Theory Techn.*, vol. 57, no. 10, p. 2498–2507, 2009.
- [29] C. Gu, Z. Peng and C. Li, "High-Precision Motion Detection Using Low-Complexity Doppler Radar With Digital Post-Distortion Technique," *IEEE Transactions on Microwave Theory and Techniques*, vol. 64, no. 3, pp. 961-972, 2016.
- [30] C. Gu, G. Wang, T. Inoue and C. Li, "Doppler radar vital sign detection with random body movement cancellation based on adaptive phase compensation," in *Microwave Symposium Digest (IMS)*, Seattle, 2013.
- [31] E. Yavari, B. Padasdao, V. Lubecke and O. Boric-Lubecke, "Packet radar spectrum recovery for physiological signals," in *Annu. IEEE Int. Eng. Med. Biol. Soc. Conf.*, Osaka, Japan, 2013.
- [32] W. Xu, C. Gu, C. Li and M. Sarrafzadeh, "Robust Doppler radar demodulation via compressed sensing," *Electron. Lett.*, vol. 48, no. 22, p. 1428–1430, 2012.
- [33] A. Tariq and H. Ghafouri-Shiraz, "Vital signs detection using Doppler radar and continuous wavelet transform," in *5th Eur. Conf. Antennas Propag. (EUCAP)*, 2001.
- [34] A. Droitcour, T. B. Seto, B. Park, S. Yamada, A. Vergara, C. El-Hourani, T. Shing, A. Yuen, V. Lubecke and O. Boric-Lubecke, "Non-contact respiratory rate measurement validation for hospitalized patients," in *31st Annu. Conf. IEEE EMBS*, Minneapolis, 2009.
- [35] E. F. Greneker, "Radar sensing of heartbeat and respiration at a distance with applications of the technology," in *Radar*, 1997.
- [36] C. Gu, Z. Salmani, H. Zhang and C. Li, "Antenna array technology for radar respiration measurement in motion-adaptive lung cancer radiotherapy," in *2012 IEEE Topical Conference on Biomedical Wireless*

Technologies, Networks, and Sensing Systems (BioWireless), 2012.

- [37] E. Yavari, H. Jou, V. Lubecke and O. Boric-Lubecke, "Doppler radar sensor for occupancy monitoring," in *Biomedical Wireless Technologies, Networks, and Sensing Systems (BioWireless)*, Austin, TX, 2013.
- [38] Y. Yan, C. Li, X. Yu, M. D. Weiss and J. Lin, "Verification of a non-contact vital sign monitoring system using an infant simulator," in *Annu. Int. Conf. IEEE Eng. Med. Biol. Soc. (EMBC)*, 2009.
- [39] I. Chouvarda, V. Rosso, M. O. Mendez, A. Bianchi, L. Parrino, A. Grassi, M. Terzano, S. Cerutti and N. Maglaveras, "EEG Complexity during Sleep: on the effect of micro and macro sleep structure," in *Annual International Conference of the IEEE EMBS*, Buenos Aires, Argentina, August 31 - September 4, 2010.
- [40] J. W. E. Brydnn and J. Lane, "Detection and Classification of Breathing Patterns". US Patent US 6,840,907 B1, April 2000.
- [41] M. Baboli, A. Singh, B. Soll, O. Boric-Lubecke and V. Lubecke, "Good Night: Sleep Monitoring Using a Physiological Radar Monitoring System Integrated with a Polysomnography System," *Microwave Magazine, IEEE*, vol. 16, no. 6, pp. 34-41, July 2015.
- [42] M. G. Amin, Y. D. Zhang, F. Ahmad and K. C. Ho, "Radar Signal Processing for Elderly Fall Detection," *IEEE Signal Processing Magazine*, vol. 33, no. 2, pp. 71 - 80, March 2016.
- [43] G. Sun, M. Kubota, M. Kagawa, N. Quang Vinh, A. Kurita and T. Matsui, "A screening method based on amplitude probability distribution analysis for detecting the disordered breathing using microwave radar respiration signals," in *Asia Pacific Microwave Conference Proceedings*, 2012.
- [44] G. R. Wang, H. G. Han, S. Y. Kim and T. W. Kim, "Wireless Vital Sign Monitoring Using Penetrating Impulses," *IEEE Microwave and Wireless Components Letters*, vol. 27, no. 1, pp. 94-96, 2017.
- [45] G. Vinci, S. Lindner, F. Barbon, S. Mann, M. Hofmann, A. Duda, R. Weigel and A. Koelpin, "Six-Port Radar Sensor for Remote Respiration Rate and Heartbeat Vital-Sign Monitoring," *IEEE Transactions on Microwave Theory and Techniques*, vol. 61, no. 3, pp. 2093-2107, 2013.
- [46] D. J. Cooper and M. D. Buist, "Vitalness of vital signs; and medical emergency teams," *Med. J. Austral.*, vol. 188, no. 11, pp. 630-631, 2008.
- [47] J. Kiriazi, O. Boric-Lubecke and V. Lubecke, "Radar cross section of human cardiopulmonary activity for recumbent subject," in *IEEE Annual Conference of Engineering in Medicine and Biology Society*, Minneapolis, Minnesota, 2009.
- [48] W. Massagram, N. Hafner, B. Park, V. Lubecke, A. Host-Madsen and O. Boric-Lubecke, "Feasibility of heart rate variability measurement from quadrature Doppler radar using arctangent demodulation with dc offset compensation," in *29th Annu. Conf. IEEE EMBS*, Lyon, France, 2007.
- [49] W. Massagram, N. Hafner and V. Lubecke, "Tidal volume measurement through non-contact Doppler radar with DC reconstruction," *IEEE Sensors Journal*, vol. 13, no. 9, p. 3397-3404, 2013.
- [50] P. C. Ivanov, A. Bunde, N. Amaral, S. Havlin, R. M. Baevsky, H. E. Stanley and A. L. Goldberger, "Sleep-Wake Differences in Scaling Behavior of the Human Heartbeat: Analysis of Terrestrial and Long-Term Space Flight Data," *Europhysics Letters*, vol. 48, no. 5, pp. 594-600, 1999.
- [51] C. Robert, C. Guilpin and A. Limoge, "Review of neural network applications in sleep research," *Journal of Neuroscience Methods*, vol. 79, pp. 187-193, 1998.
- [52] A. Singh, M. Baboli, X. Gao, E. Yavari, B. Padasdao, B. Soll, O. Boric-Lubecke and V. Lubecke, "Considerations for integration of a physiological radar monitoring system with gold standard clinical sleep monitoring systems," in *Engineering in Medicine and Biology Society (EMBC), 35th Annual International Conference of the IEEE*, Osaka, Japan, 3-7 July 2013.
- [53] J. Zhanga, X. Yanga, L. Luoa, J. Shaoa, C. Zhangb, J. Mab, G. Wangb and Y. L. d, "Assessing severity of obstructive sleep apnea by fractal dimension sequence analysis of sleep EEG," *Physica*, vol. A, no. 388, pp. 4407-4414, 2009.
- [54] M. Zakrzewski, A. Vehkaoja, A. S. Joutsen, K. T. Palovuori and J. J. Vanhala, "Noncontact Respiration Monitoring During Sleep With Microwave Doppler Radar," *IEEE Sensors Journal*, vol. 15, no. 10, pp. 5683 - 5693, 2015.
- [55] J. N. Hana, R. Schepersa, K. Stegenb, O. Van den Berghb and K. P. Van de Woestijnea, "Psychosomatic symptoms and breathing pattern," *Journal of Psychosomatic Research*, vol. 49, pp. 319-333, 2000.
- [56] C. Gu, R. Li, H. Zhang, A. Y. C. Fung, C. Torres, S. B. Jiang and C. Li, "Accurate Respiration Measurement Using DC-Coupled Continuous-Wave Radar Sensor for Motion-Adaptive Cancer Radiotherapy," *IEEE Transactions on Biomedical Engineering*, vol. 59, no. 11, pp. 3117-3123, 2012.
- [57] C. Gu, "An instruments-built Doppler radar for sensing vital signs," in *8th Int. Symp. Antennas; Propag.*

EM Theory (ISAPE), 2008.

- [58] J. W. Heal, "An Animal Activity Monitor Using a Microwave Doppler System," *Medical Biological Engineering*, vol. 13, no. 2, p. 317, 1975.
- [59] A. Singh, S. Lee, M. Butler and V. Lubecke, "Activity monitoring and motion classification of the lizard *Chamaeleo jacksonii* using multiple Doppler radars," in *Engineering in Medicine and Biology Society (EMBC), 2012 Annual International Conference of the IEEE*, San Diego, CA, 2012.
- [60] M. Mercuri, P. Karsmakers, P. Leroux, D. Schreurs and Beyer, "A. Real-time fall detection and tag-less localization using radar techniques," in *IEEE 16th Annual Wireless and Microwave Technology Conference*, Florida, April, 2015.
- [61] B. Y. Su, K. C. Ho, M. J. Rantz and M. Skubic, "Doppler Radar Fall Activity Detection Using the Wavelet Transform," *IEEE Transactions on Biomedical Engineering*, vol. 62, no. 3, pp. 865-875, Nov 2014.
- [62] L. Liu and S. Liu, "Remote Detection of Human Vital Sign With Stepped-Frequency Continuous Wave Radar," *IEEE Journal of Selected Topics in Applied Earth Observations and Remote Sensing*, vol. 7, no. 3, pp. 775-782, 2014.
- [63] B. Lohman, O. Boric-Lubecke, V. Lubecke, P. Ong and M. Sondhi, "A digital signal processor for Doppler radar sensing of vital signs," *IEEE Engineering in Medicine and Biology Magazine*, vol. 21, pp. 161-164, Sept 2002.
- [64] J. Tu, T. Hwang and J. Lin, "Respiration Rate Measurement Under 1-D Body Motion Using Single Continuous-Wave Doppler Radar Vital Sign Detection System," *IEEE Transactions on Microwave Theory and Techniques*, vol. 64, no. 6, pp. 1937 - 1948, 2016.
- [65] X. Yu, C. L. Li and J. Lin, "Two-dimensional noncontact vital sign detection using Doppler radar array approach," in *Microwave Symposium Digest (MTT), 2011 IEEE MTT-S International*, Baltimore, 2011.
- [66] C. Gu, G. Wang, Y. Li and I. T, "A Hybrid Radar-Camera Sensing System With Phase Compensation for Random Body Movement Cancellation in Doppler Vital Sign Detection," *Microwave Theory and Techniques, IEEE Transactions on*, vol. 61, no. 12, pp. 4678 - 4688, 2013.
- [67] M. Zakrzewski and J. Vanhala, "Separating respiration artifact in microwave doppler radar heart monitoring by Independent Component Analysis," *SENSORS*, pp. 1368 - 1371, 2010.
- [68] B.-K. Park, S. Yamada, O. Boric-Lubecke and V. Lubecke, "Single-Channel Receiver Limitations in Doppler Radar Measurements of Periodic Motion," in *Radio and Wireless Symposium*, San Diego, 2006.
- [69] A. Rahman, E. Yavari, A. Singh, V. Lubecke and O. Boric-Lubecke, "Single-channel radar fusion for quadrature life-sign Doppler radar," in *Wireless Information Technology and Systems (ICWITS) and Applied Computational Electromagnetics (ACES), 2016 IEEE/ACES*, Honolulu, 2016.
- [70] B.-K. Park, O. Boric-Lubecke and V. M. Lubecke, "Arctangent Demodulation With DC Offset Compensation in Quadrature Doppler Radar Receiver Systems," *IEEE Transactions on Microwave Theory and Techniques*, vol. 55, no. 5, pp. 1073-1079, May, 2007.
- [71] M. Zakrzewski, H. Raitinen and J. Vanhala, "Comparison of Center Estimation Algorithms for Heart and Respiration Monitoring With Microwave Doppler Radar," *IEEE Sensors Journal*, vol. 12, no. 3, pp. 627-634, 2012.
- [72] Y. Yan, C. Li and J. Lin, "Effects of I/Q mismatch on measurement of periodic movement using a Doppler radar sensor," in *Radio and Wireless Symposium (RWS), 2010 IEEE*, New Orleans, LA, USA, 2010.
- [73] A. Singh, X. Gao, E. Yavari, M. Zakrzewski, X. H. Cao, V. Lubecke and O. Boric-Lubecke, "Data-Based Quadrature Imbalance Compensation for a CW Doppler Radar System," *IEEE Transactions on Microwave Theory and Techniques*, vol. 64, no. 4, 2013.
- [74] M. Zakrzewski, A. Singh, E. Yavari, X. Gao, O. Boric-Lubecke, J. Vanhala and K. Palovuori, "Quadrature Imbalance Compensation With Ellipse-Fitting Methods for Microwave Radar Physiological Sensing," *IEEE Transactions on Microwave Theory and Techniques*, vol. 62, no. 6, pp. 1400-1408, 2014.
- [75] S. Chokroverty, "Sleep Disorders Medicine," *Elsevier*, 2009.
- [76] W. Klonowski, E. Olejarczyk and R. Stepień, "Sleep-EEG Analysis Using Higuchi's Fractal Dimension," in *International Symposium on Nonlinear Theory and its Applications*, Bruges, Belgium, 2005.
- [77] M. K. Weldon, *The Future X Network, A Bell Labs Perspective*, CRC Press, October, 2015.
- [78] "Samsung News Room," [Online]. Available: <https://news.samsung.com/global/samsung-unveils-new-era-of-smart-home-at-ces-2014>. [Accessed 26 June 2016].

- [79] A. Rahman, M. Baboli, O. Boric-Lubecke and V. Lubecke, "RF/wireless Indoor Activity Classification," in *Principles and Applications of RF/Microwave in Healthcare and Biosensing*, Elsevier Science & Technology Books, 2016, pp. 295-316.
- [80] T.-Y. Kao, Y. Yan, T.-M. Shen and A.-K. Chen, "Design and Analysis of a 60-GHz CMOS Doppler Micro-Radar System-in-Package for Vital-Sign and Vibration Detection," *IEEE Trans. on Microwave Theory and Techniques*, vol. 61, no. 4, pp. 1649 - 1659 , 2013 (March).
- [81] T. Kiuru, M. Metso, S. Jardak, P. Pursula, J. Häkli, M. Hirvonen and R. Sepponen, "Movement and respiration detection using statistical properties of the FMCW radar signal," in *Global Symposium on Millimeter Waves (GSMM) & ESA Workshop on Millimetre-Wave Technology and Applications*, 2016.
- [82] Y. S. Lee, P. N. Pathirana, C. L. Steinfort and T. Caelli, "Monitoring and Analysis of Respiratory Patterns Using Microwave Doppler Radar," *IEEE Journal of Translational Engineering in Health and Medicine*, vol. 2, 2014.
- [83] J. F. M. Gerrits, R. Vetter, J. R. Farserotu, C. Hennemann, M. Hübner and J.-D. Decotignie, "A low-complexity C-band radar for non-invasive respiration measurement," in *3rd International Symposium on Applied Sciences in Biomedical and Communication Technologies (ISABEL 2010)*, 2010.
- [84] C. Gu, R. Li, C. Li and S. B. Jiang, "Doppler radar respiration measurement for gated lung cancer radiotherapy," in *2011 IEEE Topical Conference on Biomedical Wireless Technologies, Networks, and Sensing Systems*, 2011.
- [85] Electronic Warfare and Radar Systems Engineering Handbook, Putu Mugu, CA: US Navy, 2013.
- [86] N. Birsan, D. Munteanu, G. Iubu and T. Niculescu, "Time-frequency analysis in Doppler radar for noncontact cardiopulmonary monitoring," in *E-Health Bioeng. Conf. (EHB)*, 2011.
- [87] A. Accardo, M. Affinito and M. Carrozzì, "Use of the fractal dimension for the analysis of electroencephalographic time series," *Biological Cybernetics*, vol. 77, no. 5, pp. 339-350, 1997.
- [88] L. A. N. Amaral, A. L. Goldberger, P. C. Ivanov and H. E. Stanley, "Scale-Independent Measures and Pathologic Cardiac Dynamics," *Physical Review Letters*, vol. 81, no. 11, 1998.
- [89] D. J. MacKay, Information Theory, Inference, and Learning Algorithms, Cambridge University Press , 2003.
- [90] S. Haykin, Neural Networks: A Comprehensive Foundation, Prentice Hall, 1998.
- [91] D. F. Specht, "Probabilistic neural networks," *Neural Networks*, vol. 3, pp. 109-118, 1990.
- [92] J. Shawe-Taylor and N. Cristianini, Support Vector Machines and other kernel-based learning methods, Cambridge University Press, 2000.
- [93] I. Rish, "An empirical study of the naive Bayes classifier," in *IJCAI Workshop on Empirical Methods in AI*, 2001.
- [94] G. Yuan, N. A. Drost and R. A. McIvor, "Respiratory rate and breathing pattern," *McMaster Univ. Med. J.*, vol. 10, no. 1, pp. 23-28, 2013.
- [95] R. Palaniappan and S. Krishnan, "Identifying individuals using ECG signals," in *Proceedings of International Conference on Signal Processing and Communications*, Bangalore, India, 2004.
- [96] R. Palaniappan, "Electroencephalogram signals from imagined activities: A novel biometric identifier for a small population," *Intelligent Data Engineering and Automated Learning – IDEAL*, vol. 4224, p. 604–611, 2006.
- [97] A. Rahman, E. Yavari, V. Lubecke and O.-B. Lubecke, "A Low IF Tag Based Motion Compensation Technique For Mobile Short Range Doppler Radar Life Sign Monitoring Device," *IEEE Transactions on Microwave Theory and Techniques*.
- [98] A. Rahman, E. Yavari, X. Gao, J. Xu, V. Lubecke and O. Boric-Lubecke, "See-through-wall life sensing using mobile Doppler radar," in *Microwave Measurement Conference (ARFTG), 2016 87th ARFTG*, San Francisco, CA, USA , 2016.
- [99] X. Li, D. Qiao, Y. Li and H. Dai, "A novel through-wall respiration detection algorithm using UWB radar," in *35th Annual International Conference of the IEEE Engineering in Medicine and Biology Society (EMBC)*, 2013.
- [100] Z. Li, W. Li, H. Lv, Y. Zhang, X. Jing and J. Wang, "A Novel Method for Respiration-Like Clutter Cancellation in Life Detection by Dual-Frequency IR-UWB Radar," *IEEE Transactions on Microwave Theory and Techniques*, vol. 61, no. 5, pp. 2086 - 2092, 2013.
- [101] Y. S. Lee and P. N. Pathirana, "Motion artifact separation in single channel Doppler radar respiration measurement," in *2015 International Symposium on Bioelectronics and Bioinformatics (ISBB)*, Beijing,

China, 2015.

- [102] C. Li and J. Lin, "Random Body Movement Cancellation in Doppler Radar Vital Sign Detection," *Microwave Theory and Techniques, IEEE Transactions on*, vol. 56, no. 12, pp. 3143-3152, 2008 - Nov.
- [103] I. Mostafanezhad and O.-B. Lubecke, "Benefits of Coherent Low-IF for Vital Signs Monitoring Using Doppler Radar," *IEEE Transactions on Microwave Theory and Techniques*, vol. 62, no. 10, pp. 2481-2487, 2014.
- [104] E. Yavari and O. Boric-Lubecke, "Low IF Demodulation for Physiological Pulse Doppler Radar," in *III MTT-S Int. Microw. Symp. Dig.*, Tampa, 2014.
- [105] J. Crols and M. Steyaert, "Low-IF topologies for high-performance analog front ends of fully integrated receivers," *Circuits and Systems II: Analog and Digital Signal Processing, IEEE Transactions*, vol. 45, no. 3, pp. 269 - 282, 1998 .
- [106] L. Chioukh, H. Boutayeb, D. Deslandes and K. Wu, "Noise and Sensitivity of Harmonic Radar Architecture for Remote Sensing and Detection of Vital Signs," *Microwave Theory and Techniques, IEEE Transactions on*, vol. 62, no. 9, pp. 1847 - 1855 , 2014 Aug.
- [107] Y. Chen, E. Gunawan, K. Soon Low, Y. Kim, C. Boon Soh, A. R. Leyman and L. Lin Thi, "Non-Invasive Respiration Rate Estimation Using Ultra-Wideband Distributed Cognitive Radar System," in *International Conference of the IEEE Engineering in Medicine and Biology Society*, 2006.
- [108] I. Mostafanezhad, O.-B. Lubecke and V. Lubecke, "A coherent low IF receiver architecture for Doppler radar motion detector used in life signs monitoring," in *Radio and Wireless Symposium (RWS) IEEE* , New Orleans, 2010.
- [109] M. C. K. Khoo, "Determinants of ventilatory instability and variability," *Respiration Physiology*, vol. 122, pp. 167-182, 2000.
- [110] Y. Kuratomi, N. Okazaki, T. Ishihara, T. Arai and S. Kira, "Variability of breath-by-breath tidal volume and its characteristics in normal and diseased subjects. Ventilatory monitoring with electrical impedance pneumography," *Jpn. J. Med.*, vol. 24, no. 2, p. 141-149, 1985.
- [111] M. A. Cretikos, R. Bellomo, K. Hillman, J. Chen, S. Finfer and A. Flabouris, "Respiratory rate: The neglected vital sign," *Med. J. Austral*, vol. 188, p. 657-659, 2008.
- [112] A. Rahman, V. Lubecke, G. Xiaomeng and O. Boric-Lebecke, "High Dynamic Range DC Coupled CW Doppler Radar for Accurate Respiration Characterization and Identification," in *89th ARFTG Microwave Measurement Symposium*, Honolulu, 2017.
- [113] "Biometrics Institute," Biometrics Institute Limited, [Online]. Available: <http://www.biometricsinstitute.org/pages/types-of-biometrics.html>. [Accessed 6 6 2017].